

# Study on the New Advanced Techniques in Free-Space Optical Communication Systems

FSO 通信システムの  
新高度化技術に関する研究

February, 2018

Yuwei SU

ス ユウエイ

# Study on the New Advanced Techniques in Free-Space Optical Communication Systems

FSO 通信システムの  
新高度化技術に関する研究

February, 2018

Waseda University

Graduate School of Fundamental Science and Engineering  
Department of Computer Science and Communications Engineering,  
Research on Ubiquitous Communication System

Yuwei SU

ス ユウエイ

## Acknowledgements

I want to take this opportunity to thank my supervisor, Prof. Dr. Takuro Sato Sensei, very much for his valuable and continual support on my research. He is so kind-hearted and willing to help me not only on the research but also on my living here in Japan. I would like to thank him for encouraging my research and for providing a good study environment during the period of my Ph.D course at FSE, Waseda University. His advices on both study as well as on my future career have been priceless. I confirm that I will continue to be benefited by his patient teaching and forward-looking guidance in my future life. It is my great honor to study under his supervision.

Besides, I appreciate Matsumoto Sensei, Shimamoto Sensei and Tsuda sensei very much of their great efforts on reviewing my thesis and presentation slides, giving help to improve the quality, and endless help on my research. I want to take this opportunity to thank the defense committees and FSE's help and effort as well.

I would like to say thanks to Pro. Dr. Matsumoto, my supervisor during Master's course, for all of his help. He has been very warmhearted with my research and I greatly appreciate him for giving me his time, advice, and encouragement during this process.

I also want to thank my research partners: Dr. Fan Bai from Sato Lab, Dr. Jun Wu from Shanghai Jiaotong University, Dr. Xiaole Sun from Arizona University, Dr. Abdelmoula Bekkali and Dr. Dimitar from Matsumoto Lab a lot for all the encouragements, discussions and information sharing on my research.

Special thanks go to my beloved parents for their help, endless support on my life and research. They always try to support me with whatever means they have. The family affection is always my great treasure.

Finally, I would like to thank the China Scholarship Council (CSC) which enable me to extend and pursue graduate studies in Japan.

# Abstract

In this thesis, we emphasize the necessity of developing the free-space optical(FSO) communication systems. Then we analyze the most significant constraint, atmospheric turbulence, in effecting the laser beam transmission. In order to improve the system performance, we propose to take four main techniques into the FSO system designment. Based on the simulation results, we can have the conclusion that the proposed methods could mitigate the channel fading caused by the atmospheric turbulence, efficiently. Detail contents of each chapter is given as follows:

In Chapter 1, titled “Introduction”, we would give a brief introduction to: the concept and the current development situation of the FSO system; both the advantages and the constraints of the FSO communications; and our mainly research contribution in the FSO field.

In Chapter 2, titled “Channel Effects”, the analysis about the influence of the atmospheric channel to the laser beam transmission is demonstrated. The atmospheric turbulence will lead to intensity fluctuations and polarization distortions of the optical wave. Unfortunately, these detrimental effects have far-reaching consequences on the FSO system. In this chapter, we explain the physical form of the atmospheric turbulence, analyze the turbulence spectrum models, introduce the statistic model describing the intensity fluctuations and establish the mathematical model describing the polarization distortions of the optical wave propagating through the atmosphere channel. According to the estimation, we can find that the optical polarization is far more stable than the optical intensity suffered from the turbulence disturbing.

In Chapter 3, titled “Related Techniques”, based on the channel analysis in chapter 2, we propose four methods to be applied in FSO system designment:

1. The orthogonal frequency division multiplexing (OFDM) technology has the advantages in against channel dispersion and time varying environment;
2. The method aperture average mitigates the channel fading by increasing the size of the receiving lens. The aperture average promoting on the plane/spherical/Gaussian wave are also discussed;
3. The multiple reception reduces the weight and cost of the FSO system by replacing one huge lens to several smaller lenses. We establish the mathematical model of the correlation coefficient between different lenses responding to their central distance and the turbulence conditions. The intensity relationship between two individual lenses are presented;
4. The polarization modulation (PM) modulates signals into optical polarization states to promote the system performance, since the optical polarization is the most stable property when laser beam propagating through the atmosphere channel. Three types of PM methods are expressed in this section.

In Chapter 4, titled “Applications and Improvements”, we analyze the performance of the FSO systems applying the technologies discussed in Chapter 3. It includes:

1. The performance of the OFDM FSO system with aperture average is simulated. The numerical result can present that the optimum OFDM modulation index is between 0.1% to 1% and the proposal can reduce the system average bit-error-rate (BER) under the varying atmospheric turbulence strength;
2. The multiple reception scheme is replacing one huge lens to several smaller lenses. Under the condition of the identical receiving area, we run the simulations about the multiple reception OFDM FSO systems. The numerical result can show that the diversity reception is an efficient method to improve the FSO system performance and the superior performance comes from a lower correlation coefficient;
3. Based on the analysis in Chapter 2, the optical polarization is the most stable property of the laser beam when propagating through the

atmospheric channel. In order to take full advantages of the polarization stability, we modulate the OFDM signal into a consecutive linear polarization state and name this method as consecutive polarization modulation (CPolM). Based on a comparison with the intensity modulation (IM) -based OFDM FSO system, the CPolM-based OFDM FSO system emerges the superiority in mitigating channel effects;

4. The linear polarization state is not suitable in a mobile environment, since a random rotation will lead to a misalignment of the polarized direction. Hence, we apply the circular polarization states to represent signals and simulate the system working in the space-to-ground channel. Comparing the numerical results of the circular polarization shift keying (CPolSK) -based FSO system with the IM-based FSO system, we can find the proposed system needs about 3dB less signal-to-noise ratio (SNR) than the conventional system to achieve the same level of BER.

In Chapter 5, titled “Conclusion”, the main discoveries of this dissertation are finally summarized up with regard to all the four techniques. The potential underwater environment, quantum communications and pointing, acquisition and tracing (ATP) techniques in FSO systems are listed as well for future studies.

# Contents

<b>1</b>	<b>Introduction</b>	<b>1</b>
1.1	Overview . . . . .	1
1.2	Main Research Contribution . . . . .	4
<b>2</b>	<b>Channel Effects</b>	<b>6</b>
2.1	Kolmogorov Theory of Turbulence . . . . .	7
2.2	Index of Refraction and Rytov Variance . . . . .	7
2.3	Intensity Distribution Model . . . . .	8
2.3.1	Lognormal Distribution . . . . .	9
2.3.2	Gamma-Gamma Distribution . . . . .	10
2.3.3	Polarization Fluctuation . . . . .	11
<b>3</b>	<b>Related Techniques</b>	<b>17</b>
3.1	OFDM . . . . .	17
3.1.1	OFDM Signal Description . . . . .	17
3.1.2	Discrete Fourier Transform . . . . .	20
3.1.3	Cyclic Prefix . . . . .	23
3.1.4	Spectral Efficiency . . . . .	26
3.1.5	Real and Complex components of an OFDM Signal . . . . .	26
3.2	Aperture Average . . . . .	28
3.2.1	Plane Wave . . . . .	29
3.2.2	Spherical Wave . . . . .	30
3.2.3	Gaussian-beam Wave . . . . .	32
3.3	Multiple Reception . . . . .	33
3.3.1	Correlation Coefficient . . . . .	33
3.3.2	Correlation Lognormal Distribution . . . . .	36
3.4	Polarization Modulation . . . . .	37
3.4.1	PolSK . . . . .	38

3.4.2	CPolM . . . . .	38
3.4.3	CPolSK . . . . .	39
<b>4</b>	<b>Applications and Improvements</b>	<b>40</b>
4.1	OFDM FSO System with Aperture Average . . . . .	40
4.2	Multiple Reception OFDM FSO System . . . . .	45
4.3	CPolM-Based OFDM FSO System . . . . .	51
4.3.1	CPolM-Based OFDM FSO System Structure . . . . .	51
4.3.1.1	Transmitter . . . . .	51
4.3.1.2	Receiver . . . . .	54
4.3.2	System Performance . . . . .	56
4.3.2.1	Theoretical Analysis . . . . .	57
4.3.2.2	Numerical Results Analysis . . . . .	59
4.4	CPolSK-Based FSO System Working in Space-to-Ground Channel . .	64
4.4.1	Space-to-Ground FSO Channel . . . . .	64
4.4.1.1	Intensity Fluctuation . . . . .	64
4.4.1.2	Polarization Fluctuation . . . . .	65
4.4.2	CPolSK-Based FSO System Structure . . . . .	70
4.4.2.1	Transmitter . . . . .	70
4.4.2.2	Receiver . . . . .	72
4.4.3	System Performance . . . . .	74
4.4.3.1	Theoretical Analysis . . . . .	74
4.4.3.2	Numerical Results Analysis . . . . .	76
<b>5</b>	<b>Conclusion</b>	<b>80</b>
5.1	Summary and discussion . . . . .	80
5.2	Future work . . . . .	82

# List of Figures

2.1	Kolmogorov Theory of Turbulence. [1]	8
2.2	Probability Density of Lognormal Distribution.	9
2.3	Probability Density of Gamma-Gamma Distribution.	11
2.4	Linear Polarization Fluctuation Distribution under Different Turbulence Strength. [2]	16
3.1	Structure for An OFDM Modulation/Demodulation System. [3,4]	18
3.2	OFDM Subcarriers in Time Domain.	20
3.3	Spectrum of OFDM Subcarriers.	20
3.4	Diagram for OFDM Transmitter. [3,4]	22
3.5	Diagram for OFDM Receiver. [3,4]	22
3.6	Transmitted OFDM Signal without Cyclic Prefix. [3,4]	23
3.7	Received OFDM Signal without Cyclic Prefix. [3,4]	24
3.8	Transmitted OFDM Signal with Cyclic Prefix. [3,4]	24
3.9	Received OFDM Signal with Cyclic Prefix. [3,4]	25
3.10	Diagram of The IQ Modulator for Complex Signals. [3,4]	27
3.11	Aperture Averaging Factor versus Diameter of Lens for Plane Wave.	30
3.12	Aperture Averaging Factor versus Diameter of Lens for Spherical Wave.	31
3.13	Aperture Averaging Factor versus Diameter of Lens for Gaussian Wave.	33
3.14	Dual Receiver.	34
3.15	Correlation Coefficient under Different Central Distance and Turbulence Condition. [5]	36
3.16	Correlation Lognormal Distribution between Two Individual Lens.	37
3.17	Principle of The PolSK.	38
3.18	Principle of The CPolSK.	39
4.1	Architecture of OFDM FSO System with Aperture Average.	40
4.2	Average SNR in Different Subcarrier Number $n$ and Optical Modulation Index $m_n$ .	43

4.3	Average BER versus Average SNR with Different Receiving Diameters under Varying Turbulence Strength. . . . .	43
4.4	Ternary Receiver. [5] . . . . .	45
4.5	Ternary Diversity Reception OFDM FSO System Architecture. [5] . .	46
4.6	Average BER versus Average SNR under Different Reception Scheme. [5]	48
4.7	Average BER versus Average SNR under Different Modulation Scheme. [5] . . . . .	48
4.8	Outage Probability versus Threshold under Different Reception Scheme. [5] . . . . .	49
4.9	Diagram of The CPolM-Based OFDM FSO System Transmitter. [6] .	51
4.10	Mapping Relation in The CPolM-Based OFDM FSO System. [6] . . .	52
4.11	Polarization States in The Transmitter. [6] . . . . .	53
4.12	Diagram of The CPolM-Based OFDM FSO System Receiver. [6] . . .	54
4.13	Polarization States in The Receiver. [6] . . . . .	55
4.14	Effects of $\eta$ to The $\langle \text{SER} \rangle$ Performance of CPolM-Based OFDM FSO System Transmitting 16-QAM Signal. [6] . . . . .	60
4.15	Effects of $L_0$ and $l_0$ to The $\langle \text{SER} \rangle$ Performance of CPolM-Based OFDM FSO System Transmitting 16-QAM Signal. [6] . . . . .	61
4.16	Comparison of $\langle \text{SER} \rangle$ Versus $\langle P_r \rangle$ in the CPolM- and IM-Based OFDM FSO System Transmitting 16-QAM Signal. [6] . . . . .	62
4.17	Comparison of The $P_{out}$ in The CPolM- and IM-Based OFDM FSO System Transmitting 16-QAM Signal. [6] . . . . .	63
4.18	Polarization Characters of the CPolSK-Based FSO System Working in Space-to-Ground Links. [7] . . . . .	69
4.19	Diagram of the CPolSK-Based FSO System Transmitter. [7] . . . . .	70
4.20	Polarization States in The Transmitter. [7] . . . . .	71
4.21	Diagram of the CPolSK-Based FSO System Receiver. [7] . . . . .	72
4.22	Polarization States in The Receiver. [7] . . . . .	73
4.23	Effects of $C_n^2(0)$ and $v$ to The $\langle BER \rangle$ Performance of CPolSK-Based FSO System Working in Space-to-Ground Channel. [7] . . . . .	76
4.24	Effects of $C_n^2(0)$ and $v$ to The $P_{out}$ Performance of CPolSK-Based FSO System Working in Space-to-Ground Channel. [7] . . . . .	77
4.25	Comparison of $\langle BER \rangle$ Versus $\langle SNR \rangle$ in the CPolSK- and OOK-Based FSO System Working in Space-to-Ground Channel. [7] . . . . .	78

# List of Tables

1.1	Existing FSO Standards. [2]	4
4.1	Parameters for Figure 4.3.	44
4.2	Parameters for Figure 4.6, Figure 4.7, Figure 4.8.	50
4.3	Simulation Parameters	59
4.4	Simulation Parameters	79

# Chapter 1

## Introduction

Free space optics (FSO) is a line-of-sight technology which utilizes the laser to provide optical bandwidth connections. It has acquired more and more attentions in the past a few years, since researches about the wireless radio frequency (RF) transmission have met with the bottleneck. The optical frequency can provide a wider communication bandwidth and a higher data transmission speed than the traditional RF band. Since the laser beam is inherent narrow, the carrier of the FSO system performs an outstanding directivity and can also supply for ultra-long distance (transmission distance $>20\text{km}$ ) communications. The optical telescopes for the FSO communications are more portable and more energy efficient than the antennas for the RF communications. The FSO system could be an ideal alternative option in some special situations (transmission distance between 10km to 20km), as natural disaster areas, mountainous areas, etc., in which the optical fiber system is too expensive or impossible to be established. Recently, the last mile problem (transmission distance $<10\text{km}$ ) is growing more and more serious and the FSO communication is considered as a desired solution. [1, 5, 6, 8–50]

### 1.1 Overview

With the increasing requirement to the wider transmission bandwidth and the high speed local area network (LAN), traditional communication equipments, such as the copper-based infrastructures, the digital subscriber line (DSL), the cable modems and the transmission system 1 (T1s), can no longer satisfied all the demands. A scheme of the higher-speed connections to the outside world has acquired more and more interests. At present, there are only 5 percent of the large corporations are settled on the backbone fiber network. And as many as 75 percent companies are distributed within one mile distance around the backbone optical fiber (called as the

last mile problem). FSO has been able to reach a transmission rate of 2.5 gigabit per second (Gbps). The text, image, voice, and video data can be transmitted through the free space environment with an optical link without the optical fiber facility. In the United States, the pilot FSO networks have already been built up in some of the major cities. In Europe, companies are eager to find a substitute high-speed accessing method to the optical fiber systems. Thus the FSO technology has received a growing attention. [1, 23–26]

Existing commercial FSO transceivers can afford the data rate from 10 Mbps to 1.25 Gbps. This transmission speed is much higher than that of digital subscriber lines or coaxial cables and can totally fulfill the requirement of broadband communications. The laser diodes on the market can produce the optical pulses duration only 100 picosecond (100 trillionths of a second) each. The on and off switching rate of such laser diodes can support the communication speed as high as 9.6 Gbps. However, this kind of device has not yet been used in the FSO applications. [1, 27–38]

Typical FSO system is applying the optical wave with 850 and 1550 nm wavelength. Unlicensed electromagnetic frequency signal is modulated on the optical frequency carriers which are operated in the relative low-power for the eye-safety. Nevertheless, the communication quality is restricted by the optical power limitation. The FSO systems can support broadband communications through the horizontal near-earth channel in the transmission distance of a range from hectometre order to kilometre order depending on the atmosphere conditions. It is enough to sustain the FSO links from customers to the backbone. In order to remit the channel fading caused by the bad weather, the FSO devices are arranged as a network structure. Each FSO transceiver is set to communicate with several nearest FSO devices. And this method can make sure that the information is transmitted reliably through an optimal network path. [1, 6, 39–45]

Be sensitive to the fog weather is restricting developing of the commercial near-earth FSO systems. Based on both of the theory and experiment data, fog effects the FSO system performance the most seriously. In order to reduce the foggy influence, the FSO system should have a link margin when designing a commercial FSO link. An automatic extension to the optical power is an efficient method to overcome the optical power loss caused by the fog weather. On the other hand, the communication quality of FSO links is also remitted by the channel absorption. What's more, the atmospheric turbulence is another influence factor to the laser propagation and will cause the optical scintillation on the receiving plane. [1, 46, 49, 51–65]

When fixing the link margin, another important parameter called the link availability should be considered. It is defined as the fraction of the total operating time that the communication interrupts ascribed by the fog or other weather influence. Based on the application, the link availability is varied to adapt the requirements. Considering a private enterprise network environment of the connection between two offices located in dividing places, it requires about 99.9% uptime and the related nine hours of downtime in one year. When it is in commercial public telecommunication carrier-class environment of connecting the important business customers, it requires about 99.999% uptime and the related 5 minutes of downtime in one year. This is the reason why it is called five-nine benchmark and it is also regarded as the conventional fiber optical communication operating level. [1, 2, 66, 67]

The conception of FSO is conceived in the 1960s. When it comes to the 1970s, the atmosphere condition influence to the communication quality and the speedy increasing of the optical fiber technology declined the development of FSO system. However, in the environment of building-to-building, aircraft-to-aircraft, satellite-to-satellite and ground-to-space, FSO technology is a suitable method to provide high speed connections. Since the laser beam is inherent narrow, FSO system performs a remarkable directivity and available for ultra-long distance ( $>20\text{km}$ ) links. The FSO devices are more portable and energy efficient than the RF devices. When the optical fiber system is too expensive or impossible to be established (in natural disaster area, mountainous area, etc.), FSO system could be an alternative option (10km 20km). FSO system is also considered as a solution to the last-mile problem ( $<10\text{km}$ ). In the 2006s, Japan Aerospace Exploration Agency (JAXA) first successfully tested the communication connection between the low altitude orbit satellite and an optical ground station (NICT, Koganei, Tokyo) using laser beams. The fact that FSO becomes an inseparable part of the modern information system based on the way of accumulated experience. In 2013s, the Lunar Laser Communication Demonstration (LLCD) is NASA's first high-rate, two-way, space laser communication demonstration. This project successful demonstrate the communication connection between the ground-based laser component installation and space terminal that will reach lunar orbit can transmit the data rate at 600 Mbps over laser, and transmission distance is over 238 km. Moreover, the use of modified FSO technology for high-speed, low-range underwater applications becomes more popular in the current time. [1, 3–5, 47, 48, 50, 68–102]

Most existing FSO standards, shown in Table 1.1, are relevant to the indoor system. In view of the advantages of the FSO system, International Telecommunication Union (ITU) has started to develop the outdoor FSO standards since 2006. [2]

Table 1.1 Existing FSO Standards. [2]

Standards		Wavelength	Data Rate
IEEE 802. 11		850–950nm	1 and 2 Mbps
IrDA	SIR	850–900nm	2.4 to 115.2 kbps
	MIR		0.576 and 1.152 Mbps
	FIR		4 Mbps
	VFIR		16 Mbps
	UFIR		96 Mbps
	Giga-IR		0.576 and 1.024 Gbps
VLCA	CP-1221	380-780nm	4.8 kbps
	CP-1222		
	CP-1223		
IEEE 802. 15. 7	PHY I	380-780nm	11.6 to 266.6 kbps
	PHY II		1.25 to 96 Mbps
	PHY III		12 to 96 Mbps

## 1.2 Main Research Contribution

In this thesis, we take four techniques to mitigate the channel fading of FSO system: orthogonal frequency division multiplexing (OFDM); aperture average; spatial diversity and polarization modulation.

OFDM can be simply seen as a kind of time diversity. We take it here as the modulation scheme of the system for its advantages against channel dispersion and time-varying environment.

Aperture average is an efficient method to mitigate channel fading in FSO system. The increasing size of receiving lens would reduce the fluctuation of the received light intensity and promote the performance of the system. In this thesis, we implement aperture average into the OFDM FSO system. Analyze the aperture averaging factor versus diameter of receiving lens in different kinds of wave model (Plane wave; Spherical wave; Gaussian-beam wave). Find out the optimal optical modulation index for each subcarrier. Simulate the performance of the system and find that aperture average could improve the system performance efficiently and the system ensemble average BER has a boundary in a certain atmospheric turbulence condition.

Aperture average is the method to implement large size lens into the receiver terminal. However, the augment of the receiving lens radius would increase both of the system weight and cost, exponentially. In this thesis, we take the method of multiple reception to replace one big lens to several small lenses. Most of the previous research about FSO multiple reception are seeing the receivers independent which means the

central distance between any two of the receiving lenses is long enough. This would make a difficulty in the design of FSO system. When the receiving lenses are not far from each other, they can't be seen as independent individuals. Thus, the received light intensity would obey a joint probability density function with correlation coefficient. We analyze the correlation coefficient and joint probability distribution function in multiple reception OFDM FSO system. Especially, we simulate the performance of dual reception and ternary reception system. We compare the ensemble average signal-to-noise ratio (SNR), ensemble average bit-error-rate (BER) and outage probability (OP) of dual reception and ternary reception system in different correlation coefficient. We can find that the receiver with three lenses perform more preminent than dual reception and single reception OFDM FSO system. Its clear that multiple reception is an available method to mitigate the channel fading in OFDM FSO system.

Furthermore a novel FSO system configuration, named as the consecutive polarization modulation (CPolM) -based OFDM FSO system, transmits the OFDM signal basing on a novel modulation scheme abbreviated as CPolM. We establish the mathematic model about the system performance and present a comparison between the CPolM- and the intensity modulation (IM) -based OFDM FSO system. The numerical results show that the proposed system has an advantage in promoting the performance of the FSO system.

Finally, we analyze the performance of a circular polarization shift keying (CPolSK) - based FSO system working in space-to-ground channel. Mathematic models associating the system performance with the Stocks parameters are established. Based on the polarization estimation, we set up the channel parameters and run the simulation about the proposed system performance. In the our simulation results, when it is compared with the conventional on-off-keying (OOK) -based FSO system, CPolSK-based system shows a significant advantage in improving the system performance.

# Chapter 2

## Channel Effects

In regard to the FSO technology, the fundamental limitation of communication reliability generates from the channel environment which it propagates through atmosphere as an unguided link. The atmosphere interacts with optical beam due to the composition of atmosphere, which corresponds to the aerosols known as molecules and suspended particles. Under this interaction effects that produces a variety of optical phenomenon including the absorption at specific optical wavelength, scattering and optical scintillation due to the variation of the atmosphere's refractive index under the effect of temperature. Thus, it arises the degradation of the transmission performance, resulting in the power losses, amplitude fluctuation, phase aberration and changes in the degree of polarization (DOP). Understanding of the effect of atmosphere environment induced channel fading at quality of received signal becomes a primary challenge in FSO issue. This section explains this challenge and introduces the statistical models for describing the irradiance fluctuation in varying degrees of turbulence strength. [1, 2, 5, 6, 32, 47, 48, 50]

The study on turbulence is one of important branches of the research on fluid mechanics. In 1883, Reynold conducted an experiment in glass tube with fluid, which is the earliest exploration on turbulence. Most of classical theories of atmospheric turbulence were based on the work of Kolmogorov, who developed a statistical theory of turbulence that derived from dimensional analysis and additional approximations. In the analysis of optical field, instead of velocity fluctuations, we more concerned about the index of refraction fluctuations, which we called optical turbulence, caused by the temperature fluctuations. The optical turbulence fluctuates randomly in time and space would lead to the intensity and polarization fluctuations. In order to describe this kind of fluctuations, several probability distribution function (PDF) models were developed. In this chapter, we first introduce the spectrum function about the index of refraction. Then lead to two well-known intensity PDF models:

Lognormal distribution and Gamma-Gamma distribution. Finally, we will derive one polarization spectrum model. [1, 2, 5, 6, 32, 47, 48, 50]

## 2.1 Kolmogorov Theory of Turbulence

The classical theory of turbulence is based on the research of Kolmogorov in 1941. The atmospheric turbulence structure is shown in Figure 2.1. The energy injection at large scales is from either wind shear or convection. Under the cascade theory, the wind velocity increasing creates smaller and partial unstable air cells called "eddies". The larger eddies separate into smaller eddies with a continuum eddy size from a macroscale  $L_0$  (outer scale of the atmospheric turbulence) to a microscale  $l_0$  (inner scale of the atmospheric turbulence). The turbulent eddies of which scale sizes smaller than the inner scale  $l_0$  would be disappeared. And the remained energy would be converted into heat. Kolmogorov analyzed random fluctuations in both the magnitude and direction of the velocity field, in terms of three hypotheses: 1.The small-scale structure of turbulence is statistically homogeneous, isotropic, and independent of the large-scale structure; 2.The motion associated with the small-scale structure is uniquely determined by the frictional force and inertial force of the fluid; 3.When Reynolds number is large, eddies between scale sizes  $l_0$  and  $L_0$  form the inertial sub-range, instead of frictional force, the motion is determined by inertial force. [1, 2, 5]

## 2.2 Index of Refraction and Rytov Variance

In the study of optical wave propagation through the atmosphere, the index of refraction fluctuations caused by the temperature fluctuations is one of the most important parameters. It can be expressed as a function of position  $R$  and time  $t$ :

$$n(R, t) = n_0 + n_1(R, t). \quad (2.1)$$

Where  $n_0 = \langle n(R, t) \rangle \approx 1$  is the mean value of the index of refraction in atmosphere and  $n_1$  is the fluctuation in the index of refraction. For optical frequency, time variations in index of refraction are negative. Therefore, the function (2.1) can be written as:

$$n(R) = 1 + n_1(R). \quad (2.2)$$

Kolmogorov power-law spectrum is a generally accepted result as a power spectral density for refractive-index fluctuations [1]:

$$\Phi_n(\kappa) = 0.033C_n^2\kappa^{-11/3}. \quad (2.3)$$

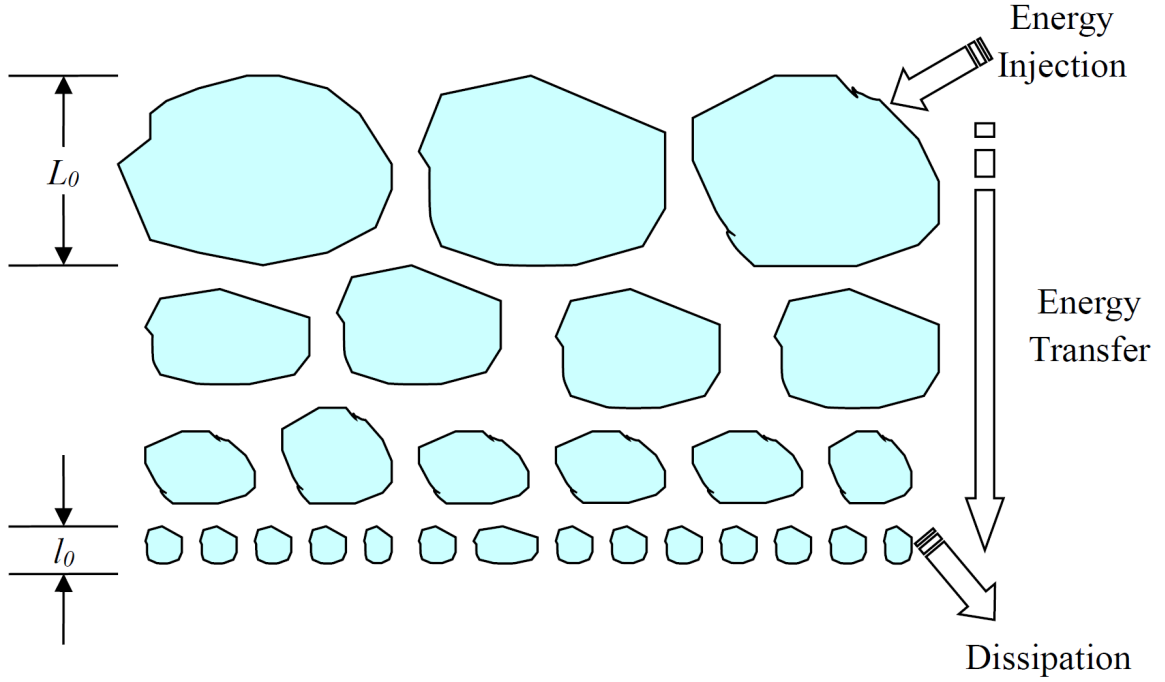


Figure 2.1 Kolmogorov Theory of Turbulence. [1]

The quantity  $C_n^2$  denotes the refractive index structure parameter. It is normally used to measure the strength of the fluctuations of index of refraction  $n$ . And  $\kappa$  is the scalar spatial frequency (in units of rad/m).

The traditional way to distinguish the weak strength turbulence and the strong strength turbulence is to calculate the value of Rytov variance. Assuming that the optical wave (optical wave number is  $k=2\pi/\lambda$ ) propagating path length is  $L$ , Rytov variance can be calculated by [1]:

$$\sigma_R^2 = 1.23k^{7/6}C_n^2L^{11/6}. \quad (2.4)$$

The situation  $\sigma_R^2 < 1$ ,  $\sigma_R^2 > 1$  and  $\sigma_R^2 = 1$  present weak turbulence, strong turbulence and moderate turbulence.

### 2.3 Intensity Distribution Model

For the influence of atmospheric turbulence can be seen as a random process, a development for a practical PDF is necessary. In this section, we present two typical mathematical scintillation distribution models: Lognormal distribution and Gamma-Gamma distribution. The two are performing well in predicting the observed phenomena. [1, 2, 5, 6, 32, 47, 48, 50]

### 2.3.1 Lognormal Distribution

We assume that the light intensity can be represented by a log-amplitude  $x$ . It can be written as:

$$I = I_0 \exp(2x - 2\langle x \rangle), \quad (2.5)$$

where  $\langle x \rangle$  denotes the ensemble average value of the log-amplitude  $x$ . Based on the Rytov approximation, the logarithm of the irradiance can be seen as Gaussian distribution. The PDF for the Lognormal distribution represented by the log-amplitude  $x$  can be written as:

$$f_x(x) = \frac{1}{\sqrt{2\pi\sigma_x^2}} \exp\left\{-\frac{(x - \langle x \rangle)^2}{2\sigma_x^2}\right\}. \quad (2.6)$$

Where  $\sigma_x^2$  is the variance of log-amplitude  $x$  and  $I_0$  presents the light intensity absenting the turbulence effects. Combining the Equation (2.5) and (2.6), the PDF of light intensity is:

$$\begin{aligned} f_C(C) &= \frac{I_0}{2I} \frac{1}{\sqrt{2\pi\sigma_x^2}} \exp\left\{-\frac{[\ln(I) - \ln(I_0)]^2}{8\sigma_x^2}\right\} \\ &= \frac{1}{C} \frac{1}{\sqrt{2\pi \cdot 4\sigma_x^2}} \exp\left\{-\frac{[\ln(C)]^2}{2 \cdot 4\sigma_x^2}\right\}, \end{aligned} \quad (2.7)$$

where  $C = I/I_0$ . In the Figure 2.2, the probability density of Lognormal distribution under different atmospheric turbulence can be shown as:

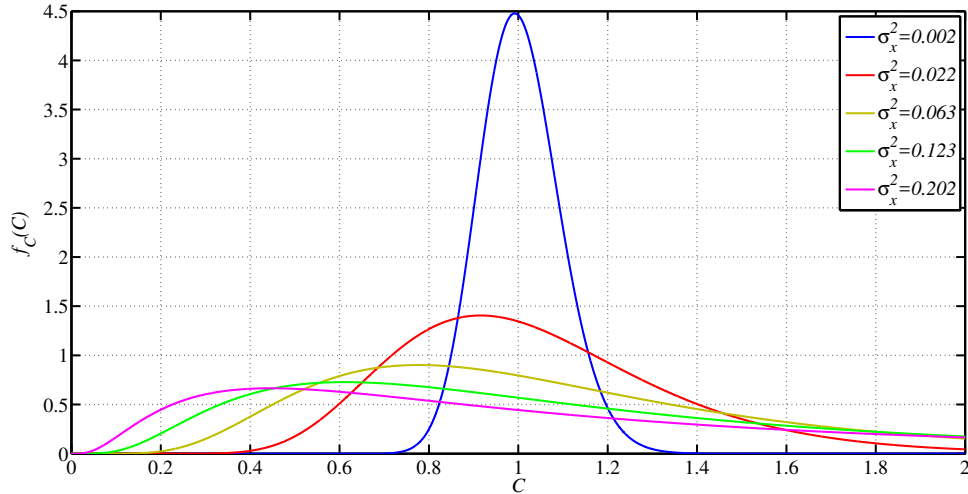


Figure 2.2 Probability Density of Lognormal Distribution.

### 2.3.2 Gamma-Gamma Distribution

Gamma-Gamma distribution function is a widely accepted statistical model in describing the intensity fluctuation (scintillation), since it is not only satisfying the weak turbulence region but also available for the moderate-to-strong turbulence region. It regards the scintillation as modulated by two independent random factors both following a Gamma distribution. The probability density function (PDF) of the Gamma-Gamma distribution is [1, 2, 5, 6, 32, 47, 48, 50]:

$$f_C(C) = \frac{2(\alpha\beta)^{\frac{\alpha+\beta}{2}}}{\Gamma(\alpha)\Gamma(\beta)} C^{\frac{\alpha+\beta-2}{2}} K_{\alpha-\beta} \left( 2\sqrt{\alpha\beta C} \right), C = \frac{P_r}{\langle P_r \rangle} > 0, \quad (2.8)$$

where  $P_r$  is the received optical power, the symbol  $\langle \cdot \rangle$  denotes the ensemble average value over scintillation,  $K_n(\cdot)$  is the modified Bessel function of the second kind of order  $n$ ,  $\alpha$  and  $\beta$  denote small- and large-scale factors can be expressed as [1]:

$$\alpha = [\exp(\sigma_{\ln X}^2) - 1]^{-1}, \quad (2.9)$$

$$\beta = [\exp(\sigma_{\ln Y}^2) - 1]^{-1}. \quad (2.10)$$

$\sigma_{\ln X}^2$  and  $\sigma_{\ln Y}^2$  are the small- and large-scale log-irradiance variances can be written as [1]:

$$\sigma_{\ln X}^2 = \sigma_{\ln X}^2(l_0) - \sigma_{\ln X}^2(L_0), \quad (2.11)$$

$$\sigma_{\ln Y}^2 = \frac{0.51\sigma_{PL}^2}{\left(1 + 0.69\sigma_{PL}^{12/5}\right)^{5/6}}, \quad (2.12)$$

where

$$\sigma_{\ln X}^2(l_0) = 0.16\sigma_R^2 \left( \frac{\eta_{l_0} Q_{l_0}}{\eta_{l_0} + Q_{l_0}} \right)^{7/6} \cdot \left[ 1 + 1.75 \left( \frac{\eta_{l_0}}{\eta_{l_0} + Q_{l_0}} \right)^{1/2} - 0.25 \left( \frac{\eta_{l_0}}{\eta_{l_0} + Q_{l_0}} \right)^{7/12} \right], \quad (2.13)$$

$$\sigma_{\ln X}^2(L_0) = 0.16\sigma_R^2 \left( \frac{\eta_{L_0} Q_{L_0}}{\eta_{L_0} + Q_{L_0}} \right)^{7/6} \cdot \left[ 1 + 1.75 \left( \frac{\eta_{L_0}}{\eta_{L_0} + Q_{L_0}} \right)^{1/2} - 0.25 \left( \frac{\eta_{L_0}}{\eta_{L_0} + Q_{L_0}} \right)^{7/12} \right], \quad (2.14)$$

$$\sigma_{PL}^2(l_0) = 3.86\sigma_R^2 \left\{ \left(1 + \frac{1}{Q_{l_0}^2}\right)^{11/12} \left[ \sin\left(\frac{11}{6} \arctan Q_{l_0}\right) + \frac{1.51}{(1 + Q_{l_0}^2)^{1/4}} \sin\left(\frac{4}{3} \arctan Q_{l_0}\right) - \frac{0.27}{(1 + Q_{l_0}^2)^{7/24}} \sin\left(\frac{5}{4} \arctan Q_{l_0}\right) \right] - 3.5Q_{l_0}^{-5/6} \right\}. \quad (2.15)$$

The related parameters are given by [1]:

$$Q_{l_0} = \frac{10.89L}{kl_0^2}, \quad \eta_{l_0} = \frac{2.61}{1 + 0.45\sigma_R^2 Q_{l_0}^{1/6}}, \quad Q_{L_0} = \frac{64\pi^2 L}{kL_0^2}, \quad \eta_{L_0} = \frac{\eta_{l_0} Q_{L_0}}{\eta_{l_0} + Q_{L_0}}, \quad (2.16)$$

where  $l_0$  is the inner scale of turbulence in the order from  $1mm$  to  $10mm$  and  $L_0$  is the outer scale of turbulence in meter-scale. The symbol  $\sigma_R^2 = 1.23C_n^2 k^{7/6} L^{11/6}$  denotes Rytov variance for a plane wave, in which  $C_n^2$  is the index of the refraction structure constant and in the range from  $10^{-17}m^{-2/3}$  to  $10^{-13}m^{-2/3}$ ,  $k$  denotes the optical wave number and  $L$  is the transmission distance. Figure 2.3 shows the probability density of Gamma-Gamma distribution under different atmospheric turbulence.

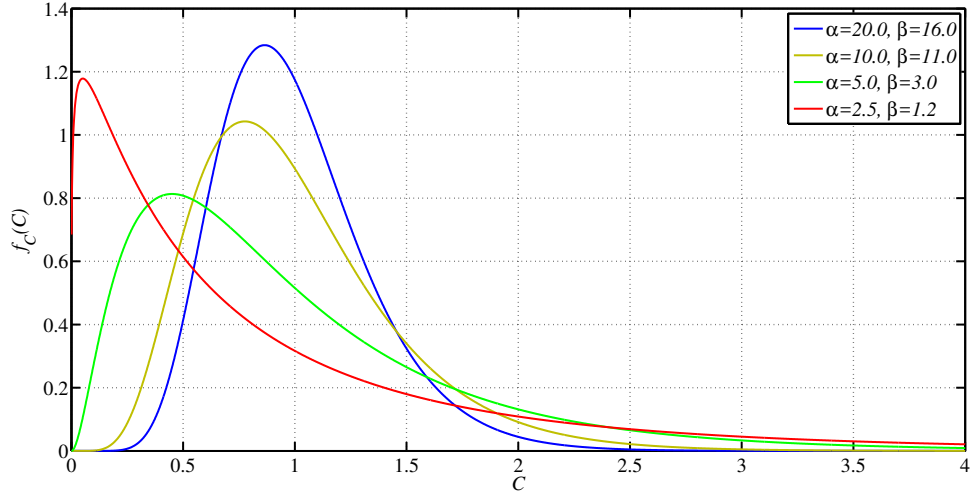


Figure 2.3 Probability Density of Gamma-Gamma Distribution.

### 2.3.3 Polarization Fluctuation

Assuming the turbulence is homogeneous and isotropic. Behaviors of an optical wave propagating through the atmosphere follow Helmholtz equation [2, 6, 38]:

$$\nabla^2 E + k^2 n^2 E + 2\nabla [E \cdot \nabla \ln(n)] = 0, \quad (2.17)$$

where  $E$  is the optical wave electric vector,  $n$  denotes the refractive-index and  $n = 1 + n_1$ .

Substituting a perturbation series for  $E$  into equation (2.17) and reserving the zero order and first order terms  $E = E_0 + E_1$ , the distorted optical wave can be expressed as:

$$\nabla^2(E_0 + E_1) + k^2(1 + n_1)^2(E_0 + E_1) + 2\nabla[(E_0 + E_1) \cdot \nabla \ln(1 + n_1)] = 0, \quad (2.18)$$

where  $|E|$  is assumed as the form of  $|n_1 E_0|$  and  $n_1 \ll 1$ . Thus, we can collate the high order terms of  $n_1$  to zero. By expanding the  $\ln(1 + n_1)$  in the power series about  $n_1$ , we can obtain:

$$\nabla^2 E_0 + k^2 E_0 = 0, \quad (2.19)$$

$$\nabla^2 E_1 + k^2 E_1 = -2k^2 n_1 E_0 - 2\nabla(E_0 \cdot \nabla n_1), \quad (2.20)$$

Assuming the incident plane wave to be linearly polarized on the X direction when propagating through the Z direction, it can be expressed as  $E_0 = A_0 e^{ikz} \vec{x}$ . The corresponding distorted component in y direction of the scattered wave can be represented by the equation:

$$\nabla^2 E_{1y} + k^2 E_{1y} = -2A_0 e^{ikz} \frac{\partial^2 n_1}{\partial y \partial x} \quad (2.21)$$

has the well-known solution [2, 6, 38]

$$E_{1y} = \frac{1}{2\pi} \int_V \frac{\partial^2 n_1(r')}{\partial y' \partial x'} A_0 e^{ikz'} \frac{e^{ik|r-r'|}}{|r-r'|} dV'. \quad (2.22)$$

If we let  $\Delta\theta = E_{1y}/E_0$  then

$$\Delta\theta = \frac{1}{2\pi} \int_V \frac{\partial^2 n_1(r')}{\partial y' \partial x'} e^{-ik(z-z')} \frac{e^{ik|r-r'|}}{|r-r'|} dV'. \quad (2.23)$$

For  $\lambda \ll l_0$ , which is a reasonable hypothesis in the optical frequency.  $l_0$  is the inner scale of the atmospheric turbulence. The optical distortion is only generated with the refractive index fluctuation within a narrow cone along with the propagating direction. The corresponding vertex angle can be calculated as  $\psi = \lambda/l_0$ . In the realistic situation, the propagating path is so much greater than the beam spot scale:

$$(z - z')^2 \gg (x - x')^2 + (y - y')^2, \quad (2.24)$$

the term  $|r - r'|$  can be reasonably approximated to the one dimensional parameter  $(z - z')$ . However, for the exponential term, the relative magnitudes described as in

equation (2.24) is not available any more. The frequency of the phase changing for  $|r - r'|$  should also be fully taken into account. Considering the zero order and the first order terms of the  $|r - r'|$  power series expansion [2, 6, 38]:

$$k|r - r'| = k(z - z') + k \frac{(x - x')^2 + (y - y')^2}{2(z - z')}. \quad (2.25)$$

The error in phase under this approximation is [6, 38]

$$k \frac{[(x - x')^2 + (y - y')^2]^2}{(z - z')^3} = \frac{k\rho^4}{(z - z')^3}. \quad (2.26)$$

where  $\rho^2 = (x - x')^2 + (y - y')^2$ . Since  $\rho \approx \psi L$ , where  $L$  denotes the transmission distance and  $\psi = \lambda/l_0$  is the vertex angle as defined previously, then the approximation of the distortion of phase in the exponential term is neglectful if:

$$L \ll \frac{l_0^4}{2\pi\lambda^3}. \quad (2.27)$$

Under these conditions the integral equation (2.23) can be simplified as [2, 6, 38]:

$$\Delta\theta(r) = \frac{1}{2\pi} \int_V \frac{\partial^2 n_1(r') e^{ik\{[(x-x')^2+(y-y')^2]/2(z-z')\}}}{\partial x' \partial y'} \frac{1}{(z - z')} dV'. \quad (2.28)$$

This expression is the exact solution to the function [2, 6, 38]:

$$\frac{\partial^2 \Delta\theta}{\partial x^2} + \frac{\partial^2 \Delta\theta}{\partial y^2} + 2ik \frac{\partial \Delta\theta}{\partial z} + 2 \frac{\partial^2 n_1}{\partial x \partial y} = 0. \quad (2.29)$$

Based on the spectral expansion,  $n_1$  can be presented as:

$$n_1(x, y, z) = n_1(z, 0, 0) + \iint_{-\infty}^{\infty} [1 - e^{i(\kappa_2 x + \kappa_3 y)}] d\nu(\kappa_2, \kappa_3, z) \quad (2.30)$$

and

$$\frac{\partial^2 n_1}{\partial x \partial y} = \iint_{-\infty}^{\infty} \kappa_2 \kappa_3 e^{i(\kappa_2 x + \kappa_3 y)} d\nu(\kappa_2, \kappa_3, z) \quad (2.31)$$

Similarly  $\Delta\theta$  can be represented as

$$\Delta\theta = \Delta\theta(z, 0, 0) + \iint_{-\infty}^{\infty} [1 - e^{i(\kappa_2 x + \kappa_3 y)}] d\alpha(\kappa_2, \kappa_3, z). \quad (2.32)$$

Substituting the equation (2.31) and (2.32) into (2.29) yields [2, 6, 38]:

$$\begin{aligned} & \iint_{-\infty}^{\infty} (\kappa_2^2 + \kappa_3^2) e^{i(\kappa_2 x + \kappa_3 y)} d\alpha(\kappa_2, \kappa_3, z) + 2ik \frac{\partial \Delta\theta}{\partial z}(z, 0, 0) \\ & + 2ik \iint_{-\infty}^{\infty} [1 - e^{i(\kappa_2 x + \kappa_3 y)}] \frac{\partial}{\partial z} [d\alpha(\kappa_2, \kappa_3, z)] \\ & + 2 \iint_{-\infty}^{\infty} \kappa_2 \kappa_3 [e^{i(\kappa_2 x + \kappa_3 y)}] d\nu(\kappa_2, \kappa_3, z) = 0. \end{aligned} \quad (2.33)$$

Letting  $x=y=0$  in (2.33) and subtracting this from (2.33) gives for the relation between the random amplitudes  $d\alpha$  and  $d\nu$ ,

$$2ik \frac{\partial}{\partial z} [d\alpha(\kappa_2, \kappa_3, z)] - (\kappa_2^2 + \kappa_3^2) d\alpha(\kappa_2, \kappa_3, z) - 2\kappa_2\kappa_3 d\nu(\kappa_2, \kappa_3, z) = 0. \quad (2.34)$$

The solution of (2.34) is:

$$d\alpha(\kappa_2, \kappa_3, z) = -i \frac{\kappa_2\kappa_3}{k} \int_0^z dz' e^{-(i/2k)[(\kappa_2^2 + \kappa_3^2)(z-z')]} d\nu(\kappa_2, \kappa_3, z'). \quad (2.35)$$

In order to obtain the spectral function of  $\Delta\theta$ , we can average the product term of the spectral amplitude of  $\Delta\theta$  and the corresponding complex conjugate [2, 6, 38]:

$$\begin{aligned} & \langle d\alpha(\kappa_2, \kappa_3, z) d\alpha^*(\kappa_2', \kappa_3', z) \rangle \\ &= \frac{\kappa_2\kappa_2'\kappa_3\kappa_3'}{k^2} \int_0^z dz' \int_0^z dz'' e^{-(i/2k)[(\kappa_2^2 + \kappa_3^2)(z-z')]} \\ & \cdot e^{(i/2k)[(\kappa_2'^2 + \kappa_3'^2)(z-z'')]} \langle d\nu(\kappa_2, \kappa_3, z') d\nu^*(\kappa_2', \kappa_3', z'') \rangle. \end{aligned} \quad (2.36)$$

Based on the spectral expansion theory, we know that [2, 6, 38]

$$\begin{aligned} & \langle d\alpha(\kappa_2, \kappa_3, z) d\alpha^*(\kappa_2', \kappa_3', z) \rangle \\ &= \delta(\kappa_2 - \kappa_2') \delta(\kappa_3 - \kappa_3') S_{\Delta\theta}(\kappa_2, \kappa_3, 0) d\kappa_2 d\kappa_2' d\kappa_3 d\kappa_3' \end{aligned} \quad (2.37)$$

where  $S_{\Delta\theta}$  is the two dimensional spectral density of the correlation equation for describing the distortion of  $\Delta\theta$  in a certain  $x-y$  plane and  $S_N$  is the two dimensional spectral density for describing the fluctuation of the refractive index. Substituting (2.36) into (2.35) and:

$$S_{\Delta\theta}(\kappa_2, \kappa_3, 0) = \frac{\kappa_2^2\kappa_3^2}{k^2} \int_0^z dz' \int_0^z dz'' S_N(\kappa_2, \kappa_3, z' - z'') \cdot e^{(i/2k)[(\kappa_2^2 + \kappa_3^2)(z' - z'')]} \quad (2.38)$$

Letting  $z' - z'' = \xi$  and  $2\eta = z' + z''$ . Considering the upper bound on  $z$  to be  $L$ . Then integrates the  $\eta$  and we can obtain that:

$$S_{\Delta\theta}(\kappa_2, \kappa_3, 0) = \frac{2\kappa_2^2\kappa_3^2}{k^2} \int_0^z d\xi (z - \xi) S_N(\kappa_2, \kappa_3, \xi) \cdot \cos \left[ \frac{(\kappa_2^2 + \kappa_3^2)\xi}{2k} \right]. \quad (2.39)$$

Since the laser beam is natural narrow, the function  $S_N(\kappa_2, \kappa_3, 0)$  usually falls to zero very fast as  $\kappa\xi \geq 1$ , we have [2, 6, 38]:

$$S_{\Delta\theta}(\kappa_2, \kappa_3, 0) = \frac{2\kappa_2^2\kappa_3^2 z}{k^2} \int_0^z d\xi S_N(\kappa_2, \kappa_3, \xi) \cdot \cos \left[ \frac{(\kappa_2^2 + \kappa_3^2)\xi}{2k} \right]. \quad (2.40)$$

Since the function  $S_N(\kappa_2, \kappa_3, 0)$  usually falls to zero very fast as  $\kappa\xi \geq 1$  where  $\kappa = \sqrt{\kappa_2^2 + \kappa_3^2}$ . Under this situation  $(\kappa_2^2 + \kappa_3^2)\xi/2k \geq \kappa/2k$ . The optical frequency is

extremely high, therefore the  $\lambda \ll l_0$ . Letting  $\kappa_{max}$  to be the largest wave number with which value  $S_N$  is non-zero and  $l_0 \approx 1/\kappa_{max}$ , we can obtain that  $l/k \ll 1/\kappa_{max}$ . If  $\kappa_{max} \ll k$ , then  $(\kappa_2^2 + \kappa_3^2)\xi/2k \ll 1$  and  $\cos(\kappa_2^2 + \kappa_3^2)\xi/2k \rightarrow 1$  in the efficient area of integral equation. Thus (2.40) can be simplified to [2, 6, 38]:

$$S_{\Delta\theta}(\kappa_2, \kappa_3, 0) = \frac{2\kappa_2^2\kappa_3^2L}{k^2} \int_0^L S_N(\kappa_2, \kappa_3, \xi)d\xi \quad (2.41)$$

where  $L$  is defined as the observation position of  $x$ .

Since  $S_N$  falls to zero very fast, we can rearrange the integration area to the infinity without influence the calculation result.

$$\int_0^\infty S_N(\kappa_2, \kappa_3, \xi)d\xi = \pi\Phi_N(\kappa_2, \kappa_3, 0) \quad (2.42)$$

where  $\Phi_N(\kappa)$  is the three dimensional spectral density of describing the index of refraction fluctuations, the spectral density of the polarization distortion can be approximate to [2, 6, 38]:

$$S_{\Delta\theta}(\kappa_2, \kappa_3, 0) = \frac{2\pi L}{k^2} \kappa_2^2 \kappa_3^2 \Phi_N(\kappa_2, \kappa_3, 0). \quad (2.43)$$

This kind of expression can be seen as a two dimensional Fourier analysis in the  $x - y$  plane, the correlation function of the distortions of  $\Delta\theta = E_{1y}/E_0$  [2, 6, 38]:

$$R_{\Delta\theta}(\rho) = \iint_{-\infty}^{\infty} S_{\Delta\theta}(\kappa_2, \kappa_3, 0) \cos(\kappa \cdot \rho) d\kappa_2 d\kappa_3. \quad (2.44)$$

The variance of  $\Delta\theta$  can be calculated from (2.44) by letting  $\rho \rightarrow 0$ , then  $R_{\Delta\theta}(0) = \langle |\Delta\theta|^2 \rangle = \langle |E_{1y}/E_0|^2 \rangle$ .

In this analysis, a well-known Kolmogorov spectrum is adopted [2, 6]:

$$\Phi_n(\kappa) = 0.033C_n^2\kappa^{-11/3}, l_0 \leq \kappa \leq L_0, \quad (2.45)$$

where  $\kappa = (\kappa_2^2 + \kappa_3^2)^{1/2}$  is the scalar wave number, take equation (2.45) into equation (2.44) and the variance of  $\Delta\theta$  can be modified as follow:

$$\sigma_{\Delta\theta}^2 = \frac{0.007C_n^2\pi L}{k^2} \left( l_0^{-\frac{7}{3}} - L_0^{-\frac{7}{3}} \right). \quad (2.46)$$

Considering  $\Delta\theta$  follows a zero-mean Gaussian distribution, and the PDF of  $\Delta\theta$  can be indicated as:

$$f_{\Delta\theta}(\Delta\theta) = \frac{1}{\sqrt{2\pi\sigma_{\Delta\theta}^2}} \exp\left(-\frac{\Delta\theta^2}{2\sigma_{\Delta\theta}^2}\right). \quad (2.47)$$

If giving an estimation to equation (2.20), taking  $l_0 = 1mm$ ,  $L_0 = 10m$ ,  $L = 2km$ , the optical wavelength  $\lambda = 1550nm$ , and  $C_n^2$  is from  $10^{-17}m^{-2/3}$  to  $10^{-13}m^{-2/3}$ , we can get the magnitude of  $\sigma_{\Delta\theta}^2$  is from  $10^{-22}rad^2$  up to  $10^{-18}rad^2$ . The variance has a very small value which means the polarization state of an optical wave in the atmosphere have a remarkable stability [2,6]. In Figure 2.4, we present the polarization fluctuation distribution under different turbulence strength (weak, moderate and strong).

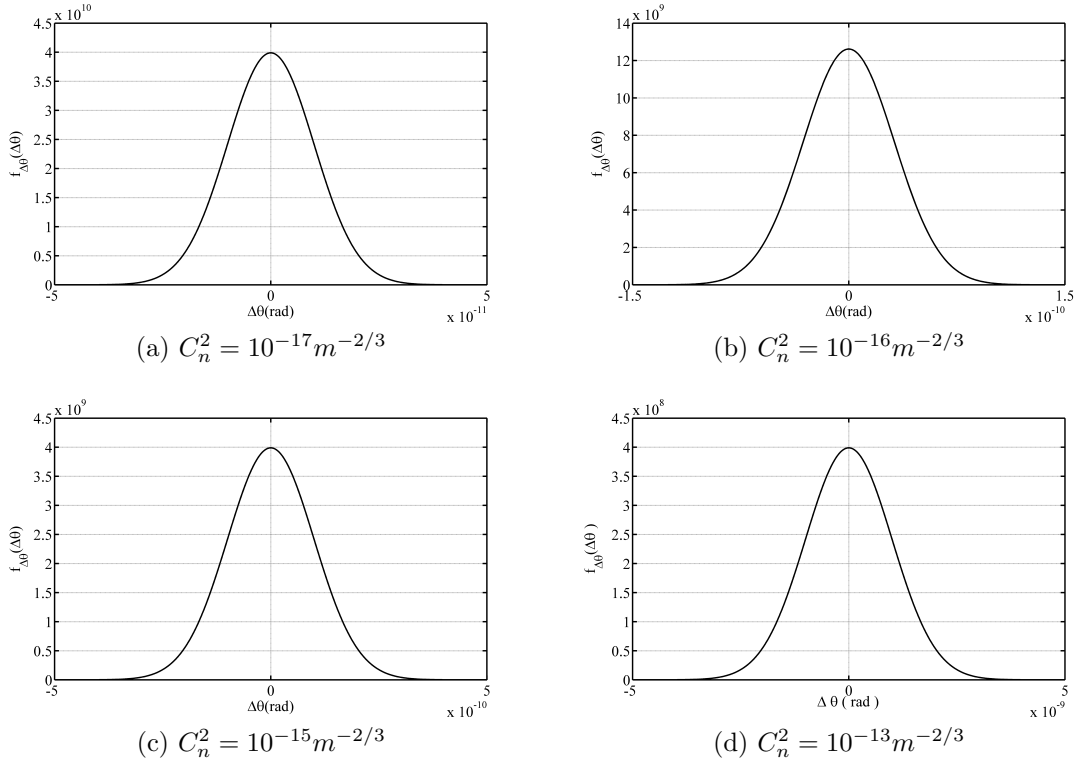


Figure 2.4 Linear Polarization Fluctuation Distribution under Different Turbulence Strength. [2]

We can find that: firstly, the polarization distortion  $\Delta\theta$  is increasing with the turbulence strength; secondly, even in the extremely strong turbulence ( $C_n^2 = 10^{-13}m^{-2/3}$ ), the possibility of the polarization distortion becoming greater than  $5 \times 10^{-9}$  rad is about zero. That inspires us, instead of two orthogonal polarization states, to investigate a consecutive polarization modulation scheme that can take the utmost of the polarization state stability.

# Chapter 3

## Related Techniques

### 3.1 OFDM

The term, Orthogonal Frequency Division Multiplexing, known as OFDM was first appeared in 1966 by the seminal paper of Chang [3, 4]. The research of OFDM was not popular until 1990s. With the prosperities of very large-scale integrated (VLSI) CMOS chips and digital broadband developing, bandwidth limit and complex computation system was no more a problem. Since 1995, OFDM has been widely applied in communication standards: ITU-T G. hn; IEEE 802.11a, g, n, ac; IEEE 802.15.3a; IEEE 802.16e; IEEE 802.20. It is also known as the core technology of the long-term evolution (LTE) which is a representative standard for the fourth generation mobile communications. Optical OFDM was first mentioned in 1996 [5, 6, 32, 48, 73]. In 2001, Dixon et al. proposed the advantages of OFDM in against optical channel dispersion and time varying environment in his paper [3, 4]. In this master thesis we used OFDM as modulation to mitigate the channel fading in atmospheric turbulence channel.

#### 3.1.1 OFDM Signal Description

OFDM belongs to a broader class named multicarrier modulation (MCM). The modulation structure of MCM systems associate with the equation model below is shown in Figure 3.1. In Figure 3.1, the IQ modulator/demodulator is a typical expression of the complex multiplier which is widely utilized in the MCM systems. The mathematic expression for MCM signal  $s(t)$  is given as:

$$s(t) = \sum_{m=-\infty}^{+\infty} \sum_{k=1}^N X_{mk} s_k(t - mT_s), \quad (3.1)$$

where

$$s_k(t) = \delta(t) \cdot \exp(j2\pi f_k t), \quad (3.2)$$

$$\delta(t) = \begin{cases} 1, & (0 < t < T_s) \\ 0, & (t < 0, t > T_s) \end{cases}, \quad (3.3)$$

where  $X_{mk}$  represents the  $m$ th symbol on the  $k$ th subcarrier.  $s_k$  denotes the waveform of the  $k$ th subcarrier.  $f_k$  is the frequency of the  $k$ th subcarrier.  $N$  denotes the total amount of subcarriers.  $T_s$  denotes the symbol period and  $\delta(t)$  is the pulse shaping function.

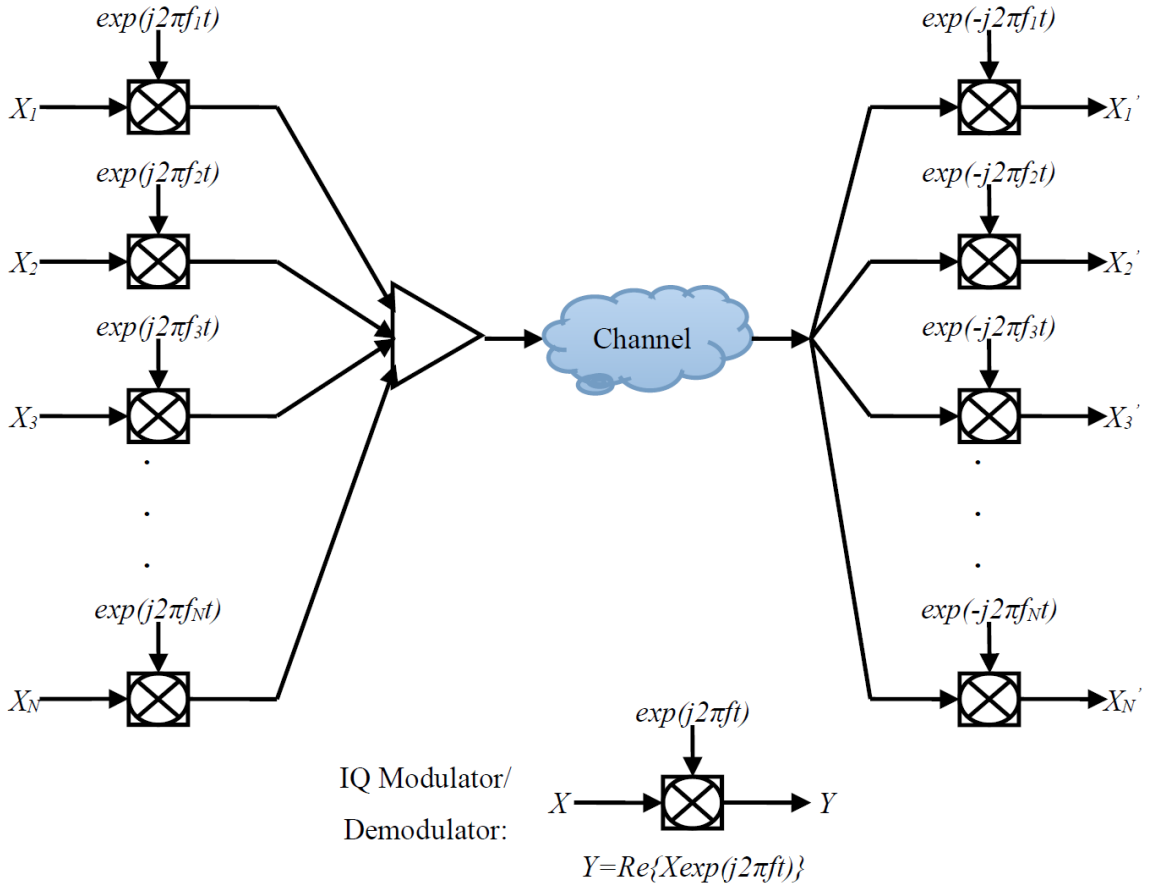


Figure 3.1 Structure for An OFDM Modulation/Demodulation System. [3, 4]

A valid detector should contain a bunch of correlators that match the relevant subcarrier waveform or filters match the relevant subcarrier frequency as shown in Figure 3.1. When the received signal is output from the relevant filter, the expression of the information symbol  $X'_{mk}$  is given as:

$$X'_{mk} = \frac{1}{T_s} \int_0^{T_s} r(t - mT_s) s_k^* dt = \frac{1}{T_s} \int_0^{T_s} r(t - mT_s) \exp(-j2\pi f_k t) dt, \quad (3.4)$$

where the received  $m$ th time domain signal on the  $k$ th subcarrier denoted by the symbol  $r(\cdot)$ .

The typical MCM technology applies subcarriers with non-overlapped frequency and the related transceiver systems should be implemented with huge numbers of oscillators and filters at not only the transmitter but also the receiver terminations [3,5]. The most serious problem of MCM technique may be that it demands too much bandwidth resources. The reason is in the filters and oscillators designment we have to leave enough channel spacing which is a several-fold of the symbol rate. Thus, the spectral efficiency will be greatly limited. The OFDM approach, using the orthogonal overlapped subcarriers to transmit signals, has been proposed as a solution to improve the spectral usage rate [3,4]. Because the frequency of subcarriers is overlapped, bandwidth efficiency would be increased sharply and because the subcarriers are orthogonal, the design of filters and oscillators would be cost-effective. In one symbol period, the condition of two separate subcarriers keeping orthogonal is:

$$\int_0^{T_s} \cos(2\pi f_i t + \phi_i) \cdot \cos(2\pi f_j t + \phi_j) dt = 0, \quad (3.5)$$

where  $f_i$  and  $f_j$  are the frequency of the  $i$ th and  $j$ th subcarriers.  $\phi_i$  and  $\phi_j$  represent initial phase of the  $i$ th and  $j$ th subcarriers. Function (3.5) can be written as:

$$\begin{aligned} & \frac{1}{2} \int_0^{T_s} \cos[2\pi(f_i - f_j)t + \phi_i - \phi_j] dt + \\ & \frac{1}{2} \int_0^{T_s} \cos[2\pi(f_i + f_j)t + \phi_i + \phi_j] dt = 0. \end{aligned} \quad (3.6)$$

Integrate equation (3.6), the result is:

$$\begin{aligned} & \frac{\sin[2\pi(f_i + f_j)T_s + \phi_i + \phi_j]}{2\pi(f_i + f_j)} - \frac{\sin(\phi_i + \phi_j)}{2\pi(f_i + f_j)} + \\ & \frac{\sin[2\pi(f_i - f_j)T_s + \phi_i - \phi_j]}{2\pi(f_i - f_j)} - \frac{\sin(\phi_i - \phi_j)}{2\pi(f_i - f_j)} = 0. \end{aligned} \quad (3.7)$$

The condition to satisfied function (3.7) in different  $\phi_i$  and  $\phi_j$  is:

$$\Delta f = f_i - f_j = n/T_s \quad \text{or} \quad \Delta T = \frac{1}{\Delta f} = \frac{T_s}{n}. \quad (3.8)$$

Where  $n$  is integer. Equation (3.8) gives us a conception that the cosine period of OFDM subcarriers should be  $1/n$  of one symbol period. In Figure 3.2, we present seven OFDM subcarriers in one symbol period  $T_s$ .

In Figure 3.3, we present the spectrum of the seven OFDM subcarriers as shown in Figure 3.2. We can find that in frequency domain, for a certain subcarrier  $k$ , it has a central frequency  $f_k$ , where others are zero. Thus the difficulties in filters and oscillators design would be reduced.

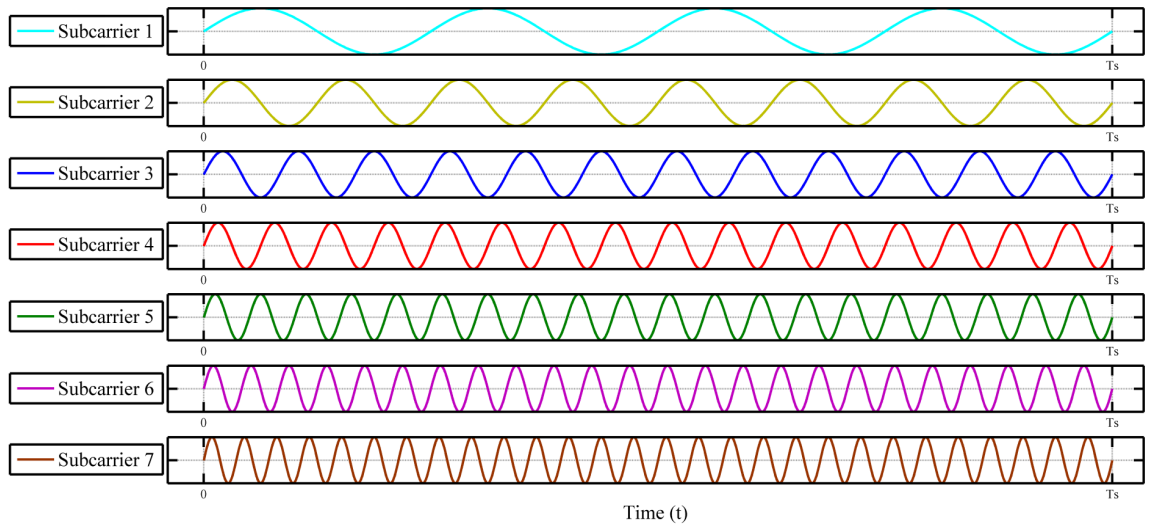


Figure 3.2 OFDM Subcarriers in Time Domain.

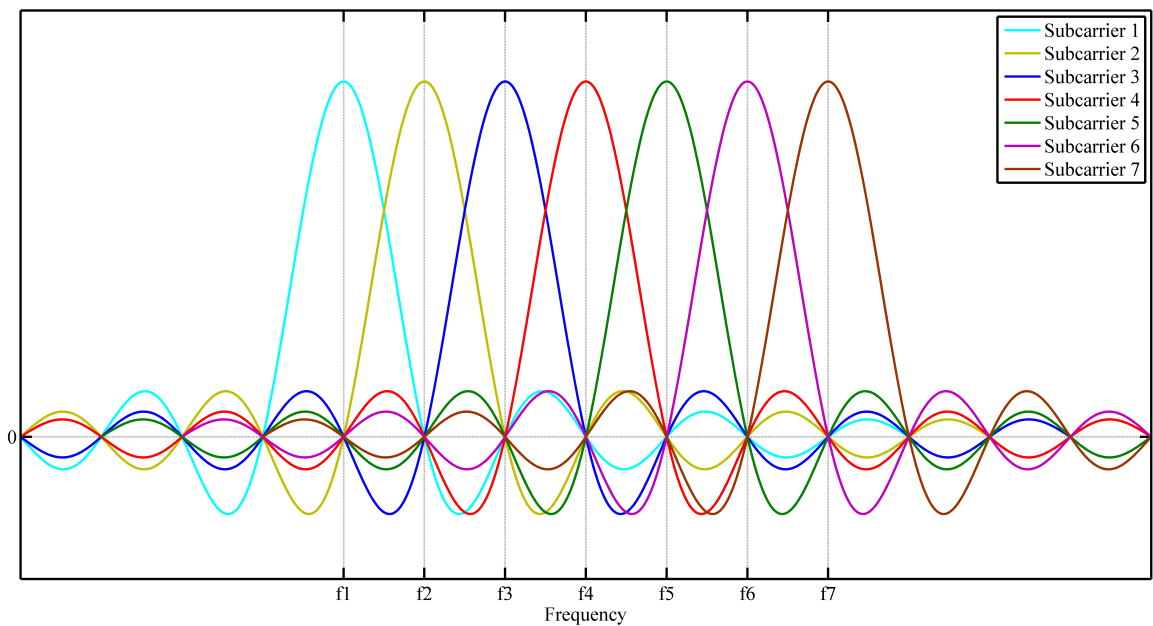


Figure 3.3 Spectrum of OFDM Subcarriers.

### 3.1.2 Discrete Fourier Transform

In OFDM technology, the information is carried on a large number of subcarriers. In this case, the effect of transmission channel on each subcarrier could be modeled as a flat channel. In this situation, the system would be consisted with an extremely complex architecture involving many oscillators and filters at both transmitting and

receiving terminals. By the work of Weinstein and Ebert, the OFDM modulation needs an Inverse Discrete Fourier Transform (IDFT). And the OFDM demodulation could be realized by implement Discrete Fourier Transform (DFT) [3]. If we concentrate our attention on a certain OFDM symbol, looking back to the Equation (3.1), assuming that we sample  $s(t)$  at every interval of  $T_s/N$ . The  $m$ th sample of  $s(t)$  from Equation (3.1) should be written as:

$$s_m = \sum_{k=1}^N NX_k \cdot \exp \left[ j2\pi f_k \cdot \frac{(m-1)T_s}{N} \right]. \quad (3.9)$$

With the orthogonality condition of Equation (3.8) and the convention that:

$$f_k = \frac{k-1}{T_s}, \quad (3.10)$$

and substituting Equation (3.10) into Equation (3.9), we have:

$$s_m = \sum_{k=1}^N NX_k \cdot \exp \left[ j2\pi \cdot \frac{(k-1)(m-1)}{N} \right] = F^{-1}(X_k). \quad (3.11)$$

Where  $F(\cdot)$  is the Fourier Transform. Similarly, in the receiving terminal, the received signal  $X'_k$  is:

$$X'_k = F(r_m). \quad (3.12)$$

Where  $r_m$  is the sampled signal with the interval  $T_s/N$ .

In terms of Equation (3.11) and (3.12), it is clear that the discrete value of the transmitted OFDM signal  $s(t)$  can be represented by an  $N$ -point IDFT of the information symbol  $X_k$ , and the received information symbol  $X'_k$  can be seen as an  $N$ -point DFT of the receive signal. The advantages for DFT/IDFT introduced into OFDM are [3]:

1. FFT/IFFT is much more common and higher efficient algorithm methods in the implementation of DFT/IDFT. When it is used into processing Equation (3.11) and Equation (3.12), the number of complex multiplication calculation could be reduced from  $N^2$  to  $0.5 \cdot N \cdot \log_2(N)$ , which is approximately linear with the number of subcarriers  $N$  [4].
2. When DFT/IDFT implemented in OFDM, since the signal over orthogonal subcarriers can be modulated and demodulated just with IFFT and FFT algorithm, the system architecture can be simplified by saving large numbers of complex oscillators and filters [3, 4].

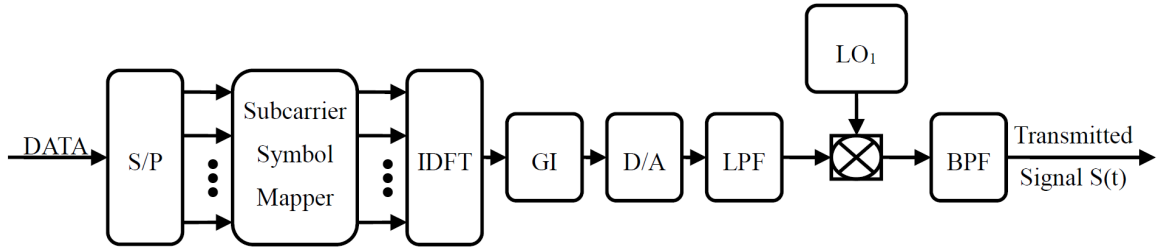


Figure 3.4 Diagram for OFDM Transmitter. [3, 4]

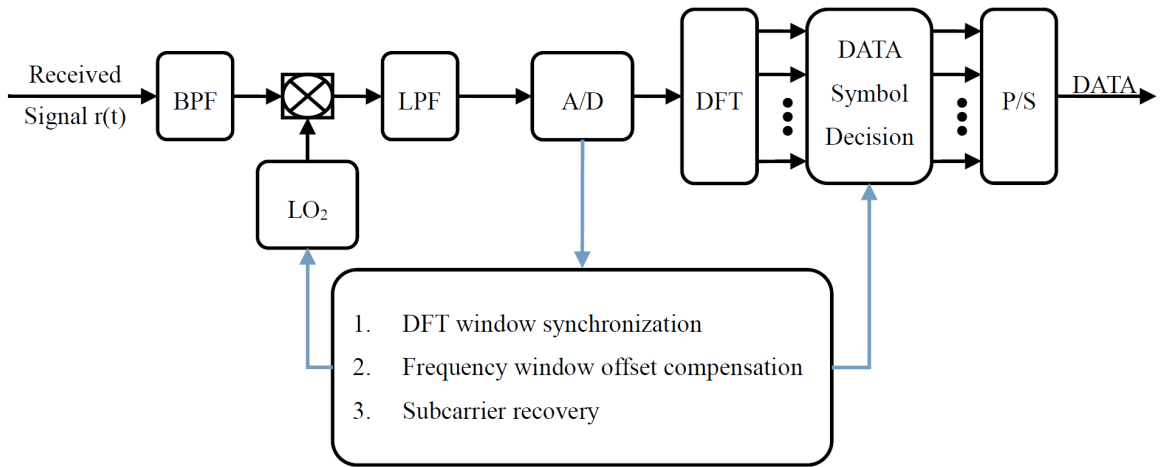


Figure 3.5 Diagram for OFDM Receiver. [3, 4]

Conceptions of the OFDM transceiver architectures are shown in Figure 3.4 and Figure 3.5. D/A is the abbreviation of the Digital-to-Analog Converter. It is used to convert the discrete signal  $s_m$  to the analog signal  $s(t)$ . A/D is the abbreviation of the Analog-to-Digital Converter. It is used to convert the received analog signal  $r(t)$  to the discrete signal  $r_m$ . S/P and P/S are Serial-to-Parallel and Parallel-to-Serial Converter, GI is Guard Time Insertion, LPF is Low Pass Filter, BPF is Band Pass Filter, LO presents Local Oscillator.

At the transmit terminal, the form of input data is serial bits. Firstly, serial data is processed by Serial-to-Parallel Converter and converted into a lot of parallel data pipes. Each data pipe is mapped into certain information on the corresponding subcarrier for one OFDM symbol. Then the data would be processed by IDFT and converted to the digital time domain signal. In order to reduce the inter-symbol-interference (ISI) caused by channel dispersion, a guard interval should be inserted

into the real-time signal. The baseband real-time signal can be modulated on a proper subcarrier by an IQ modulator. In the receiving terminal, the OFDM signal will be downconverted to baseband by an IQ demodulator. The analog signal would be processed by an A/D Converter and converted into digital signal. Then perform DFT to the digital signal and the data is converted into frequency domain. After demodulated by the Data Symbol Decision device and Parallel-to-Serial Converter, the signal would be recovered.

### 3.1.3 Cyclic Prefix

One of the most significant technologies for OFDM is the cyclic prefix insertion. Firstly, if we consider two consecutive OFDM symbols that transmitted on a dispersive channel with a delay spread. For simplicity, each OFDM symbol is carried by only two subcarriers with the fast delay and slow delay spread at  $t_d$ , which called "fast subcarrier" and "slow subcarrier", respectively [3, 4]. Figure 3.6 shows that one

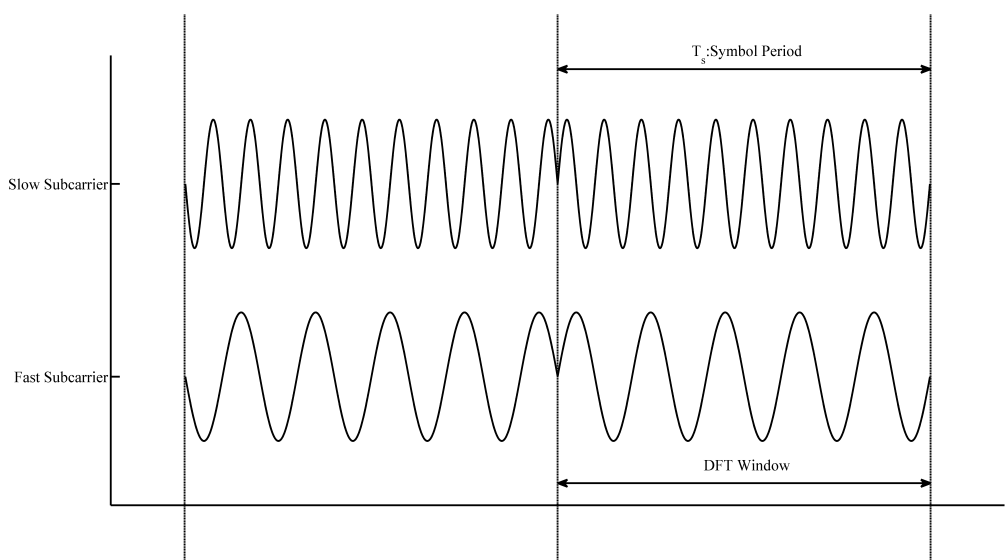


Figure 3.6 Transmitted OFDM Signal without Cyclic Prefix. [3, 4]

certain OFDM symbol. Let the fast subcarrier and the slow subcarrier carry the identical symbol, respectively. At the transmitter, the two symbols are transmitted, simultaneously. When received the two symbols, assuming that the slow subcarrier has a  $t_d$  delay to the fast subcarrier, as shown in Figure 3.7. If the DFT window contains the entire fast subcarrier OFDM symbol, part of the slow subcarrier OFDM symbol will stay out of the DFT window boundary. The interference is therefore

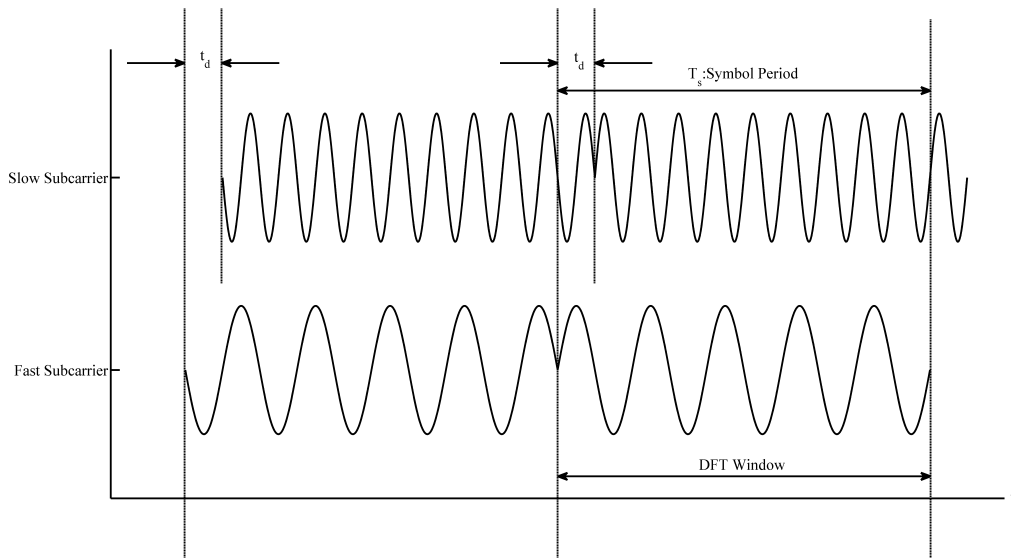


Figure 3.7 Received OFDM Signal without Cyclic Prefix. [3, 4]

generated between the neighboring OFDM symbols. This effects caused by the channel dispersion is called ISI. What's more, the inter-carrier interference (ICI) effects appear after the subcarriers orthogonality misleading caused by the incomplete of the slow subcarrier OFDM symbol waveform in the DFT window [3, 4].

Cyclic prefix is deemed as a solution to ISI and ICI brought by he channel dispersion [3, 4]. The principle of this method is to add a cyclic waveform extension, denoted by  $\Delta G$ , in front of each symbol as a guard interval. As shown in Figure 3.8,

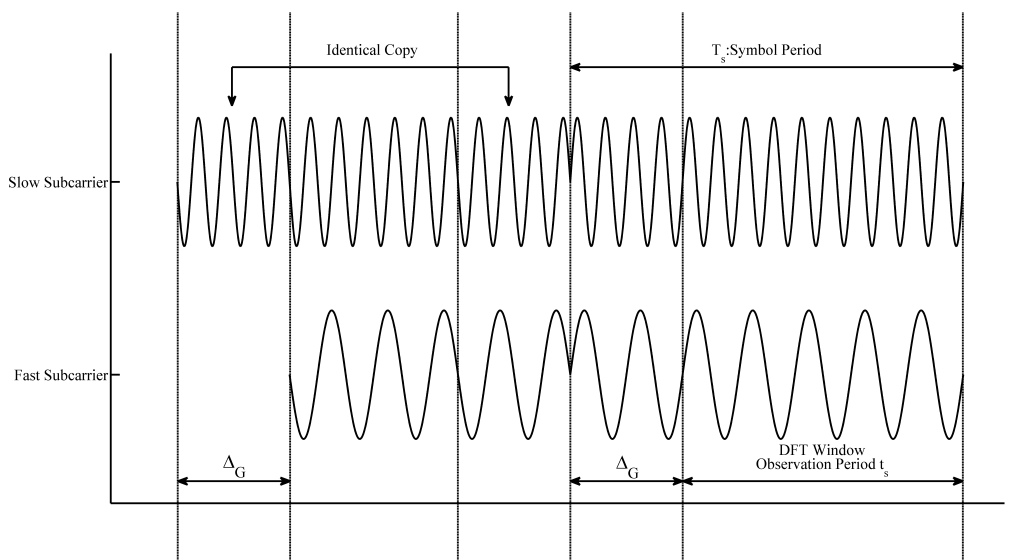


Figure 3.8 Transmitted OFDM Signal with Cyclic Prefix. [3, 4]

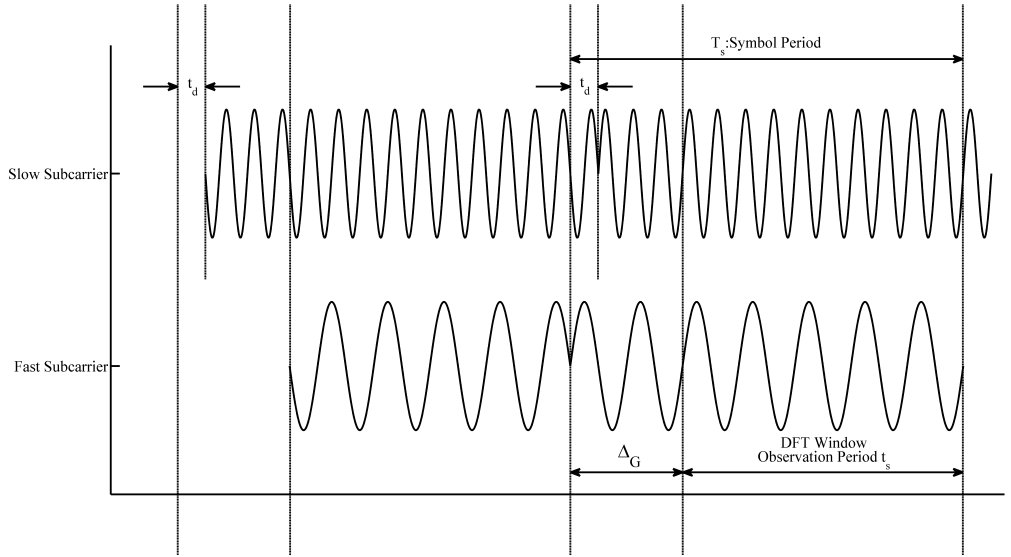


Figure 3.9 Received OFDM Signal with Cyclic Prefix. [3,4]

we shift an identical copy of the waveform in the end part of DFT window forward by a whole observation period ( $t_s$ ) as the guard interval. In Figure 3.9, the OFDM signal is received with cyclic prefix. When the received signals in Figure 3.9 have suffered the identical channel dispersion as the signals shown in Figure 3.7 and the DFT window has covered the entire fast subcarrier OFDM symbol, from Figure 3.9 we can find that the intact slow subcarrier OFDM symbol is still contained within the DFT window. A part of the guard interval has been merged into the DFT window and has taken the place of the identical version which has been delayed by the channel dispersion. In this condition, the received slow subcarrier OFDM symbol is an identical copy of the transmitted slow subcarrier OFDM symbol even suffered a phase shift distortion. This phase shift distortion can be eliminated by the channel estimation algorithm and corrected by the symbol decision. Thus, we can obtain an essential condition to refrain ISI in OFDM communication, given by:

$$t_d < \Delta_G. \quad (3.13)$$

It is clear that to revise the OFDM symbols, there are two significant problems that need to be solved [3,4]:

1. How to build a DFT window synchronization procedure, in order to select an appropriate DFT window.
2. How to build a channel estimation procedure or a subcarrier recovery procedure to deal with the phase shift for each subcarrier.

These two problems are hot topics in OFDM research. The two signal processing procedures are actively discussed in a lot of articles [3–6, 32, 48, 73].

A concise method to process the cyclic prefix may be to describe the received signal in the identical expression as the transmitted signal  $s(t)$  in equation (3.1) and to expand the pulse shape expression described in equation (3.3) to the guard interval, written as:

$$\delta(t) = \begin{cases} 1, & (-\Delta_G < t \leq t_s) \\ 0, & (t \leq -\Delta_G, t > t_s) \end{cases}. \quad (3.14)$$

The utilization of the cyclic prefix brought another benefit which is the cyclic prefix waveforms can be seen as signboards contained by the parallel OFDM symbols. It is quite useful in signal synchronizing.

### 3.1.4 Spectral Efficiency

In DDO-OFDM systems, the result of OFDM implemented in RF spectrum can not be used directly. Therefore, in order to implement these results in analyzing the optical spectral efficiency, we change our motivation to the spectral efficiency of optical spectrum for CO-OFDM technology [3]. Assume the amount of subcarriers is  $N$ , the symbol period for each OFDM symbol is denoted by  $T_s$  and the symbols are modulated on all subcarriers by the CO-OFDM technology. Thus, the symbol rate can be expressed as:

$$R = \frac{N}{T_s}. \quad (3.15)$$

Considering the wavelength division multiplex (WDM) channel, each wavelength channel with CO-OFDM modulation, we are concentrated on the optical spectrum. Defined the first value zero in the optical spectrum as the boundary partitioning different frequency channels. The bandwidth  $B_{OFDM}$  can be calculated as:

$$B_{OFDM} = \frac{2}{T_s} + \frac{N-1}{t_s}, \quad (3.16)$$

where  $t_s$  denotes the period of DFT window. In the real systems, the value of  $N$  is quite large. Therefore, the total bandwidth efficiency  $B_e$  can be estimated as:

$$B_e = \frac{2R}{B_{OFDM}} = \frac{2t_s}{T_s}. \quad (3.17)$$

### 3.1.5 Real and Complex components of an OFDM Signal

In the starting and the ending stage of a digital processing, the essence of OFDM signals is represented as the modality of the complex variables. However, during

the transmitting stage the OFDM signal should be modulated as a real variable signal. When dealing with this complex value along with real value mutual conversion, the frequency upconversion and the frequency downconversion processing, in another word, the baseband along with the passband conversion is necessary. A complex multiplier (mixer), as well as, the combination of IQ modems can realize this kind of conversion. The upconversion procedure can be fully expressed by an mathematic model as:

$$S_C(t) = \Re [S(t) \exp j2\pi f_c t] = \Re [S(t)] \cdot \cos(2\pi f_c t) - \Im [S(t)] \cdot \sin(2\pi f_c t). \quad (3.18)$$

Where  $S_C(t)$  is the real variable signal modulated on the passband at the central frequency of  $f_C$ ,  $S(t)$  is the complex variable signal modulated on the baseband,  $\Re$  denotes the real component and  $\Im$  indicates the imaginary component of the complex variable. Normally, the IQ modulator as shown in Figure 3.1 can be consisted of a pair of LOs with a 90-degree difference as shown in Figure 3.10.

The downconversion of real variable to complex variable of an OFDM signal could be designed as a reverse procedure of the upconversion. The schematic diagram of reversing the baseband signal  $X$  to the passband signal  $Y$  is shown in Figure 3.10. The high developed silicon technique is able to design a 60 GHz data rate mixed-signal integrated circuit (IC) [3–6, 32, 48, 73].

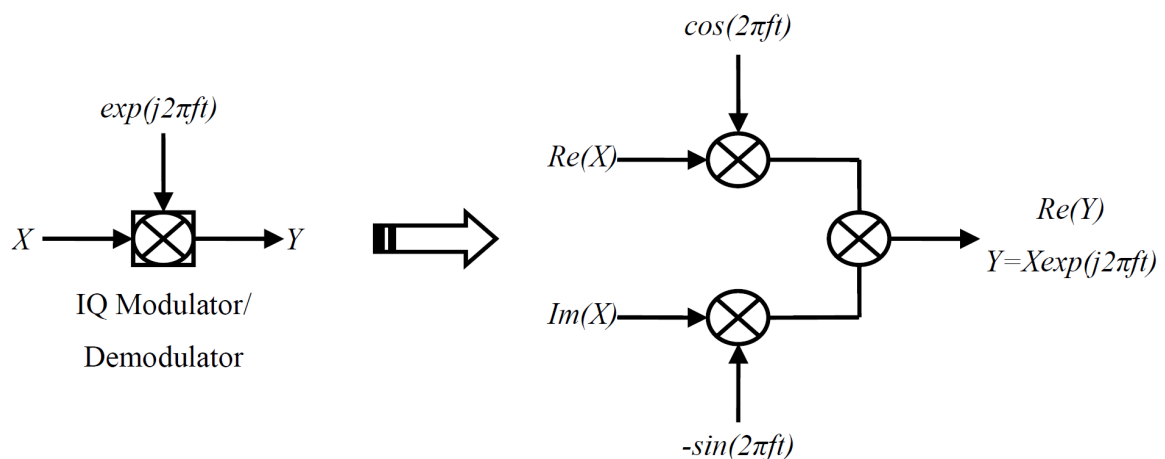


Figure 3.10 Diagram of The IQ Modulator for Complex Signals. [3, 4]

Discrete multi-tone (DMT) is one of the interesting variations of OFDM modulation [3, 4]. Its advantage is using just real variable signals even at the baseband.

It could be achieved by constraining the special condition that the OFDM signals should be must modulated as in equation (3.11):

$$X_{N-k} = X_k^*. \quad (3.19)$$

That means the OFDM information symbols for the subcarriers  $k$  and  $N-k$  are complex conjugate to each other. In this condition,  $s_m$  in Equation (3.11) is calculated as a real variable signal. Because both transmitted and received signals are real value, IQ modulation and demodulation are not necessary. The IC design become much simpler and more cost-effective, consequently. Therefore, DMT technique has been extensively used in the practical digital subscriber line (DSL) instruments.

## 3.2 Aperture Average

If the receiving aperture in an FSO communication system is smaller than the correlation width of the irradiance fluctuations, then the receiver behaviors can be seen as a “point aperture”. However, with the size of receiving aperture increasing beyond the irradiance correlation width, the receiver would detect several correlation patches and the scintillation at the detector in the image plane would be decrease. This effect is defined as aperture averaging. It is intentionally used in the detector of communication systems to reduce scintillation and, consequently, improve the mean signal-to-noise ratio (SNR) [1, 5, 29, 32, 48, 67, 80, 81].

The decrease in scintillation associated with increasing telescope collecting area had been recognized in early astronomical measurements made in the 1950s [29, 67, 80, 81]. These same measurements showed that scintillation reduction through aperture averaging would cause a shift of the relative frequency content of the irradiance power spectrum toward lower frequenciesnamely, averaging out the fastest fluctuations. More recently, aperture averaging effects have been studied in the context of laser beam propagation through atmospheric turbulence [1, 5, 29, 32, 48, 67, 80, 81].

The reduction in scintillation due to aperture averaging can be obtained from a definition of a ratio of the received optical power fluctuation when using one large size aperture over the received optical intensity fluctuations when using a point aperture. The normalized variance to describe the received optical intensity fluctuations is the same as the flux variance of irradiance fluctuations defined by [1]:

$$\begin{aligned} \sigma_I^2(D) &= \frac{\langle P^2 \rangle - \langle P \rangle^2}{\langle P \rangle^2} \\ &= \frac{16}{\pi D^2} \int_0^D \rho B_I(\rho, L) \left[ \arccos\left(\frac{\rho}{D}\right) - \frac{\rho}{D} \sqrt{1 - \left(\frac{\rho}{D}\right)^2} \right] d\rho, \end{aligned} \quad (3.20)$$

where  $P$  is the received optical power,  $D$  is the (hard) aperture diameter of a circular aperture,  $B_I(\rho, L)$  is the irradiance covariance in the receiving aperture. The change of variable  $x = \rho/L$  permits us to rewrite Equation (3.20) as:

$$\sigma_I^2(D) = \frac{16}{\pi} \int_0^1 x B_I(xD, L) \left[ \arccos(x) - x\sqrt{1-x^2} \right] dx \quad (3.21)$$

The aperture averaging factor (or coefficient)  $A$  for a circular aperture of diameter  $D$  is defined by the ratio  $A = \sigma_I^2(D)/\sigma_I^2(0)$ , where  $\sigma_I^2(0) = B_I(0, L)$  is the scintillation index for a point aperture ( $D = 0$ ). In this case we write:

$$A = \frac{\sigma_I^2(D)}{\sigma_I^2(0)} = \frac{16}{\pi} \int_0^1 \frac{x B_I(\rho, L)}{B_I(0, L)} \left[ \arccos(x) - x\sqrt{1-x^2} \right] dx \quad (3.22)$$

Define  $b_I(\rho, L) = B_I(\rho, L)/B_I(0, L)$  is the normalized covariance function. And Equation (3.22) can be rewritten as:

$$A = \frac{\sigma_I^2(D)}{\sigma_I^2(0)} = \frac{16}{\pi} \int_0^1 x b_I(\rho, L) \left[ \arccos(x) - x\sqrt{1-x^2} \right] dx \quad (3.23)$$

Consider a situation that the transmitted distance is  $L$ , the diameters of the receiving lens is  $D$  and the wave number of laser beam is  $k$ . We will calculate the irradiance flux variance under general irradiance fluctuation conditions on the optical axis in the plane of the photodetector behind the receiver collecting lens.

### 3.2.1 Plane Wave

The on-axis irradiance flux variance of a plane wave in the plane of the photodetector is given by [1]:

$$\sigma_{I,PL}^2(D) = 8\pi^2 k^2 L \int_0^1 \int_0^{+\infty} \kappa \Phi_n(\kappa) \exp\left(-\frac{D^2 \kappa^2}{16}\right) \left(1 - \cos \frac{L \kappa^2 \xi}{k}\right) d\kappa d\xi. \quad (3.24)$$

Consider  $\Phi_n(\kappa)$  as a conventional Kolmogorov power-law spectrum and in the absence of inner scale and outer scale effects, the irradiance flux variance in Equation (3.24) can be calculate as a simple expression:

$$\sigma_{I,PL}^2(D) = \exp \left[ \frac{0.49\sigma_R^2}{\left(1 + 0.65d^2 + 1.11\sigma_R^{12/5}\right)^{7/6}} + \frac{0.51\sigma_R^2 \left(1 + 0.69\sigma_R^{12/5}\right)^{-5/6}}{1 + 0.9d^2 + 0.62d^2\sigma_R^{12/5}} \right] - 1, \quad (3.25)$$

where

$$d = \sqrt{\frac{kD^2}{4L}}. \quad (3.26)$$

In Figure 3.11, we show the aperture averaging factor  $A$  deduced from Equation (3.25) as a function of circular aperture diameter  $D$  in different turbulence condition (Weak:  $\sigma_R^2 < 1$ ; Medium:  $\sigma_R^2 = 1$ ; Strong:  $\sigma_R^2 > 1$ ) with the transmitted distance  $L = 1km$ . The wave number of the light  $k = 2\pi/\lambda = 4.05 \times 10^6 rad/m$  (wave length:  $\lambda = 1550nm$ ). The result shows that when the diameter of the receiving lens  $D$  is increased, the aperture averaging factor  $A$  can be decreased significantly, which means the fluctuation of irradiance would be reduced.

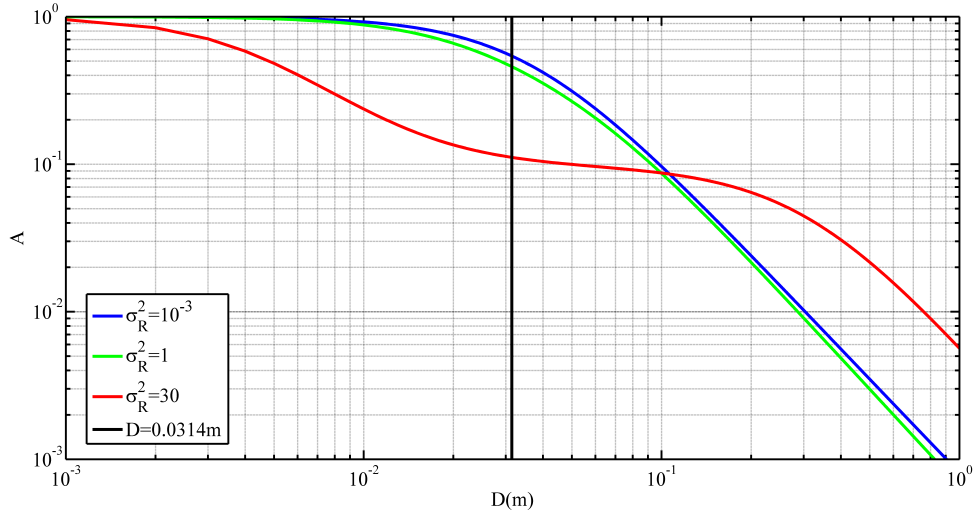


Figure 3.11 Aperture Averaging Factor versus Diameter of Lens for Plane Wave.

### 3.2.2 Spherical Wave

The on-axis irradiance flux variance of a spherical wave in the plane of the photodetector is given by [1]:

$$\sigma_{I,SP}^2(D) = 8\pi^2 k^2 L \int_0^1 \int_0^{+\infty} \kappa \Phi_n(\kappa) \exp\left(-\frac{D^2 \kappa^2 \xi^2}{16}\right) \left[1 - \cos \frac{L \kappa^2 \xi (1 - \xi)}{k}\right] d\kappa d\xi. \quad (3.27)$$

Consider  $\Phi_n(\kappa)$  as a conventional Kolmogorov power-law spectrum and in the absence of inner scale and outer scale effects, the irradiance flux variance in Equation

(3.27) can be calculate as a simple expression:

$$\sigma_{I,SP}^2(D) = \exp \left[ \frac{0.2\sigma_R^2}{\left(1 + 0.18d^2 + 0.19\sigma_R^{12/5}\right)^{7/6}} + \frac{0.21\sigma_R^2 \left(1 + 0.23\sigma_R^{12/5}\right)^{-5/6}}{1 + 0.9d^2 + 0.21d^2\sigma_R^{12/5}} \right] - 1, \quad (3.28)$$

In Figure 3.12, we show the aperture averaging factor  $A$  deduced from Equation (3.28) as a function of circular aperture diameter  $D$  in different turbulence condition (Weak:  $\sigma_R^2 < 1$ ; Medium:  $\sigma_R^2 = 1$ ; Strong:  $\sigma_R^2 > 1$ ) with the transmitted distance  $L = 1km$ . The wave number of the light  $k = 2\pi/\lambda = 4.05 \times 10^6 rad/m$  (wave length:  $\lambda = 1550nm$ ). The result shows that when the diameter of the receiving lens  $D$  is increased, the aperture averaging factor  $A$  can be decreased significantly, which means the fluctuation of irradiance would be reduced.

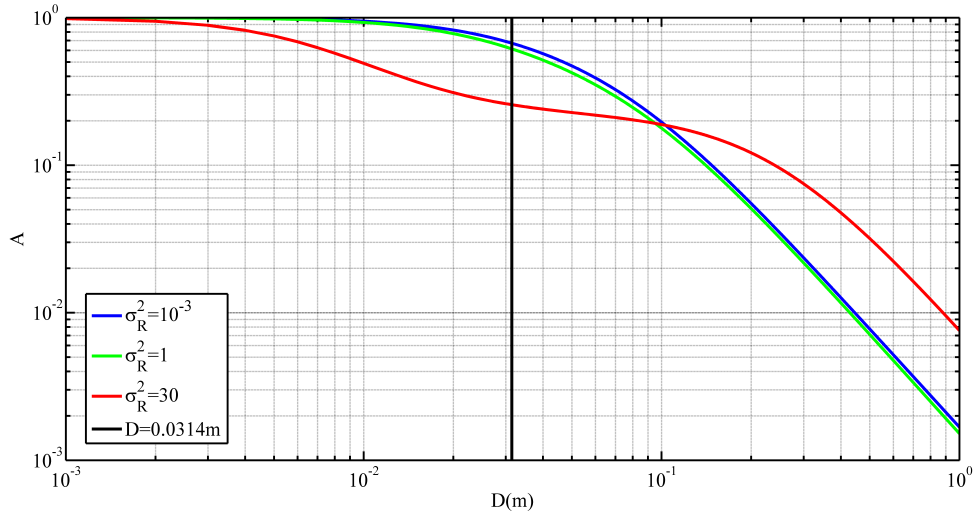


Figure 3.12 Aperture Averaging Factor versus Diameter of Lens for Spherical Wave.

### 3.2.3 Gaussian-beam Wave

The on-axis irradiance flux variance of a spherical wave in the plane of the photodetector is given by [1]:

$$\sigma_I^2(D) = 8\pi^2 k^2 L \int_0^1 \int_0^{+\infty} \kappa \Phi_n(\kappa) \exp \left\{ -\frac{L\kappa^2}{k(\Lambda + \Omega)} \left[ (1 - \bar{\Theta}\xi)^2 + \Lambda\Omega\xi^2 \right] \right\} \left\{ 1 - \cos \left[ \frac{L\kappa^2}{k} \left( \frac{\Omega - \Lambda}{\Omega + \Lambda} \right) \xi (1 - \bar{\Theta}\xi) \right] \right\} d\kappa d\xi. \quad (3.29)$$

Consider  $\Phi_n(\kappa)$  as a conventional Kolmogorov power-law spectrum and in the absence of inner scale and outer scale effects, the irradiance flux variance in Function (3.29) can be calculate as a simple expression:

$$\sigma_I^2(D) = \exp [\sigma_{\ln X}^2(D) + \sigma_{\ln Y}^2(D)], \quad (3.30)$$

where the index in Equation (3.30) can be denoted as:

$$\sigma_{\ln Y}^2(D) = \frac{0.51\sigma_B^2 / (1 + 0.69\sigma_B^{12/5})^{5/6}}{1 + \left[ 1.2(\sigma_R/\sigma_B)^{12/5} + 0.83\sigma_R^{12/5} \right] / (\Omega + \Lambda)}, \quad (3.31)$$

$$\sigma_{\ln X}^2(D) = \frac{0.49\sigma_B^2 \left( \frac{\Omega - \Lambda}{\Omega + \Lambda} \right)^2}{\left[ 1 + \frac{0.4(2 - \bar{\Theta})(\sigma_B/\sigma_R)^{12/7}}{(\Omega + \Lambda) \left( \frac{1}{3} - \frac{1}{2}\bar{\Theta} + \frac{1}{5}\bar{\Theta}^2 \right)^{6/7}} + 0.56(1 + \Theta)\sigma_B^{12/5} \right]^{7/6}}, \quad (3.32)$$

where

$$\bar{\Theta} = 1 - \Theta, \quad (3.33)$$

$$\sigma_B^2 = 3.86\sigma_R^2 \Re \left[ i^{-5/6} F_{2,1} \left( -\frac{5}{6}, \frac{11}{6}; \frac{17}{6}; \bar{\Theta} + i\Lambda \right) - \frac{11}{16}\Lambda^{5/6} \right]. \quad (3.34)$$

The parameters X and Y are large-scale factor and small-scale factor that we talk about in Chapter 2.  $\Theta$  and  $\Lambda$  are the refraction parameter and the diffraction parameter of Gaussian-beam in the receiving plane.  $\Omega$  denotes a nondimensional parameter characterizing the spot radius of the collecting lens.  $\sigma_B^2$  is Rytov variance for a beam wave.  $F_{2,1}(\cdot, \cdot; \cdot)$  is the Hypergeometric Function.

We set a collimated Gaussian-beam wave. Beam radius in the transmitter  $W_0 = 2mm$  and the spot radius of the collecting lens (soft aperture diameter)  $\Omega = 16L/kD^2$ . In Figure 3.13, we show the aperture averaging factor  $A$  deduced from Equation (3.30) as a function of circular aperture diameter  $D$  in different turbulence condition

(Weak:  $\sigma_R^2 < 1$ ; Medium:  $\sigma_R^2 = 1$ ; Strong:  $\sigma_R^2 > 1$ ) with the transmitted distance  $L = 1km$ . The wave number of the light  $k = 2\pi/\lambda = 4.05 \times 10^6 rad/m$  (wave length:  $\lambda = 1550nm$ ). The result shows that when the diameter of the receiving lens  $D$  is increased, the aperture averaging factor  $A$  can be decreased significantly, which means the fluctuation of irradiance would be reduced.

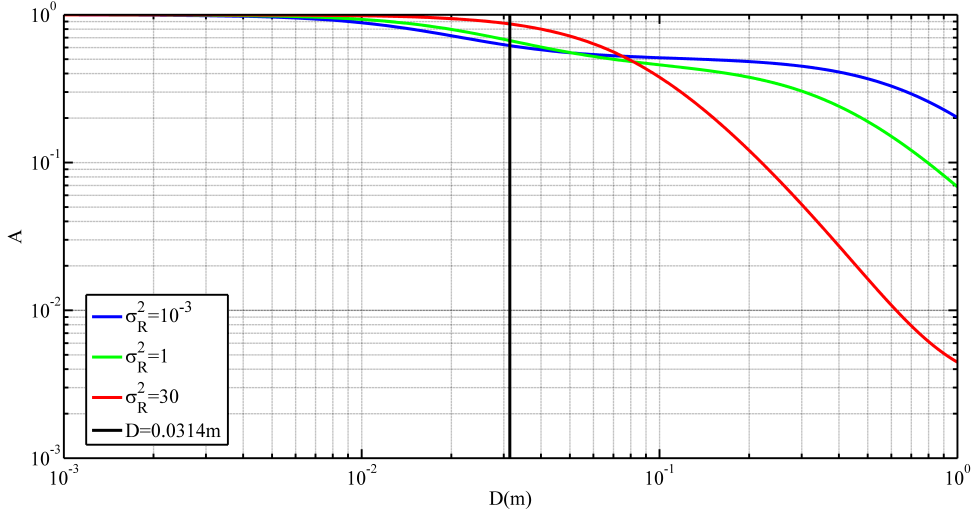


Figure 3.13 Aperture Averaging Factor versus Diameter of Lens for Gaussian Wave.

### 3.3 Multiple Reception

In last section, we analyze the performance of aperture average implement in FSO system. The result shows that the increasing size of receiving lens is benefit to promoting the system performance [29, 67, 81]. However, the increasing lens' radius would lead to the cost and the weight of the receiving terminal increase exponentially. It is kind of a trend to replace one big lens to several smaller receivers [5, 27, 32, 48, 66]. Most of the previous research on FSO communication system with multiple receivers concerned each reception being independent with others, which meant the distance between two individuals was long enough [28, 31, 33, 68, 79–81]. This non-quantitative definition would made difficulties in the design of FSO system.

#### 3.3.1 Correlation Coefficient

In the theory used to derive the atmospheric turbulence, optical field propagation can be seen as a random process. In order to obtain the PDF of the multiple reception

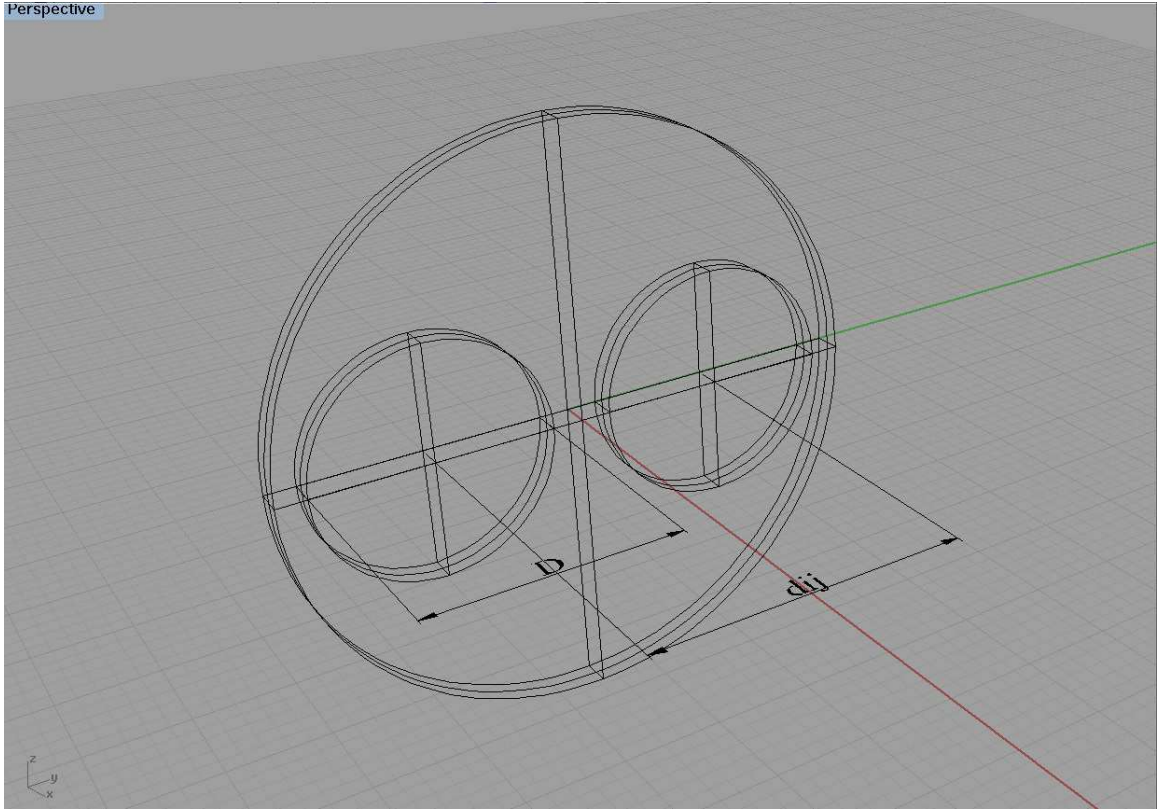


Figure 3.14 Dual Receiver.

system, it is not only to know the value distribution for each receiver, but also the correlation coefficient between any two receivers [5, 32, 48]. Consider  $lens_i$  and  $lens_j$  as two individual receivers with central distance  $d_{ij}$  and diameter  $D$  as shown in Figure 3.14. The received light intensity of  $lens_i$  and  $lens_j$  have average value  $I_i$  and  $I_j$ . Correlation coefficient  $\gamma_{ij}$  of  $lens_i$  to  $lens_j$  is defined as:

$$\gamma_{ij}(d_{ij}, D) = \frac{B_{ij}(I_i, I_j, d_{ij}, D)}{\sqrt{\sigma_i^2 \sigma_j^2}}. \quad (3.35)$$

$B_{ij}(I_i, I_j, d_{ij}, D)$  is the spatial covariance of  $lens_i$  to  $lens_j$ . The  $\sigma_i^2$  and  $\sigma_j^2$  are the variance of  $lens_i$  and  $lens_j$ . In order to characterize the irradiance and the scintillation index of receiver induced channel fading, we use the light irradiance spatial covariance function which can be presented as:

$$B_{ij}(I_i, I_j, d_{ij}, D) = \frac{\langle I_i I_j \rangle}{\langle I_i \rangle \langle I_j \rangle} - 1, \quad (3.36)$$

and

$$\sigma_i^2(D) = B_{ii}(I_i, 0, D) = \frac{\langle I_i^2 \rangle}{\langle I_i \rangle^2} - 1, \quad (3.37)$$

$$\sigma_j^2(D) = B_{jj}(I_j, 0, D) = \frac{\langle I_j^2 \rangle}{\langle I_j \rangle^2} - 1. \quad (3.38)$$

Based on the extended Rytov theory, we can express the light intensity as  $I = I_0 \exp(2x - 2\langle x \rangle)$  which we have discussed in Chapter 2. In this case, we can use the log-amplitude  $x$  and its variance  $\sigma_x^2$  of the optical wave to express two points on-axis log-amplitude variance. It is defined as:

$$\begin{aligned} B_{x,ij}(r_i, r_j, L) &= \langle (x_i x_j)^2 \rangle - (\langle x_i x_j \rangle)^2 \\ &= \frac{1}{2} \Re \mathfrak{e} [E_2(r_i, r_j, L) + E_3(r_i, r_j, L)]. \end{aligned} \quad (3.39)$$

Consider the plane wave model, which means  $r_i = r_j = 0$ . Where  $E_2, E_3$  are two second-order statistical moments can be represented as:

$$E_2(0, 0, L) = 4\pi^2 k^2 L \int_0^1 \int_0^{+\infty} \kappa \Phi_n(\kappa) \exp\left(-\frac{\kappa^2 D^2}{16}\right) J_0(\kappa d_{12}) d\kappa d\xi, \quad (3.40)$$

$$E_3(0, 0, L) = -4\pi^2 k^2 L \int_0^1 \int_0^{+\infty} \kappa \Phi_n(\kappa) \exp\left(-\frac{\kappa^2 D^2}{16} - i \frac{L \kappa^2 \xi}{k}\right) J_0(\kappa d_{12}) d\kappa d\xi, \quad (3.41)$$

where  $\xi = 1 - z/L$  and  $J_0(\cdot)$  is Bessel function of the first kind and zero order. Therefore the spatial covariance for the plane wave model can be written as:

$$\begin{aligned} B_{x,ij}(r_i, r_j, L) &= \exp [4B_{x,ij}(0, 0, L)] - 1 \\ &= \exp \{2\Re \mathfrak{e} [E_2(0, 0, L) + E_3(0, 0, L)]\} \\ &= \exp \left\{ 8\pi^2 k^2 L \int_0^1 \int_0^{+\infty} \kappa \Phi_n(\kappa) \exp\left(-\frac{\kappa^2 D^2}{16}\right) \right. \\ &\quad \left. J_0(\kappa d_{12}) \left[ 1 - \cos\left(\frac{L \kappa^2 \xi}{k}\right) \right] d\kappa d\xi \right\} - 1. \end{aligned} \quad (3.42)$$

Based on Rytov Theory,  $I_i, I_j, \sigma_i^2$  and  $\sigma_j^2$  are the variables versus atmospheric turbulence situation, which can be described by Rytov Variance  $\sigma_R^2$ . Hence if we set the diameters of each lens as a certain value (It is 10cm in Figure 3.15), the correlation coefficient is a function of the receivers setting and turbulence condition, as showed in Figure 3.15. From the Figure 3.15, we can find that when the size of each receiver is a steady state value, the correlation coefficient would be decreased when the central distance between two individual receivers is increased. And it would be increased when the atmospheric turbulence condition is getting stronger [5].

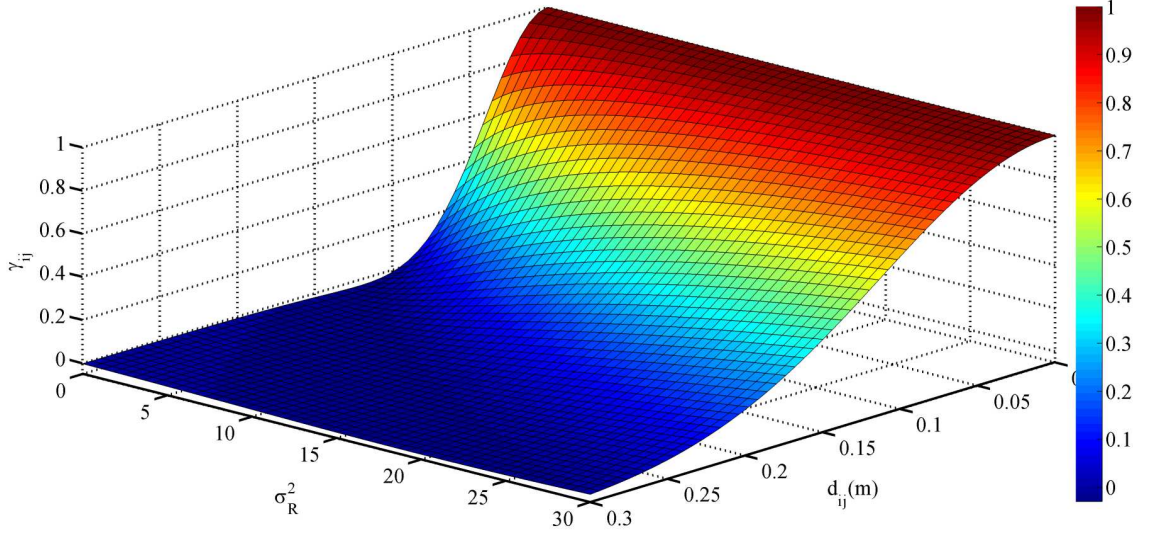


Figure 3.15 Correlation Coefficient under Different Central Distance and Turbulence Condition. [5]

### 3.3.2 Correlation Lognormal Distribution

Consider the Lognormal distribution, the log-amplitude  $x$  is under Gaussian distribution. Assume there are  $n$  receivers and the received intensity of each lens is under the Lognormal distribution. Thus, with the correlation coefficient is known, the correlation distribution of the log-amplitude  $x$  at  $n$  receivers in plane wave model can be expressed as [5, 32, 48]:

$$f_x(x) = \frac{1}{(2\pi)^{n/2} |C_x|^{1/2}} \cdot \exp \left\{ -\frac{1}{2} [(x_1 - \langle x_1 \rangle) \cdots (x_n - \langle x_n \rangle)] \cdot C_x^{-1} \cdot [(x_1 - \langle x_1 \rangle) \cdots (x_n - \langle x_n \rangle)]^T \right\}, \quad (3.43)$$

Where  $[\cdot]^T$  denotes the matrix transpose.  $C_x$  is the covariance matrix of the log-amplitude  $x$  at  $n$  receivers in plane wave model, which can be written as:

$$C_x = \begin{bmatrix} \sigma_{x_1}^2 & \sigma_{x_1} \sigma_{x_2} \gamma_{12} & \cdots & \sigma_{x_1} \sigma_{x_n} \gamma_{1n} \\ \sigma_{x_2} \sigma_{x_1} \gamma_{21} & \sigma_{x_2}^2 & \cdots & \sigma_{x_2} \sigma_{x_n} \gamma_{2n} \\ \vdots & \vdots & \ddots & \vdots \\ \sigma_{x_n} \sigma_{x_1} \gamma_{n1} & \sigma_{x_n} \sigma_{x_2} \gamma_{n2} & \cdots & \sigma_{x_n}^2 \end{bmatrix}. \quad (3.44)$$

Since the received intensity can be expressed as:  $I = I_0 \exp(2x - 2\langle x \rangle)$ , the correlation distribution of the received intensity  $I$  at  $n$  receivers in plane wave model can be

written as:

$$f_I(I) = \frac{1}{2^n (2\pi)^{n/2} |C_x^{1/2}| \prod_{i=1}^n I_i} \exp \left\{ -\frac{1}{8} \left[ \ln \left( \frac{I_1}{I_{10}} \right) \cdots \ln \left( \frac{I_n}{I_{n0}} \right) \right]^T C_x^{-1} \cdot \left[ \ln \left( \frac{I_1}{I_{10}} \right) \cdots \ln \left( \frac{I_n}{I_{n0}} \right) \right] \right\}, \quad (3.45)$$

where  $I_{i0}$  denotes the average received intensity value of receiver  $i$ .  $I_i$  is the received intensity of receiver  $i$ .

Figure 3.16 expresses the correlation Lognormal distribution between two individual lens with different correlation coefficient. We can find that when the correlation

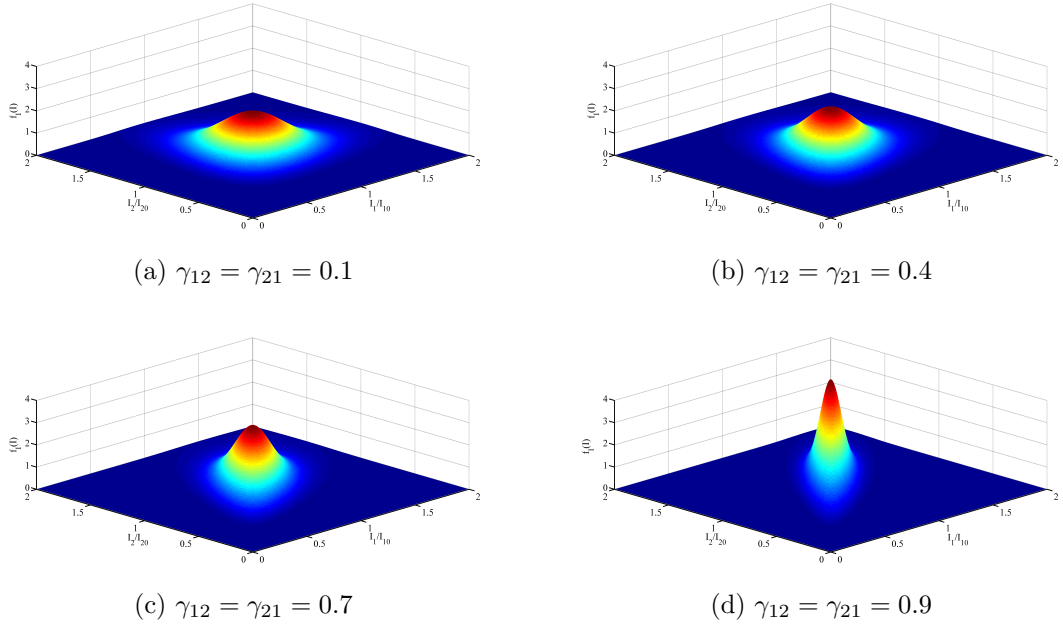


Figure 3.16 Correlation Lognormal Distribution between Two Individual Lens.

coefficient is higher, the probability distribution is more centralized [5].

### 3.4 Polarization Modulation

Based on the estimation in Chapter 2, it is obvious that the optical polarization is a much more stable property than the optical intensity while the laser beam propagating through the atmospheric channel. It inspires us to develop the polarization modulation based FSO system. In this section we are going to introduce three types of the polarization modulation schemes: the polarization shift keying (PolSK), the

consecutive polarization modulation (CPolM), the circular polarization shift keying (CPolSK).

### 3.4.1 PolSK

The PolSK modulation is the most basic polarization modulation method. In the PolSK modulation, two linear orthogonal polarization states represent datas '1' and '0', respectively [37, 50, 86, 89, 93, 97]. For instance, we can modulate the signal '1' and '0' into the horizontal and vertical polarization vectors:

$$s = \begin{cases} 1, & (|E_x|^2 = I_0 \& |E_y|^2 = 0) \\ 0, & (|E_x|^2 = 0 \& |E_y|^2 = I_0) \end{cases} \quad (3.46)$$

The corresponding principle can be expressed as in Figure 3.17:

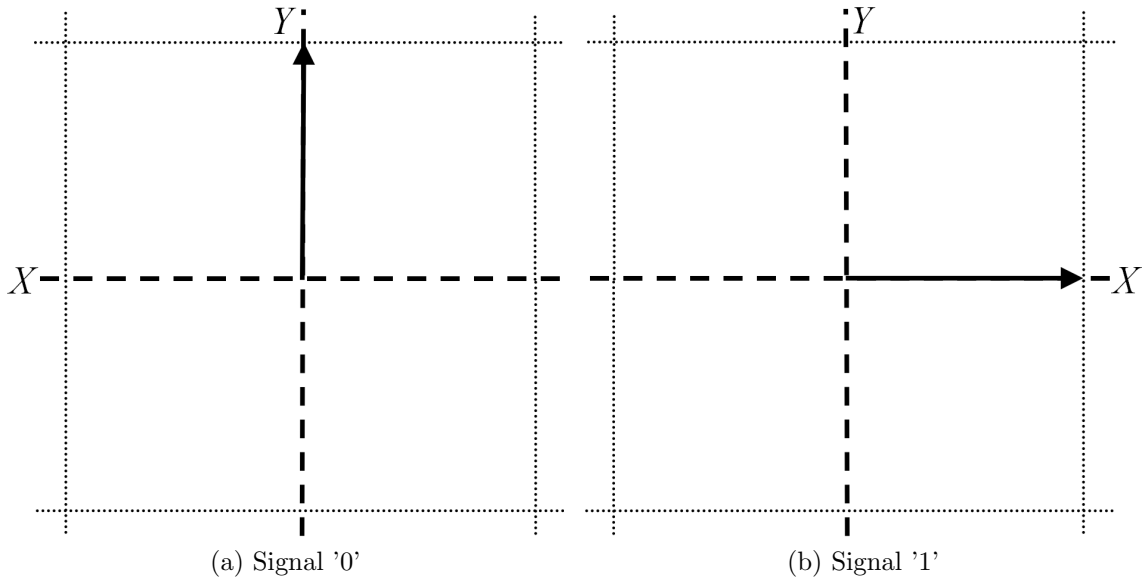


Figure 3.17 Principle of The PolSK.

### 3.4.2 CPolM

The PolSK modulation, just using two optical polarization states, doesn't take full advantages of the stability of the optical polarization in the atmosphere. Different from the conventional PolSK modulation scheme, in this thesis, the polarization state is consecutive in a certain range. We named this novel modulation scheme as CPolM [6]. More details will be analyzed and discussed in Chapter 4.

### 3.4.3 CPolSK

Neither CPolM-based nor PolSK-based FSO system is suitable in a mobile environment. The rotation of a transceiver device will lead to an angle misalignment of the linear polarization state detection. Thus, we suppose to use the left and right circular polarized light represent datas '1' and '0', respectively [2, 40, 74, 83].

$$s = \begin{cases} 1, & \left( \vec{E} = \vec{E}_x \exp(j\omega t + \phi_0) + \vec{E}_y \exp\left[j\omega t + \phi_0 - \frac{\pi}{2}\right] \right) \\ 0, & \left( \vec{E} = \vec{E}_x \exp(j\omega t + \phi_0) + \vec{E}_y \exp\left[j\omega t + \phi_0 + \frac{\pi}{2}\right] \right) \end{cases}, \quad (3.47)$$

where

$$|E_x| = |E_y|. \quad (3.48)$$

The corresponding principle can be expressed as in Figure 3.18:

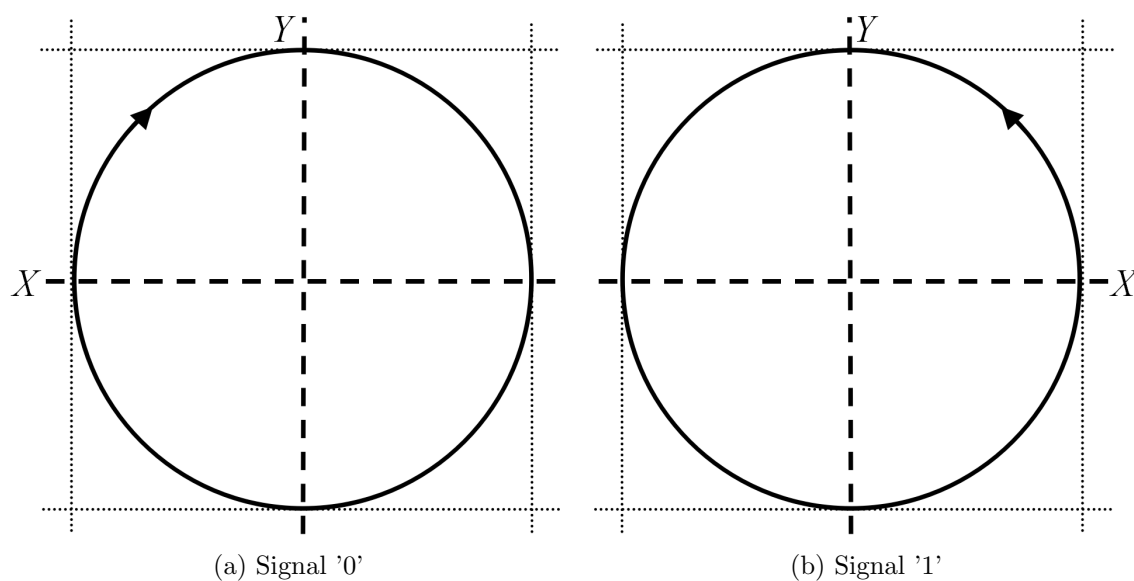


Figure 3.18 Principle of The CPolSK.

# Chapter 4

## Applications and Improvements

In this chapter, we will demonstrate the performance improvements of four different FSO systems, including: the OFDM FSO system with aperture average, the multiple reception OFDM FSO System, the CPolM-based OFDM FSO system and the CPolSK-based FSO system working in space-to-ground channel, which apply the technologies discussed in Chapter 3.

### 4.1 OFDM FSO System with Aperture Average

Based on the analysis in Chapter 3, we can find that the OFDM technology has advantages in against the time varying environment and the aperture average is an efficient technology to reduce the fluctuation of irradiance. Consider a FSO system, composed with OFDM and aperture average. The system architecture is shown as:

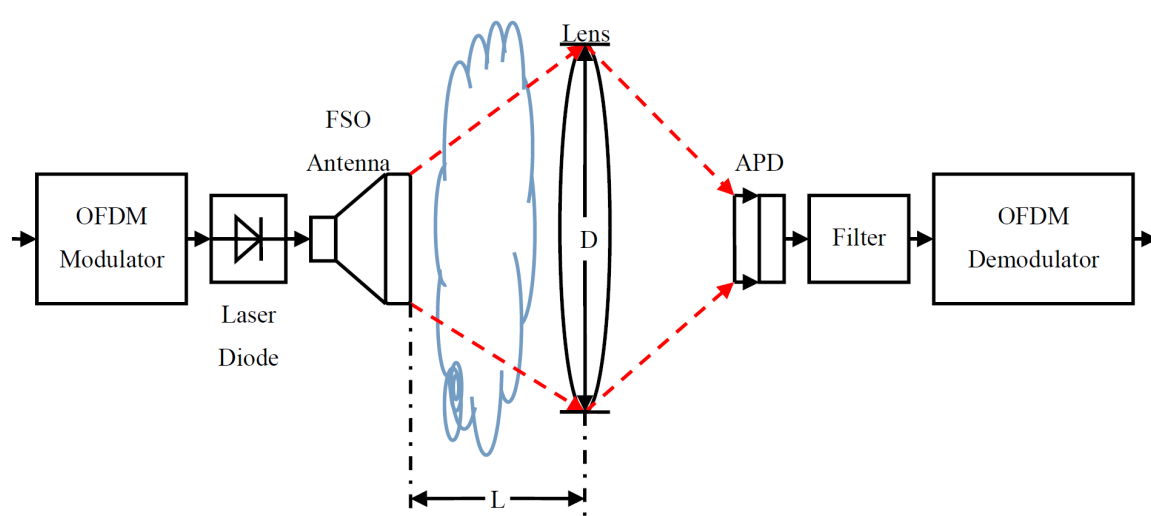


Figure 4.1 Architecture of OFDM FSO System with Aperture Average.

The electrical signal data is modulated by OFDM Modulator as we talk about in the Chapter 3 and it is converted to optical signal by laser-diode. The optical signal propagates through atmospheric turbulence and would be received by the aperture averaging receiver with a lens diameter  $D$ . The received data would be converted back to electrical signal by an avalanche photodiode (APD). After go through the filter, the signal would be demodulated by the OFDM Demodulator as we mentioned in the Chapter 3.

Considering OFDM signals are carried on  $N$  subcarriers. After upconverted to the optical angular frequency  $\omega_c$ , the signals can be written as:

$$S_{OFDM}(t) = \sum_{n=1}^N S_n(t) = \sum_{n=1}^N X_n \exp [j(\omega_n + \omega_c)t + \phi_n], \quad (0 \leq t \leq T_s). \quad (4.1)$$

Where  $\omega_n$  is the  $n$ th subcarrier angular frequency,  $\phi_n$  is the  $n$ th subcarrier initial phase,  $X_n = a_n + jb_n$  is  $n$ th subcarrier complex data symbol.  $a_n$  and  $b_n$  are the in-phase and quadrature modulation symbols. The LD would cause a nonlinearity effect messing with the desired signals. It mainly manifests as the inter-modulation distortions (IMD) which is an effect that the output optical power would be proportional to the modulating signals as [5]:

$$P_T(t) = P_t \left\{ 1 + \sum_{n=1}^N m_n s_n(t) + a_3 \left[ \sum_{n=1}^N m_n s_n(t) \right]^3 \right\}, \quad (4.2)$$

Where  $P_t$  is the average transmitted optical power,  $a_3$  is the third order nonlinearity coefficient, and  $m_n$  is the optical modulation index (OMI) for subcarrier  $n$ . The total OMI can be written as:

$$m = \frac{1}{N} \sqrt{\sum_{n=1}^N m_n^2}. \quad (4.3)$$

We assumed  $I_{ph}$  is the DC of total received photocurrent:

$$I_{ph} = \rho L_{Scint} L_{Atm} P_T \exp(2x - 2\langle x \rangle), \quad (4.4)$$

Where  $\rho$  is the responsivity of the APD.  $L_{Scint}$  is the loss due to the optical scintillation.  $L_{Atm}$  is the loss of optical power due to the atmospheric attenuation.  $x$  denotes the parameter describing intensity fluctuation follow the Lognormal distribution discussed in Chapter 2. The desired signal power can be expressed as:

$$C(x) = \frac{1}{2} m^2 I_{ph}^2. \quad (4.5)$$

We assumed the total noise power of the system is constitute by thermal noise, shot noise and relative intensity noise (RIN) process [5, 32, 48, 77]:

$$N_0(I_{ph}) = \frac{4K_B T_{abs} F B_e}{R_L} + 2qI_{ph}B_e + (RIN)I_{ph}^2 B_e, \quad (4.6)$$

where  $K_B$  is Boltzmanns constant,  $T_{abs}$  is the absolute temperature, F is the noise figure of the receiver electronics,  $R_L$  is the PD load resistor, q is the electron charge and  $B_e$  is the Electrical filter bandwidth.

The received optical power at APD can be expressed as:

$$P_R(t) = \rho L_{Scint} L_{Atm} P_T \exp(2x - 2\langle x \rangle) + N_0. \quad (4.7)$$

Thus, with the OFDM symbol duration  $T_s$ , the received signal-noise-ratio (SNR) per OFDM symbol can be expressed as:

$$SNR(x) = \frac{C(x)}{N_0} T_s. \quad (4.8)$$

The ensemble average value of  $SNR(x)$  over the Lognormal distribution can be expressed as:

$$\begin{aligned} \langle SNR \rangle &= \int_{-\infty}^{+\infty} SNR(x) f_x(x) dx \\ &= \int_{-\infty}^{+\infty} SNR(x) \frac{1}{\sqrt{2\pi\sigma_x^2}} \exp\left[-\frac{(x - \langle x \rangle)^2}{2\sigma_x^2}\right] dx. \end{aligned} \quad (4.9)$$

Figure 4.2 shows a 3-D figure of the ensemble average SNR in different subcarrier number n and optical modulation index  $m_n$ . We can find the  $\langle SNR \rangle$  has a preminent performance, when  $m_n$  is between 0.01% ~ 0.1%.

Consider the modulation of the system as M-QAM. The received bit-error-rate (BER) of the system can be given by:

$$BER(x) = 2 \left( \frac{\sqrt{M} - 1}{\sqrt{M}} \right) \text{erfc} \left[ \sqrt{\frac{3SNR(x)}{2(M-1)}} \right]. \quad (4.10)$$

The ensemble average value of BER(x) over the Lognormal distribution can be expressed as:

$$\begin{aligned} \langle BER \rangle &= \int_{-\infty}^{+\infty} BER(x) f_x(x) dx \\ &= \int_{-\infty}^{+\infty} BER(x) \frac{1}{\sqrt{2\pi\sigma_x^2}} \exp\left[-\frac{(x - \langle x \rangle)^2}{2\sigma_x^2}\right] dx. \end{aligned} \quad (4.11)$$

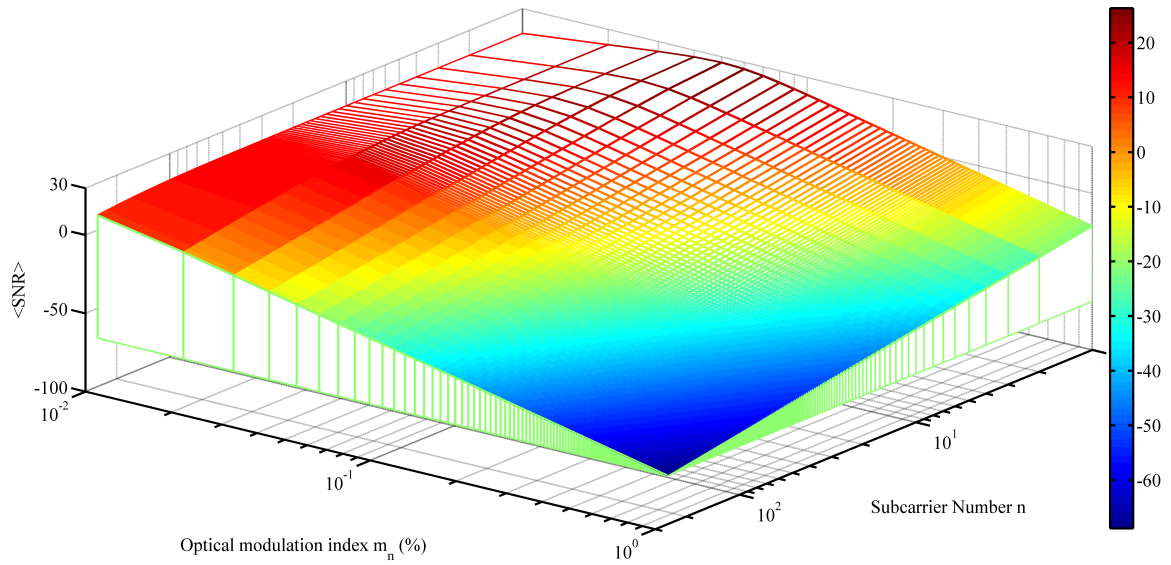


Figure 4.2 Average SNR in Different Subcarrier Number  $n$  and Optical Modulation Index  $m_n$ .

In Figure 4.3, we show the ensemble average BER versus transmitted power with different receiving lens diameters and in different atmospheric turbulence conditions (Weak Turbulence:  $\sigma_R^2 = 0.5$ ; Strong Turbulence:  $\sigma_R^2 = 30$ ), and the modulation we implement is QPSK.

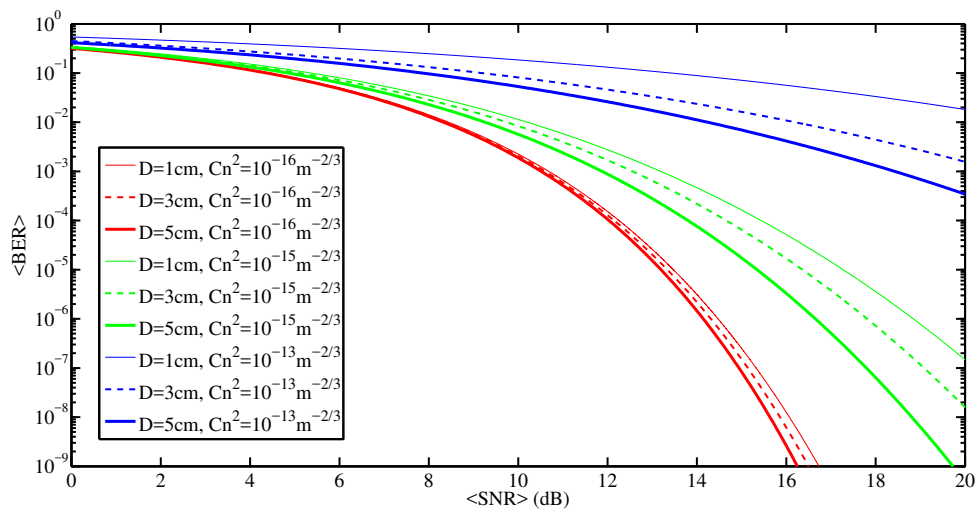


Figure 4.3 Average BER versus Average SNR with Different Receiving Diameters under Varying Turbulence Strength.

As Figure 4.3 shown, the performance of the system would be impact by the at-

atmospheric turbulence condition, significantly. OFDM FSO system in this thesis would have a better performance in a better atmospheric condition. When the transmitted power increases, the ensemble average BER of the system would be reduced. Under the condition of moderate/strong turbulence regime, the diameter increasing would reduce the  $\langle BER \rangle$  of the system, efficiently.

Table 4.1 Parameters for Figure 4.3.

Parameter	Value
Transmission Distance ( $L$ )	$2km$
Optical Wavelength ( $\lambda$ )	$1550nm$
Number of Subcarriers ( $N$ )	512
Symbol Duration ( $T_s$ )	$1.008\mu s$
Absolute Temperature ( $T_{abs}$ )	$300K$
PD Load Resistor ( $R_L$ )	$50\Omega$
Detector Responsivity ( $\rho$ )	$0.8A/W$
Relative Intensity Noise ( $RIN$ )	$-130dB/Hz$
Electron Charge ( $q$ )	$1.602 \times 10^{-19}C$
Third Order IMD ( $a_3$ )	$9 \times 10^{-4}$
Scintillation Loss ( $L_{Scint}$ )	0.9
Atmospheric Loss ( $L_{Atm}$ )	0.9
Optical Modulation Index for the nth Subcarrier ( $m_n$ )	0.1%
Noise Figure of The Receiver Electronics ( $F$ )	$2dB$

In this section, we analyze the ensemble average BER versus the ensemble average SNR performance when system has different sizes of receivers. We can have a conclusion that the FSO system performance is seriously effected by the atmospheric turbulence and the increasing size of receiver could mitigate the channel fading and promote the performance of the OFDM FSO system.

## 4.2 Multiple Reception OFDM FSO System

In this section, we will present a discussion about two influence elements, the amount of lenses and the distance between two individual lenses, of multiple reception technology in the OFDM FSO system. The dual reception architecture is demonstrated as in Figure 3.14 and the corresponding analysis is also discussed in Chapter 3. Here we consider an OFDM FSO system with ternary reception scheme. The receiver architecture is designed as Figure 4.4.  $D$  is the diameter of each lens. Consider two separate lenses  $lens_i$  and  $lens_j$ ,  $d_{ij}$  presents the central distance between  $lens_i$  and  $lens_j$ .

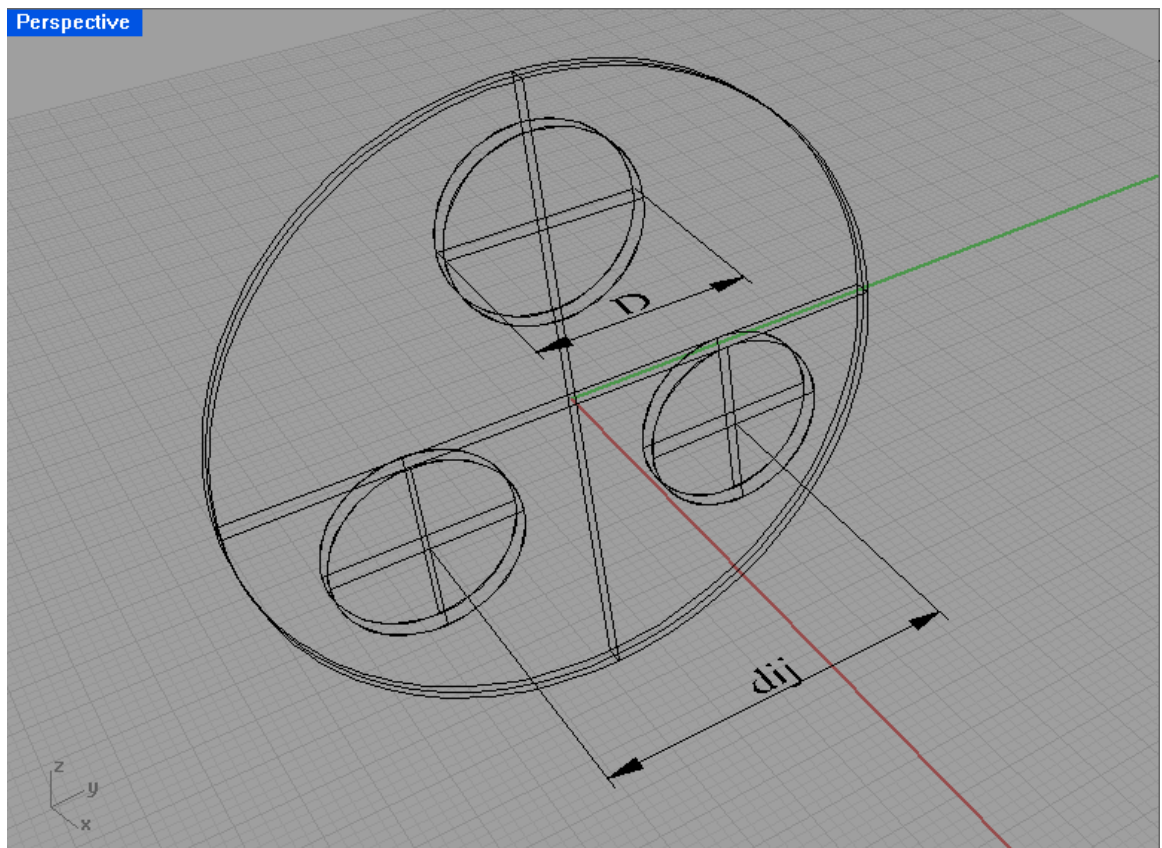


Figure 4.4 Ternary Receiver. [5]

The architecture of the system is shown in Figure 4.5. The electrical signal is modulated by OFDM Modulator and converted to optical signal by laser-diode. The optical signal propagates through atmospheric turbulence and would be received by the ternary receiver. After converted back electrical signal, the signals from three detectors would be demodulated by OFDM Demodulator and combined under equal

gain combining (EGC) scheme.

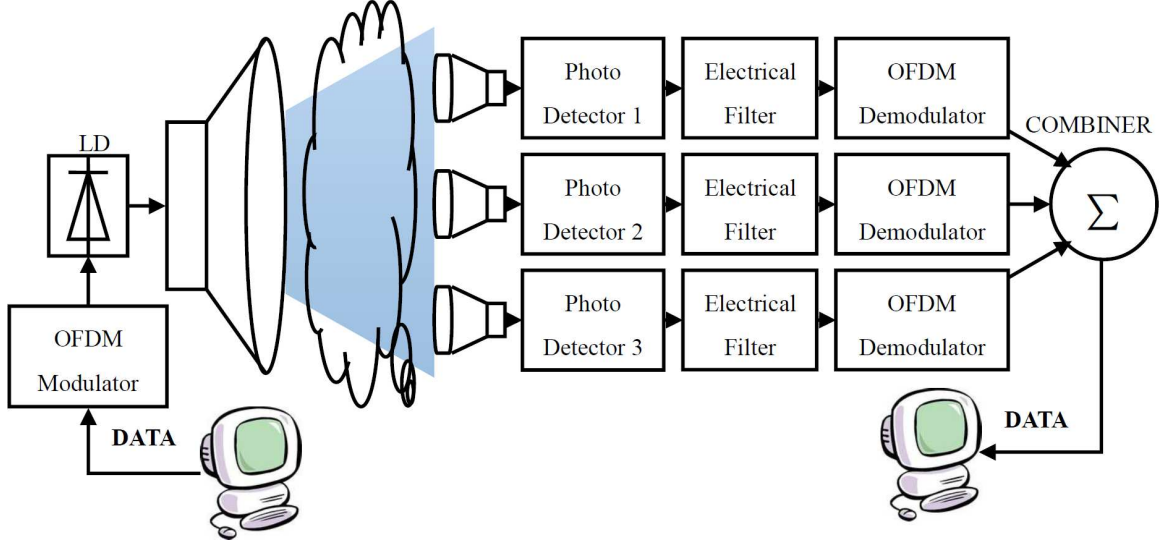


Figure 4.5 Ternary Diversity Reception OFDM FSO System Architecture. [5]

Assuming the optical wave is plane wave model and the received intensity of each receiver is under Lognormal distribution. Thus, the Equation (3.45) can be written as:

$$\begin{aligned}
 & f_{I_1, I_2, I_3}(I_1, I_2, I_3) \\
 &= \frac{1}{16\pi I_1 I_2 I_3 \sqrt{2\pi \sigma_{X_1}^2 \sigma_{X_2}^2 \sigma_{X_3}^2}} \cdot \\
 & \frac{1}{\sqrt{(1 - \gamma_{12}\gamma_{21} - \gamma_{23}\gamma_{32} - \gamma_{13}\gamma_{31} + \gamma_{12}\gamma_{23}\gamma_{31} + \gamma_{13}\gamma_{32}\gamma_{21})}} \cdot \\
 & \exp \left\{ -\frac{1}{8(1 - \gamma_{12}\gamma_{21} - \gamma_{23}\gamma_{32} - \gamma_{13}\gamma_{31} + \gamma_{12}\gamma_{23}\gamma_{31} + \gamma_{13}\gamma_{32}\gamma_{21})} \right. \\
 & \left[ \sigma_{X_2}^2 \sigma_{X_3}^2 (1 - \gamma_{23}\gamma_{32}) \ln^2 \left( \frac{I_1}{I_{10}} \right) + \right. \\
 & \sigma_{X_1}^2 \sigma_{X_3}^2 (1 - \gamma_{13}\gamma_{31}) \ln^2 \left( \frac{I_2}{I_{20}} \right) + \\
 & \sigma_{X_1}^2 \sigma_{X_2}^2 (1 - \gamma_{12}\gamma_{21}) \ln^2 \left( \frac{I_3}{I_{30}} \right) + \\
 & \sigma_{X_1}^2 \sigma_{X_2} \sigma_{X_3} (\gamma_{21}\gamma_{13} + \gamma_{31}\gamma_{12} - \gamma_{23} - \gamma_{32}) \ln \left( \frac{I_2}{I_{20}} \right) \ln \left( \frac{I_3}{I_{30}} \right) + \\
 & \sigma_{X_1} \sigma_{X_2}^2 \sigma_{X_3} (\gamma_{12}\gamma_{23} + \gamma_{32}\gamma_{21} - \gamma_{13} - \gamma_{31}) \ln \left( \frac{I_1}{I_{10}} \right) \ln \left( \frac{I_3}{I_{30}} \right) + \\
 & \left. \left. \sigma_{X_1} \sigma_{X_2} \sigma_{X_3}^2 (\gamma_{13}\gamma_{32} + \gamma_{23}\gamma_{31} - \gamma_{12} - \gamma_{21}) \ln \left( \frac{I_1}{I_{10}} \right) \ln \left( \frac{I_2}{I_{20}} \right) \right] \right\}. \tag{4.12}
 \end{aligned}$$

Consider the three receiving lenses have the same diameters and set as a regular triangle ( $d_{12} = d_{23} = d_{13}$ ). Since the optical wave is plane wave model, that lead to  $I_{10} = I_{20} = I_{30}$  and  $\gamma_{10} = \gamma_{20} = \gamma_{30}$ . The Function (4.12) can be written as:

$$f_I(I) = \frac{1}{16\pi I^3 \sqrt{2\pi\sigma_X^6(1-3\gamma^2+2\gamma^3)}} \exp \left\{ -\frac{1}{8(1-3\gamma^2+2\gamma^3)} \left[ 3\sigma_X^4(1-2\gamma+\gamma^2) \ln^2 \left( \frac{I}{I_0} \right) \right] \right\}. \quad (4.13)$$

Combining the result in section 4.1, the desired signal power can be expressed as:

$$C(I_1, I_2, I_3) = \frac{1}{2} m^2 I_{ph}^2(I_1, I_2, I_3). \quad (4.14)$$

The total noise power of the system is mainly consist of three components: thermal noise, shot noise and relative intensity noise (RIN) process:

$$N_0(I_1, I_2, I_3) = \frac{4K_B T_{abs} F B_e}{R_L} + 2q I_{ph}(I_1, I_2, I_3) B_e + (RIN) I_{ph}^2(I_1, I_2, I_3) B_e. \quad (4.15)$$

Thus, with the OFDM symbol duration  $T_s$ , the received SNR per OFDM symbol can be expressed as:

$$SNR(I_1, I_2, I_3) = \frac{T_s C(I_1, I_2, I_3)}{N_0}. \quad (4.16)$$

The ensemble average SNR and ensemble average BER over Lognormal distribution can be calculated as:

$$\langle SNR \rangle = \iiint_0^{+\infty} SNR(I_1, I_2, I_3) \cdot f_I(I_1, I_2, I_3) dI_1 dI_2 dI_3, \quad (4.17)$$

$$\langle BER \rangle = \iiint_0^{+\infty} BER(I_1, I_2, I_3) \cdot f_I(I_1, I_2, I_3) dI_1 dI_2 dI_3. \quad (4.18)$$

We set the lens diameters of single, dual and ternary reception are 12cm, 8.49cm and 6.93cm, so that the total reception area of three schemes are the same ( $36\pi cm^2$ ). For the ternary reception system, the three lenses are setting as a regular triangle. In weak atmospheric turbulence condition ( $\sigma_R^2 = 0.14$ ), we draw three picture (Figure 4.6, Figure 4.7, Figure 4.8) to have a legible view to the system performance.

In Figure 4.6, we give a comparison about the system average BER versus average SNR under different reception scheme. We can see that multiple reception is a efficient method to mitigate the FSO channel fading. The decreasing correlation coefficient would promote the performance of the system. When the correlation coefficients are the same, ternary reception is more preminent. Dual reception system with low correlation coefficient ( $\gamma = 0$ ) could perform better than the ternary reception system with high correlation coefficient ( $\gamma = 0.8$ ).

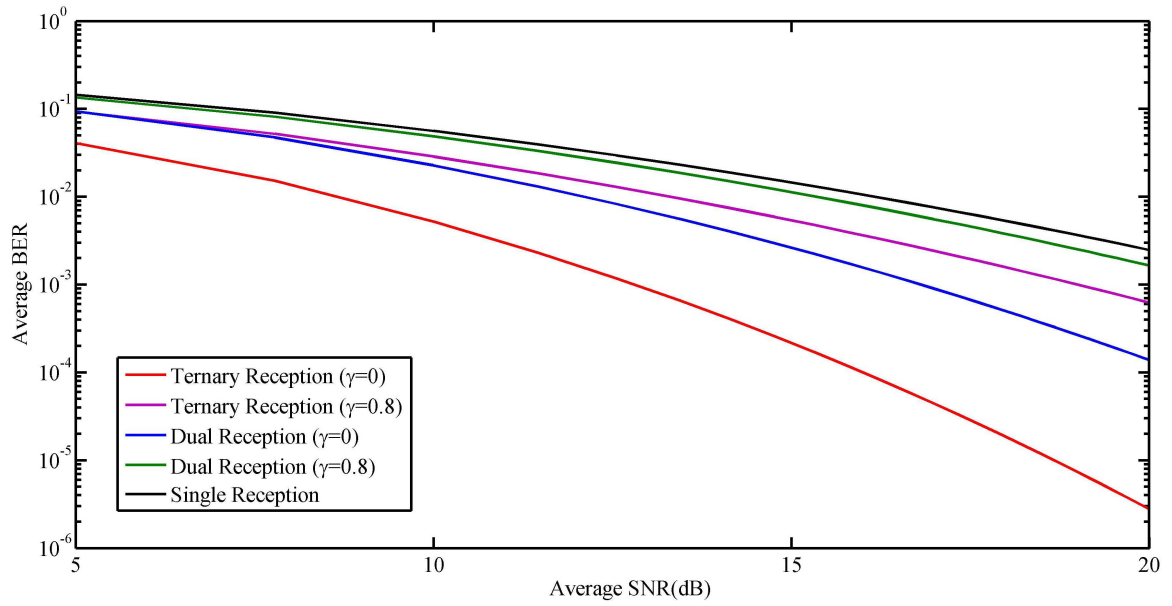


Figure 4.6 Average BER versus Average SNR under Different Reception Scheme. [5]

In Figure 4.7, we give a comparison about the system average BER versus average SNR under different modulation scheme. It is clear that the higher constellation size modulation require more received powers to reduce BER of the system.

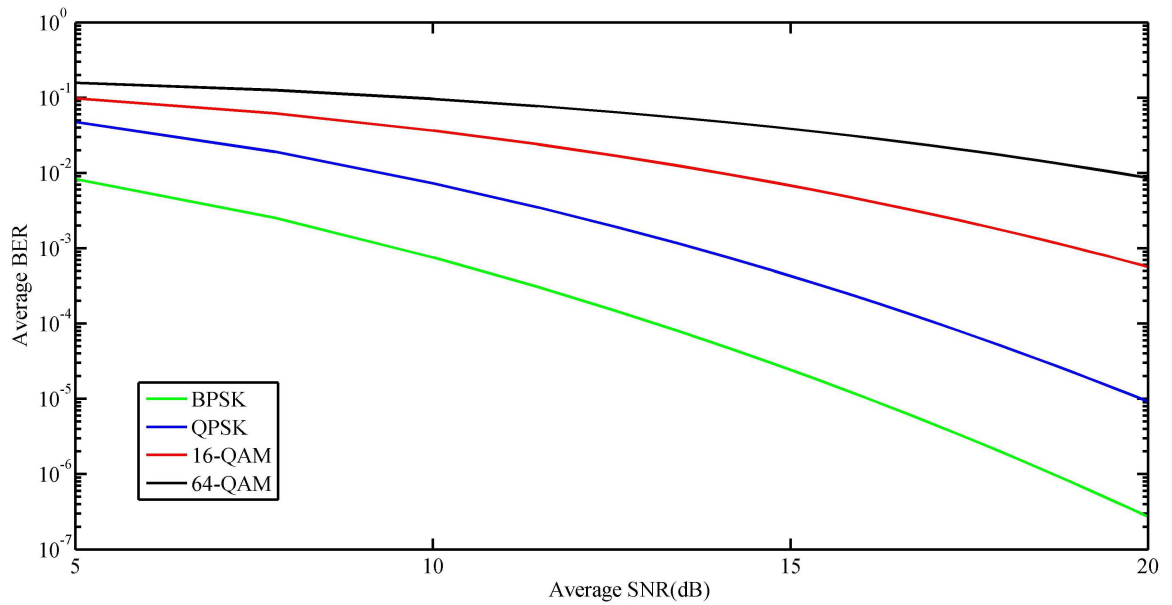


Figure 4.7 Average BER versus Average SNR under Different Modulation Scheme. [5]

Consider a threshold  $SNR_{th}$ . Only when the SNR of the system is better than

the  $SNR_{th}$ , the quality of communication is acceptable. Otherwise, we can see the communication is failed. Define the probability of the SNR falling worse than the  $SNR_{th}$  as the outage probability  $P_{outage}$ . It can be expressed as:

$$P_{outage}(SNR_{th}) = P(SNR < SNR_{th}) \quad (4.19)$$

In Figure 4.8, we give a comparison about the outage probability versus threshold  $SNR_{th}$  in different reception schemes. We can see that multiple reception is a efficient method to mitigate the OFDM FSO system outage probability. The decreasing correlation coefficient would reduce the OFDM FSO system outage probability. When the correlation coefficients are the same, ternary reception is more preminent. Dual reception system with low correlation coefficient ( $\gamma = 0$ ) could perform better than the ternary reception system with high correlation coefficient ( $\gamma = 0.8$ ).

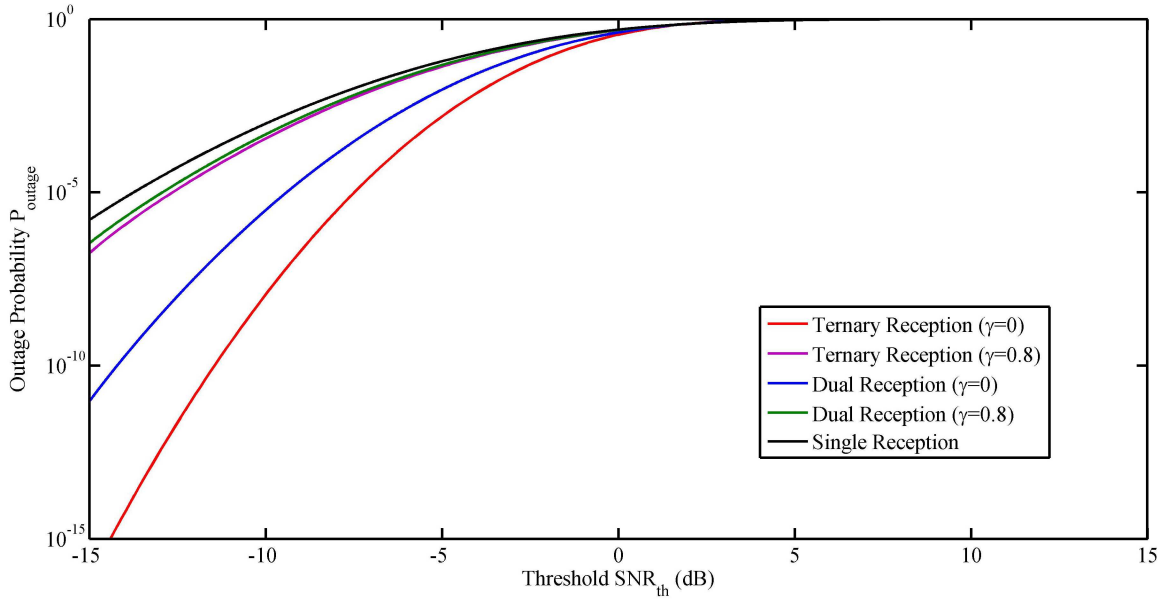


Figure 4.8 Outage Probability versus Threshold under Different Reception Scheme. [5]

In this section, we calculate the multiple reception joint probability distribution function under Lognormal distribution with correlation coefficient. We especially analyze the dual reception and the ternary reception system. The decreasing correlation coefficient would promote the performance of the system. When the correlation coefficients are the same, ternary reception is more preminent. Dual reception system with low correlation coefficient could perform better than the ternary reception system with high correlation coefficient. We can figure out that multiple reception is a efficient method to mitigate the FSO channel fading.

Table 4.2 Parameters for Figure 4.6, Figure 4.7, Figure 4.8.

Parameter	Value
Transmission Distance ( $L$ )	$2km$
Optical Wavelength ( $\lambda$ )	$1550nm$
Number of Subcarriers ( $N$ )	$512$
Symbol Duration ( $T_s$ )	$1.008\mu s$
Absolute Temperature ( $T_{abs}$ )	$300K$
PD Load Resistor ( $R_L$ )	$50\Omega$
Detector Responsivity ( $\rho$ )	$0.8A/W$
Relative Intensity Noise ( $RIN$ )	$-130dB/Hz$
Electron Charge ( $q$ )	$1.602 \times 10^{-19}C$
Third Order IMD ( $a_3$ )	$9 \times 10^{-4}$
Scintillation Loss ( $L_{Scint}$ )	$0.9$
Atmospheric Loss ( $L_{Atm}$ )	$0.9$
Optical Modulation Index for the nth Subcarrier ( $m_n$ )	$0.1\%$
Noise Figure of The Receiver Electronics ( $F$ )	$2dB$

### 4.3 CPolM-Based OFDM FSO System

Based on the estimation in Chapter 3, we can find the optical polarization is the most stable property of the laser beam when propagating through the atmospheric turbulence. However, the PolSK modulation scheme only using two orthogonal linear polarization states is unable to take the utmost of the polarization stability. That inspires us, instead of PolSK, to investigate a consecutive polarization modulation scheme.

#### 4.3.1 CPolM-Based OFDM FSO System Structure

In this section, we present the transceiver structure of the CPolM-based OFDM FSO system. A theoretical analysis for the states of the optical signal is carried out. The operation principle about the optical devices mentioned in this section can be found in [103–106].

##### 4.3.1.1 Transmitter

The structure of the transmitter in the proposed system is shown in Figure 4.9. Figure 4.10 shows the mapping relation between the OFDM signal and the polarization states. Different OFDM signal value is corresponding to different polarization state. The symbol  $\theta$  denotes the angle between polarized direction and the positive  $X$  direction.

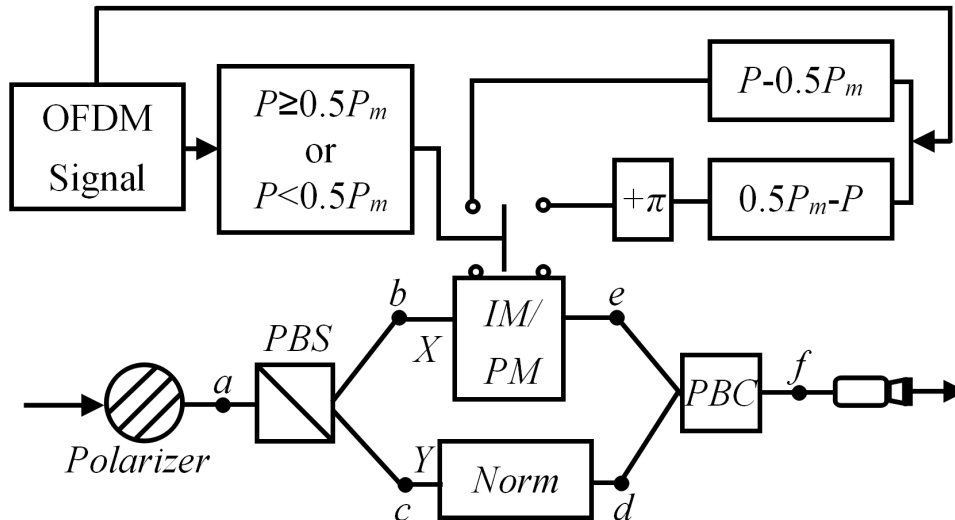


Figure 4.9 Diagram of The CPolM-Based OFDM FSO System Transmitter. [6]

Figure 4.11 illustrates the polarization states of the optical wave in points  $a$ ,  $b$ ,  $c$ ,  $d$ ,  $e$  and  $f$ . Firstly, the optical wave is polarized to  $45^\circ$  by a polarizer (as in Figure



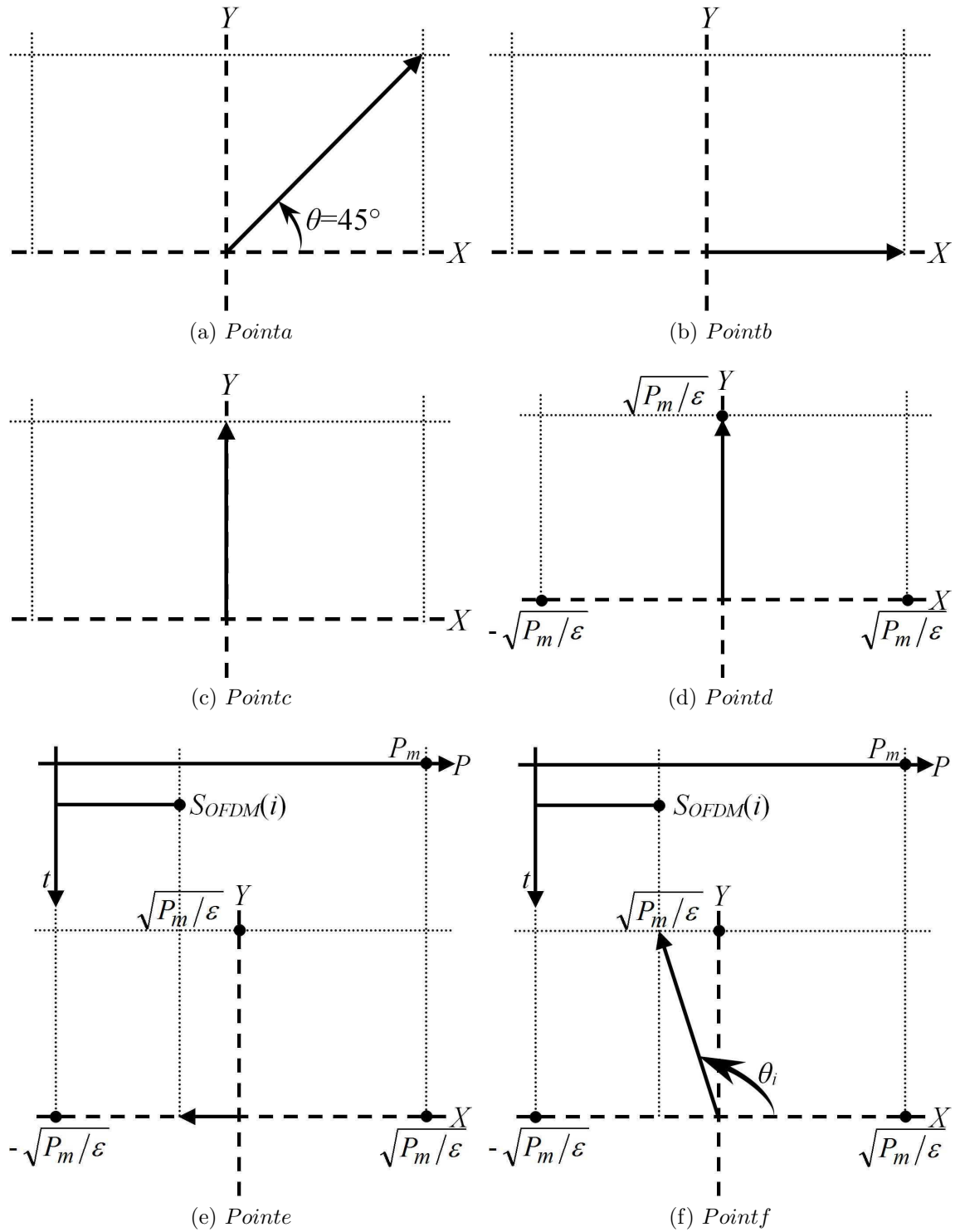


Figure 4.11 Polarization States in The Transmitter. [6]

as in Figure 4.11.(d). Finally,  $X$  component light and  $Y$  component light are combined (as in Figure 4.11.(f)) by a polarization beam combiner ( $PBC$ ) and transmitted

through the turbulence channel.

#### 4.3.1.2 Receiver

The structure of the receiver is shown in Figure 4.12. Figure 4.13 illustrates the polarization states of the optical wave in points  $f'$ ,  $g$ ,  $h$ ,  $i$ , and  $j$ . When the optical

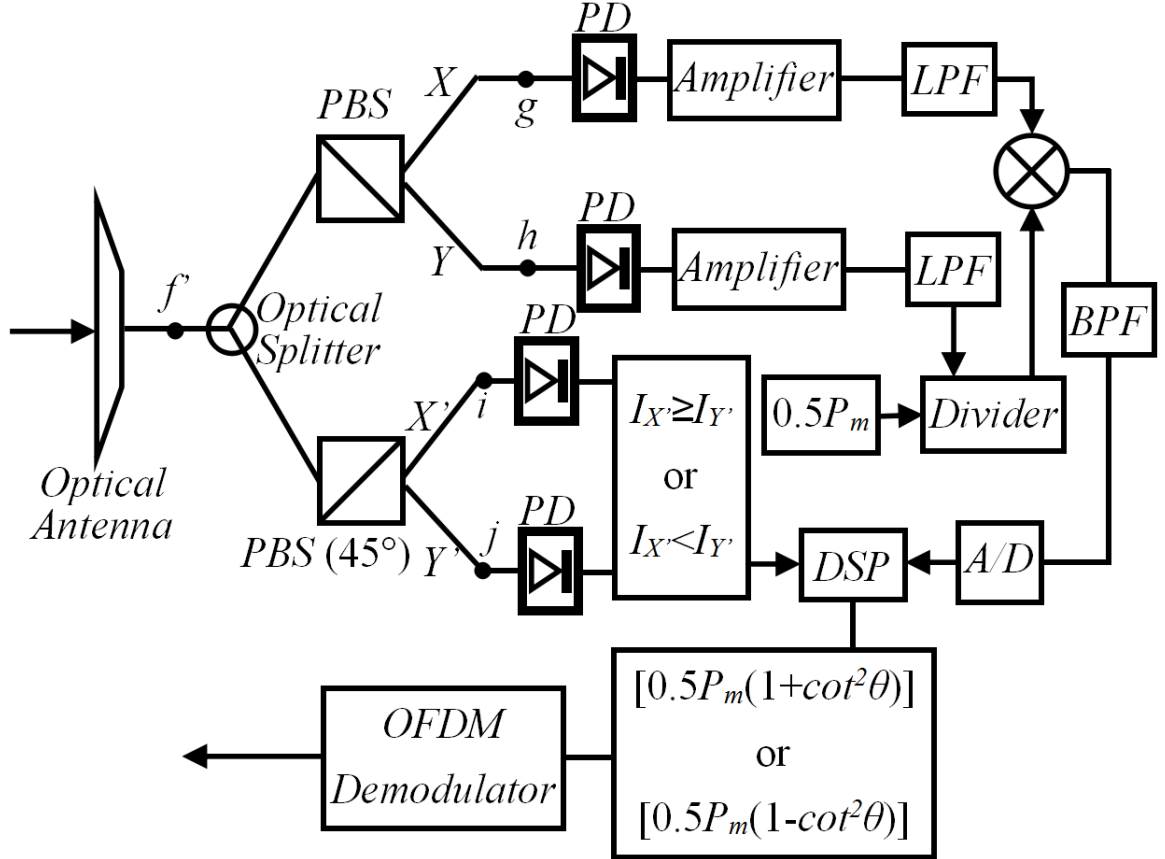


Figure 4.12 Diagram of The CPolM-Based OFDM FSO System Receiver. [6]

wave propagates through the turbulence channel to the receiver, it is collected and coupled into the optical fiber. The optical wave in the point  $f'$  (as in Figure 4.13.(a)) presents the turbulence effects on both optical intensity and polarization state. The received optical power under the turbulence influence can be expressed as:

$$P_r = \frac{1}{2} c \varepsilon E_Y^2 [1 + \cot^2(\theta + \Delta\theta)] \cdot C = \frac{C}{2} c \varepsilon [(E_X + \Delta E_X)^2 + E_Y^2], \quad (4.23)$$

where  $\Delta E_X$  is shown in Figure 5.(b) and can be calculated as:

$$\Delta E_X = E_Y \cdot \cot(\theta + \Delta\theta) - E_Y \cdot \cot(\theta) \cong E_Y \cdot (1 + \cot^2\theta) \cdot \Delta\theta. \quad (4.24)$$

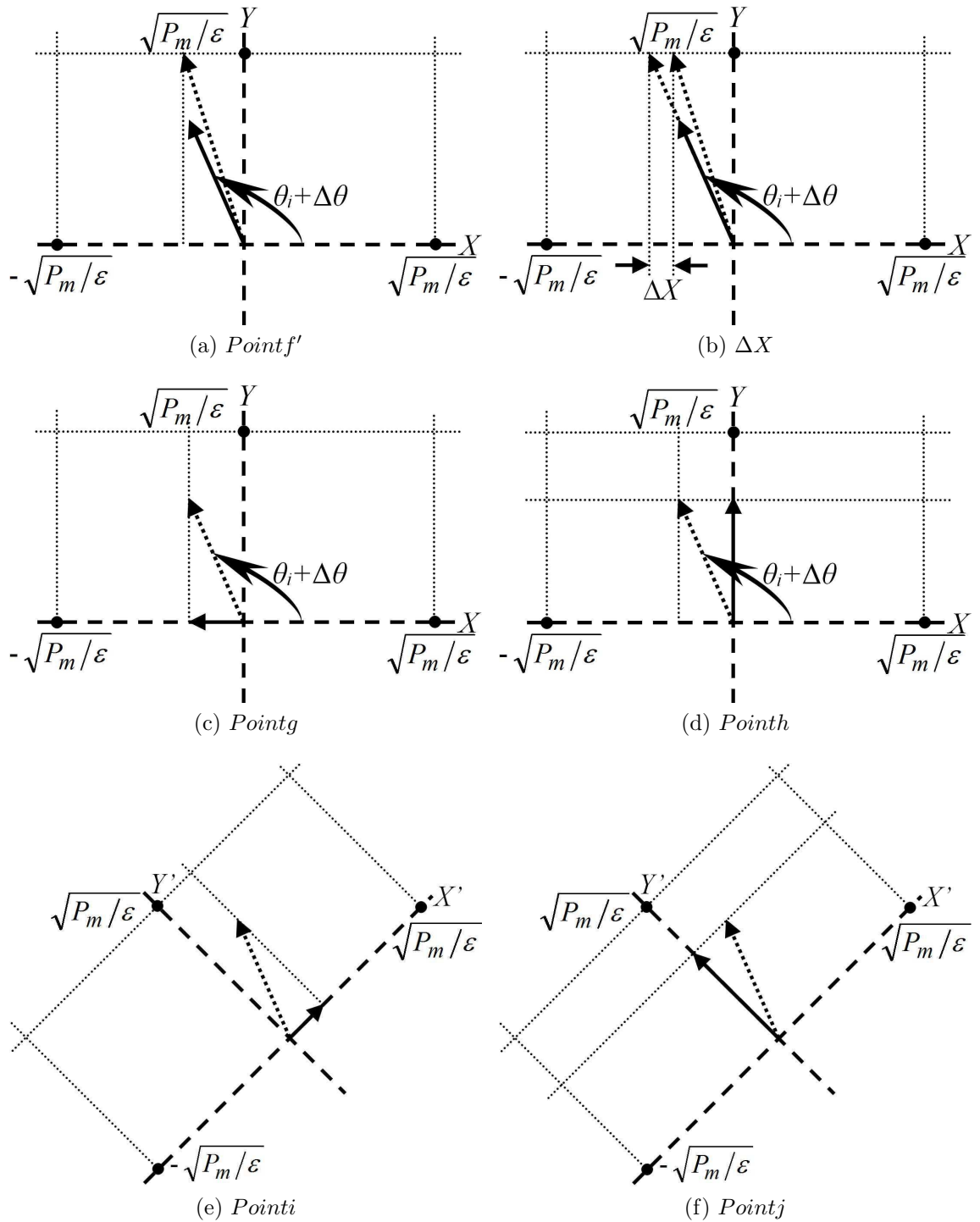


Figure 4.13 Polarization States in The Receiver. [6]

The light is split into two branches by an optical splitter. We set the ratio between the optical power in the upper branch and that in the point  $f'$  as  $\eta$ . So the optical

power in upper and lower branches can be defined as:

$$\begin{cases} P_{upper} = \eta \cdot P_r \\ P_{lower} = (1 - \eta) \cdot P_r. \end{cases} \quad (4.25)$$

The *PBS* in upper branch splits the light into original polarization directions  $X$  and  $Y$  (as in Figure 4.13.(c), 4.13.(d)). The *PBS* in lower branch splits the light into the directions  $X'$  and  $Y'$ , which are  $45^\circ$  rotated from the originals (as in Figure 4.13.(e), 4.13.(f)).

Four independent photo-detectors (*PD*) convert the optical intensity into electric current as:

$$\begin{cases} I_X = \rho\eta P_r \cos^2(\theta + \Delta\theta) + n_X \\ I_Y = \rho\eta P_r \sin^2(\theta + \Delta\theta) + n_Y = 0.5\rho\eta C P_m + n_Y \\ I_{X'} = \rho(1 - \eta) P_r \cos^2(\theta + \Delta\theta - \pi/4) + n_{X'} \\ I_{Y'} = \rho(1 - \eta) P_r \sin^2(\theta + \Delta\theta - \pi/4) + n_{Y'}, \end{cases} \quad (4.26)$$

where  $\rho$  is the responsivity of the *PDs*.  $n_X$ ,  $n_Y$ ,  $n_{X'}$  and  $n_{Y'}$  are additive white Gaussian noise (AWGN). Based on the experimental data in [102], the time-frequency component of the normalized optical intensity  $C$  is not greater than  $1000Hz$ . That gives us two advantages: 1. When  $I_Y$  pass the low-pass filter (*LPF*),  $n_Y$  can be seen as perfectly removed; 2. A divider can be implemented and do the calculation  $0.5P_m/I_Y$  (noticing  $P_m$  is constant). After multiplying the signals in  $X$  direction and  $Y$  direction, passing through the band-pass filter (*BPF*) and an analogue-to-digital conversion (A/D), the signal is processed by a digital signal processor (*DSP*). Compare the value of  $I_{X'}$  and  $I_{Y'}$ : when  $I_{X'} \geq I_{Y'}$ , the output signal should be  $0.5P_m(1 + \cot^2\theta) + N_{Total}$ ; when  $I_{X'} < I_{Y'}$ , the output signal should be  $0.5P_m(1 - \cot^2\theta) + N_{Total}$ , where  $N_{Total}$  is the total noise presented in section 4.3.2. At last, we demodulate the signal with an OFDM demodulator.

### 4.3.2 System Performance

In this section, we establish the mathematic model to describe the proposed system performance, in terms of SNR, symbol-error-ratio (SER) and the outage probability  $P_{out}$ . Then, an analysis on the effects of  $\eta$ ,  $l_0$  and  $L_0$  to the system performance is obtained from the simulation results. Finally, a comparison between the proposed system with the IM-based OFDM FSO system is discussed.

### 4.3.2.1 Theoretical Analysis

In the proposed system, at the OFDM demodulator the desired signal power for  $n$ th subcarrier can be expressed as:

$$S_n = \frac{1}{2}m_n^2 I^2, n = 1, 2, 3, \dots, N, \quad (4.27)$$

where  $m_n$  denotes the optical modulation index (OMI) for the  $n$ th subcarrier.  $N$  represents the total number of subcarriers.  $I$  is the direct current component of the signal:

$$I = \frac{1}{2}P_m = \frac{1}{2}c\varepsilon E_Y^2. \quad (4.28)$$

Hence, the total desired signal power is:

$$S = \sum_{n=1}^N S_n, n = 1, 2, 3, \dots, N. \quad (4.29)$$

Considering the total noise in the CPoIM-based OFDM FSO system is consist of the AWGN, the intermodulation distortion (IMD) and the polarization distortion:

$$N_{Total} = N_{AWGN} + N_{IMD} + N_{PolD}. \quad (4.30)$$

The  $N_{AWGN}$  is derived from the AWGN  $n_X$  which is mentioned in section 3. Firstly, considering the thermal noise, the shot noise and the relative intensity noise (RIN) are the components of the AWGN [6] and the value of  $n_X$  can be expressed as:

$$n_X = N_{th} + N_{shot} + N_{RIN}, \quad (4.31)$$

where

$$N_{th} = \frac{4K_B T_{abs} F}{T_s R_L}, N_{shot} = \frac{2q\rho\eta CI}{T_s}, N_{RIN} = \frac{RIN \cdot (\rho\eta CI)^2}{T_s}, \quad (4.32)$$

where  $K_B$  denotes the Boltzmann's constant,  $T_{abs}$  is the absolute temperature,  $F$  represents the noise figure of the receiver electronics,  $R_L$  is the  $PD$  load resistor, and  $q$  denotes the electron charge.  $T_s$  is the signal duration.  $RIN$  denotes relative intensity noise. After passing the multiplier, we get the  $N_{AWGN}$  as:

$$N_{AWGN} = \frac{n_X}{\rho\eta C} = \frac{4K_B T_{abs} F}{T_s R_L \rho\eta C} + \frac{2qI}{T_s} + \frac{RIN \cdot \rho\eta CI^2}{T_s}. \quad (4.33)$$

The IMD is usually caused by the amplifier's nonlinearity and dominated by its third order. Similar analysis as the AWGN, for  $n$ th subcarrier the IMD noise can be approximated to [6]:

$$N_{IMD,n} = \frac{\rho\eta C}{2} \left[ \frac{3}{4}a_3 m_n^3 D_2(N, n) + \frac{3}{2}a_3 m_n^3 D_3(N, n) \right]^2 \cdot I^2, \quad (4.34)$$

where  $a_3$  denotes the third order IMD. When  $N$  is large,  $D_2(N, n)$  and  $D_3(N, n)$  are defined by [6]:

$$\begin{cases} D_2(N, n) = \frac{1}{2} \left\{ N - 2 - \frac{1}{2} [1 - (-1)^N] \cdot (-1)^n \right\} \\ D_3(N, n) \cong \frac{n}{2}(N - n + 1) + \frac{1}{4} [(N - 3)^2 - 5]. \end{cases} \quad (4.35)$$

And the total IMD can be expressed as:

$$N_{IMD} = \sum_{n=1}^N N_{IMD,n}, n = 1, 2, 3, \dots, N. \quad (4.36)$$

The signal current with the effects of polarization distortion can be expressed as:

$$I_{PolD} = \frac{1}{2} \rho c \varepsilon [(E_X + \Delta E_X)^2 + E_Y^2]. \quad (4.37)$$

We should note that  $\Delta\theta$  included in  $\Delta X$  is a very small value. The power of polarization distortion can be calculated as:

$$N_{PolD} = \frac{1}{2} [(I_{PolD})^2 - I^2 (1 + \cot^2\theta)^2] \cong 2I^2 \cdot \Delta\theta \cdot \cot\theta (1 + \cot^2\theta)^2. \quad (4.38)$$

Therefore, the instantaneous SNR in the CPolM-based OFDM FSO system can be represented as the ratio:

$$SNR(\theta, \Delta\theta, C, I) = \frac{S}{N_{Total}}. \quad (4.39)$$

Considering the OFDM signal with M-QAM modulation ( $M = 2^{2t}, t = 1, 2, \dots$ ), the instantaneous SER is given by:

$$SER(\theta, \Delta\theta, C, I) = \frac{2(\sqrt{M} - 1)}{\sqrt{M}} \operatorname{erfc} \left( \sqrt{\frac{3SNR(\theta, \Delta\theta, C, I)}{2(M - 1)}} \right). \quad (4.40)$$

Assuming  $\theta$  follows uniform distribution, the average SNR and the average SER can be calculated as:

$$\langle SNR(I, \theta_{max}, \theta_{min}) \rangle = \frac{1}{\theta_{max} - \theta_{min}} \int_{\theta_{min}}^{\theta_{max}} \int_{-2\pi}^{2\pi} \int_0^{+\infty} SNR(\theta, \Delta\theta, C, I) f_{\Delta\theta}(\Delta\theta) f_C(C) dC d\Delta\theta d\theta, \quad (4.41)$$

$$\langle SER(I, \theta_{max}, \theta_{min}) \rangle = \frac{1}{\theta_{max} - \theta_{min}} \int_{\theta_{min}}^{\theta_{max}} \int_{-2\pi}^{2\pi} \int_0^{+\infty} SER(\theta, \Delta\theta, C, I) f_{\Delta\theta}(\Delta\theta) f_C(C) dC d\Delta\theta d\theta, \quad (4.42)$$

where  $\theta_{max}$ ,  $\theta_{min}$  represent the maximum and minimum value of  $\theta$ . We set  $\theta_{min} = 45^\circ$ ,  $\theta_{max} = 135^\circ$  and rewrite equation (33), (34) as:

$$\langle SNR \rangle = \frac{2}{\pi} \int_{\frac{\pi}{4}}^{\frac{3\pi}{4}} \int_{-2\pi}^{2\pi} \int_0^{+\infty} SNR(\theta, \Delta\theta, C, I) f_{\Delta\theta}(\Delta\theta) f_C(C) dC d\Delta\theta d\theta \quad (4.43)$$

$$\langle SER \rangle = \frac{2}{\pi} \int_{\frac{\pi}{4}}^{\frac{3\pi}{4}} \int_{-2\pi}^{2\pi} \int_0^{+\infty} SER(\theta, \Delta\theta, C, I) f_{\Delta\theta}(\Delta\theta) f_C(C) dC d\Delta\theta d\theta \quad (4.44)$$

The outage probability  $P_{out}$  is another important parameter in evaluating the communication link performance. When the instantaneous SNR lower than a threshold  $SNR_{th}$ , the communication can be seen as failed. Thus, the  $P_{out}$  can be defined as:

$$P_{out} = P[SNR(\theta, \Delta\theta, C, I) < SNR_{th}]. \quad (4.45)$$

#### 4.3.2.2 Numerical Results Analysis

In this section, we will give some simulation results to analyze the performance of the CPolM-based OFDM FSO system. Furthermore, a comparison between the proposed system and IM-based OFDM FSO system will be presented. The simulation parameters can be found in Table 4.3.

Table 4.3 Simulation Parameters

Parameter	Value
Transmission Distance ( $L$ )	$2km$
Optical Wavelength ( $\lambda$ )	$1550nm$
Number of Subcarriers ( $N$ )	$1024$
Symbol Duration ( $T_s$ )	$1008ns$
Absolute Temperature ( $T_{abs}$ )	$300K$
PD Load Resistor ( $R_L$ )	$50\Omega$
Detector Responsivity ( $\rho$ )	$0.8A/W$
Relative Intensity Noise ( $RIN$ )	$-130dB/Hz$
Third Order IMD ( $a_3$ )	$9 \times 10^{-4}$
Inner Scale of Turbulence ( $l_0$ )	$1mm$
Outer Scale of Turbulence ( $L_0$ )	$10m$
Optical Modulation Index for the nth Subcarrier ( $m_n$ )	$0.1\%$
Noise Figure of The Receiver Electronics ( $F$ )	$2dB$

Figure 4.14 presents the effects of the ratio  $\eta$  to the proposed system. The trend of curves clearly shows that increase the value of  $\eta$  can reduce the error probability level of the system. Especially, when turbulence in weak region, the improvement is significant. That means the system designer should increase the value of  $\eta$  as

much as possible, on the premise of no miscalculation in the comparing circuit. We can also find that system performance is sensitive to the turbulence strength. With  $C_n^2$  increasing, the turbulence getting stronger,  $\langle \text{SER} \rangle$  keeps deteriorating. Under certain turbulence strength,  $\langle \text{SER} \rangle$  will be improved when we increase the average received power  $\langle P_r \rangle$ .

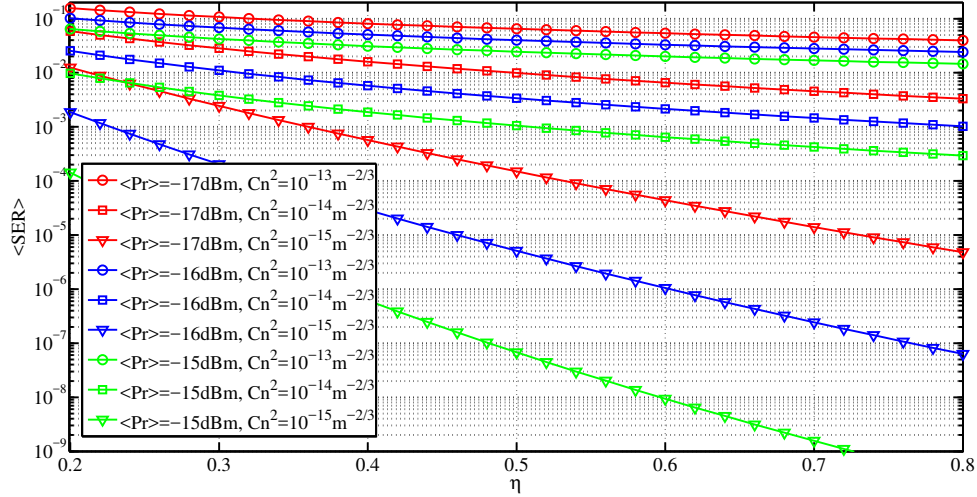
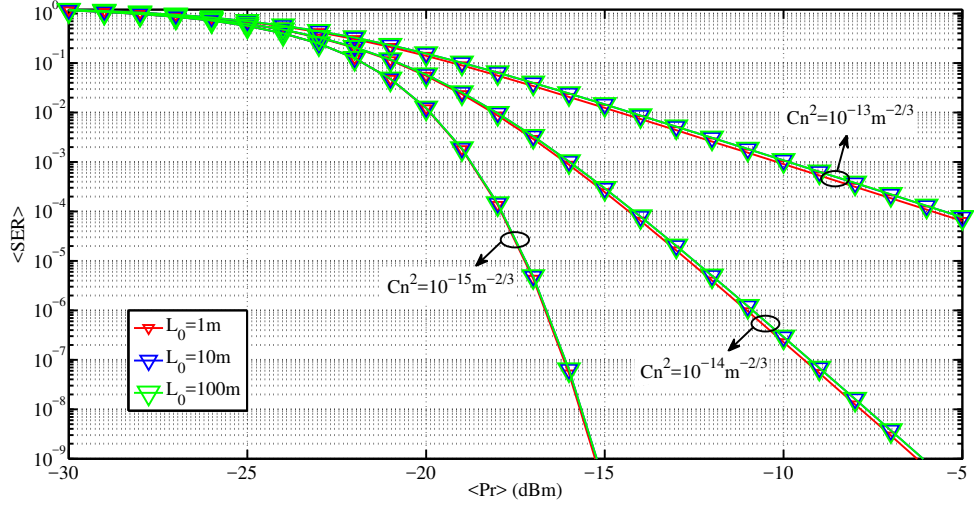


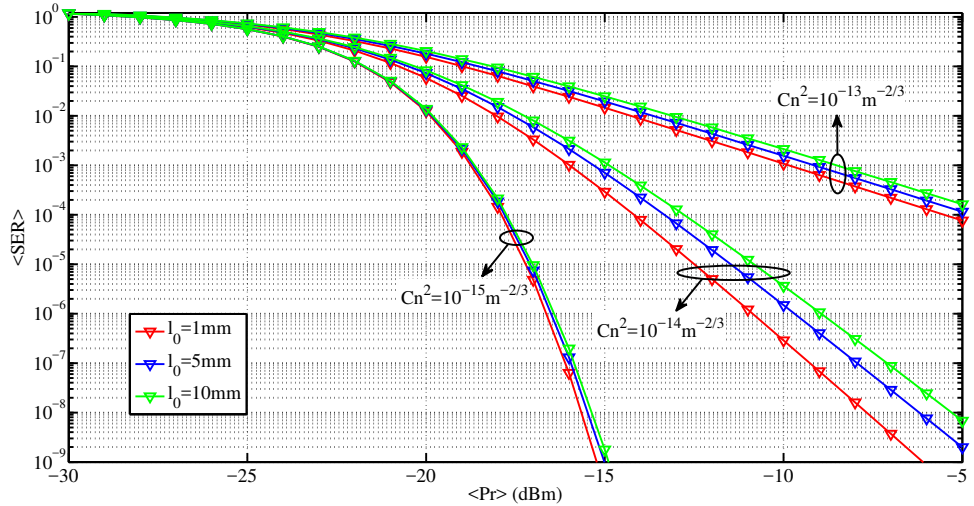
Figure 4.14 Effects of  $\eta$  to The  $\langle \text{SER} \rangle$  Performance of CPolM-Based OFDM FSO System Transmitting 16-QAM Signal. [6]

Figure 4.15 shows the performance of the proposed system under different outer-scale  $L_0$  and inner-scale  $l_0$ . From Figure 4.15.(a) we can find that curves denoting different  $L_0$  effects are overlapped, which means  $L_0$  has little impact on the system performance. On the other hand,  $l_0$  affects the system performance obviously which is presented in Figure 4.15.(b). It's worth noting that with  $l_0$  increasing, the polarization fluctuation of the optical wave will be reducing based on Equation (13). It should have led to a deterioration in the system. However, we can see the opposite trend in Figure 4.15.(b). The reason is the intensity fluctuation performs much more dominated in comparison to the polarization fluctuation.

Figure 4.16 shows a comparison of  $\langle \text{SER} \rangle$  versus  $\langle P_r \rangle$  between the CPolM- and IM-based OFDM FSO system transmitting 16-QAM signal under different turbulence regimes. We can clearly find that: The performance of both systems are sensitive to the turbulence effects. When  $\eta = 0.5$ , the CPolM-based system performs better than the IM-based system under the moderate-to-strong turbulence ( $C_n^2 = 10^{-14}\text{m}^{-2/3}, 10^{-13}\text{m}^{-2/3}$ ). The result is inverse when  $\langle P_r \rangle$  less than  $-14\text{dBm}$



(a)  $l_0=1\text{mm}$

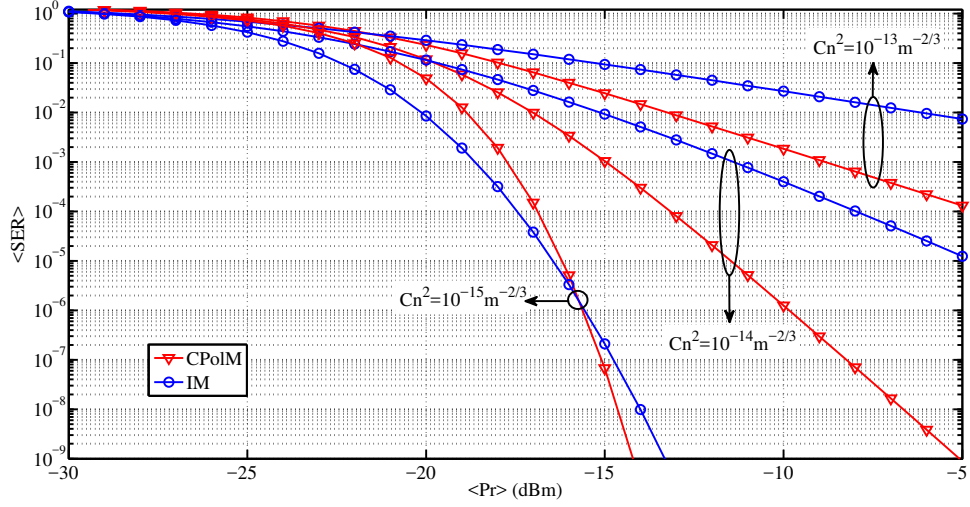


(b)  $L_0=10\text{m}$

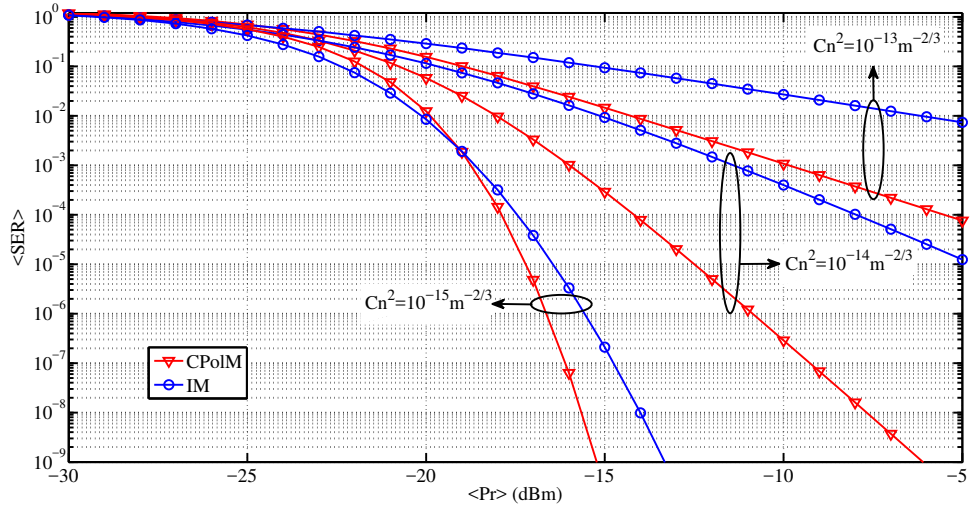
Figure 4.15 Effects of  $L_0$  and  $l_0$  to The  $\langle \text{SER} \rangle$  Performance of CPoIM-Based OFDM FSO System Transmitting 16-QAM Signal. [6]

under the weak turbulence ( $C_n^2 = 10^{-15} \text{m}^{-2/3}$ ) since a half of the signal power in the CPoIM-based system are occupied by the comparing circuit. However, when  $\langle P_r \rangle$  increasing over  $-14 \text{dBm}$ , the CPoIM-based system performs superior. When  $\eta$  equals to 0.8, the performance of the CPoIM-based system has a significant advantage.

For a fixed  $\langle P_r \rangle = -10 \text{dBm}$ . We plot the outage probability  $P_{out}$  versus variational threshold  $\text{SNR}_{th}$  in Figure 9 and compare the results between the CPoIM- and the IM-based OFDM FSO system transmitting 16-QAM signal under different turbulence



(a)  $\eta = 0.5$

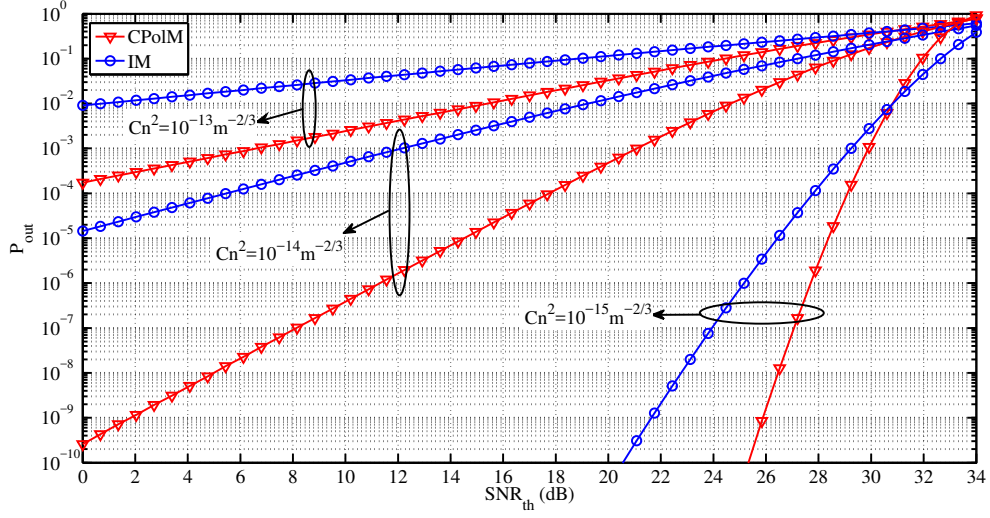


(b)  $\eta = 0.8$

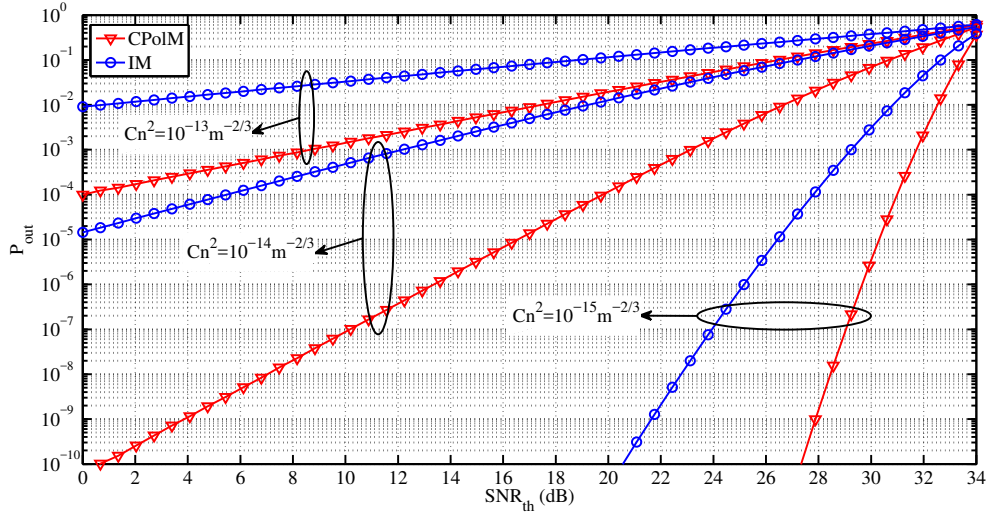
Figure 4.16 Comparison of  $\langle \text{SER} \rangle$  Versus  $\langle P_r \rangle$  in the CPolM- and IM-Based OFDM FSO System Transmitting 16-QAM Signal. [6]

regimes. It comes to the similar conclusion to Figure 8. Although still sensitive to the turbulence condition, the CPolM-based system has a significant improvement to the traditional IM-based system. Further, the increasing  $\eta$  can also reduce  $P_{out}$  of the proposed system.

In this section, we propose a CPolM-based OFDM FSO system, establish the transceiver configuration and the mathematic models to describe the system performance under the turbulence channel. We conduct the simulation to analyze the



(a)  $\eta = 0.5$



(b)  $\eta = 0.8$

Figure 4.17 Comparison of The  $P_{out}$  in The CPoIM- and IM-Based OFDM FSO System Transmitting 16-QAM Signal. [6]

performance of the proposed system and give a comparison with the conventional IM-based OFDM FSO system. The numerical results show that the CPoIM-based OFDM FSO system has a significant potential in overcoming the channel fading caused by atmospheric turbulence.

## 4.4 CPolSK-Based FSO System Working in Space-to-Ground Channel

In the past few years, more and more countries start to realize that the FSO system possesses a huge superiority in the extra-long distance signal transmissions, such as the deep space communications.

FSO system uses laser as carrier which provides a higher data rate and a wider bandwidth than the radio frequency (RF) system. Inherent narrow laser beam results a concentrated spot size in the receiving plane which represents a vast improvement of the power density after a long-distance transmission. Generally, compared to an RF antenna, an FSO telescope is more portable and more energy efficient. These are all remarkable advantages in the deep space system designing [14, 30, 36].

Conventional FSO systems modulate signals on the optical intensity which is highly sensitive to the atmospheric conditions. These effects could cause a serious channel fading in FSO links [2, 9–11, 17, 30].

In contrast, the polarization state of the optical wave is a much more stable property while propagating through the atmosphere which encourages us to develop the polarization modulation based FSO system.

However, neither the CPolM-based nor the PolSK-based FSO system is suitable in deep space communication. The rotation of a satellite will lead to an angle misalignment of the linear polarization state detection. Thus, we suppose to use the left and right circular polarized light represent datas '1' and '0', respectively.

In this section, we establish the mathematic model to describe the performance of CPolSK-based FSO system working in the space-to-ground channel. By running the simulations we analyze the related influence elements and give a comparison with the OOK-based FSO system.

### 4.4.1 Space-to-Ground FSO Channel

#### 4.4.1.1 Intensity Fluctuation

In the space-to-ground path, the atmospheric channel property is inhomogeneous and non-isotropic. The index of the refraction structure  $C_n^2$  is related to altitude  $h$ . A widely accepted model for the description of  $C_n^2$  is the so-called Hufnagel-Valley (H-V) model represented as [1]:

$$\begin{aligned} C_n^2(h) = & 0.00594(w/27)^2(10^{-5}h)^{10}exp(-h/1000) \\ & + 2.7 \times 10^{-16}exp(-h/1500) + C_n^2(0)exp(-h/100). \end{aligned} \tag{4.46}$$

where  $w$  is the pseudo-wind in the unit m/s and  $C_n^2(0)$  is a nominal value of  $C_n^2$  at the ground in  $m^{-2/3}$ . Thus, the vertical Rytov variance from the altitude  $h_0$  to  $H$  can be given as:

$$\sigma_R^2 = 2.25k^{7/6} \int_{h_0}^H (h - h_0)^{5/6} C_n^2(h) dh. \quad (4.47)$$

We set  $h_0$  as 0m and  $H$  as 20km, since normally channel over 20km can be regarded as a vacuum environment.

The Gamma-Gamma distribution (as introduced in Chapter 2) is utilized for describing the optical intensity fluctuation. It has been proved to be accurate not only in the weak turbulence region, but also the moderate-to-strong turbulence region.

#### 4.4.1.2 Polarization Fluctuation

According to the analysis in Chapter 2, the variance of linear polarization state while an optical wave propagating through the homogeneous and isotropic turbulence can be expressed as:

$$\sigma_{\Delta\theta}^2 = \frac{0.007C_n^2\pi L}{k^2} \left( l_0^{-\frac{7}{3}} - L_0^{-\frac{7}{3}} \right), \quad (4.48)$$

where  $\Delta\theta$  denotes the distortion of the polarized direction,  $L$  is the transmission distance,  $k$  denotes the optical wave number,  $l_0$  is the inner scale of turbulence in the order from 1mm to 10mm and  $L_0$  is the outer scale of turbulence in meter-scale.

In the space-to-ground channel, since  $C_n^2$  is no longer a constant, the equation above should be rewritten in integral form as:

$$\sigma_{\Delta\theta}^2 = \int_{h_0}^H \frac{0.007C_n^2(h)\pi}{k^2} \left( l_0^{-\frac{7}{3}} - L_0^{-\frac{7}{3}} \right) dh. \quad (4.49)$$

Instead of the linear polarized light, the circular polarized light is more suitable for the deep space communications coping with the rotation of a satellite. In order to describe the circular polarization characters concisely, we introduce the normalized Stocks parameters defined as:

$$\begin{cases} S_1 = \frac{\langle E_x^* E_x \rangle - \langle E_y^* E_y \rangle}{\langle E_x^* E_x \rangle + \langle E_y^* E_y \rangle} = \frac{\langle E_x^* E_x \rangle - \langle E_y^* E_y \rangle}{P}, \\ S_2 = \frac{\langle E_x^* E_y \rangle + \langle E_y^* E_x \rangle}{\langle E_x^* E_x \rangle + \langle E_y^* E_y \rangle} = \frac{\langle E_x^* E_y \rangle + \langle E_y^* E_x \rangle}{P}, \\ S_3 = \frac{j [\langle E_y^* E_x \rangle - \langle E_x^* E_y \rangle]}{\langle E_x^* E_x \rangle + \langle E_y^* E_y \rangle} = \frac{j [\langle E_y^* E_x \rangle - \langle E_x^* E_y \rangle]}{P}, \end{cases} \quad (4.50)$$

where  $E_x$  and  $E_y$  denote the optical wave electric vector in X and Y directions. The asterisk indicates the complex conjugate.  $P$  means the intensity of the optical wave. The vectors  $(S_1, S_2, S_3) = (0, 0, 1)$  and  $(S_1, S_2, S_3) = (0, 0, -1)$ , corresponding to the North and South Pole on *Poincaré* sphere, denote the right and the left circularly polarized light, respectively. In this method,  $S_3$  is the parameter we most care about and the reason will be discussed in the next section.

Consider the right circularly polarized light with polarization fluctuation, the electric vector of X and Y polarized components can be expressed as:

$$\begin{cases} E_x = E_0 + jE'_x e^{j(\phi + \phi_x)}, \\ E_y = jE_0 e^{j\phi} + E'_y e^{j\phi_y}, \end{cases} \quad (4.51)$$

where  $E_0$  and  $jE_0 e^{j\phi}$  are the original complex electric amplitude of X and Y polarized components. The parameter  $\phi$ , following zero-mean Gaussian distribution  $N(0, \sigma_\phi^2)$ , denotes the phase difference caused by the atmospheric turbulence.  $jE'_x e^{j(\phi + \phi_x)}$  and  $E'_y e^{j\phi_y}$  are the distorted complex electric amplitude derived from  $jE_0 e^{j\phi}$  and  $E_0$ , respectively.  $\phi_x$  and  $\phi_y$  are arbitrary phase transformations. The corresponding Stokes parameters can be represented as:

$$\begin{cases} S_1 = \frac{\langle E_x^* E_x \rangle - \langle E_y^* E_y \rangle}{\langle E_x^* E_x \rangle + \langle E_y^* E_y \rangle} = \frac{E_x'^2 - E_y'^2}{2E_0^2 + E_x'^2 + E_y'^2} = \frac{V_x^2 - V_y^2}{2 + V_x^2 + V_y^2}, \\ S_2 = \frac{\langle E_x^* E_y \rangle + \langle E_y^* E_x \rangle}{\langle E_x^* E_x \rangle + \langle E_y^* E_y \rangle} = \frac{-2E_0^2 \sin(\phi)}{2E_0^2 + E_x'^2 + E_y'^2} = \frac{-2 \sin(\phi)}{2 + V_x^2 + V_y^2}, \\ S_3 = \frac{j [\langle E_y^* E_x \rangle - \langle E_x^* E_y \rangle]}{\langle E_x^* E_x \rangle + \langle E_y^* E_y \rangle} = \frac{2E_0^2 \cos(\phi)}{2E_0^2 + E_x'^2 + E_y'^2} = \frac{2 \cos(\phi)}{2 + V_x^2 + V_y^2}, \end{cases} \quad (4.52)$$

where  $V_x = E_x/E_0 = \Delta\theta_x$  and  $V_y = E_y/E_0 = \Delta\theta_y$  are two independent polarization difference following zero-mean Gaussian distribution  $N(0, \sigma_{V_x}^2)$  and  $N(0, \sigma_{V_y}^2)$  as defined in section 2.3.3.

Based on the principle of interchangeability,

$$\sigma_V^2 = \sigma_{V_x}^2 = \sigma_{V_y}^2. \quad (4.53)$$

Moreover,  $V_x^2/\sigma_{V_x}^2$  and  $V_y^2/\sigma_{V_y}^2$  are following Chi-squared distribution with one degree

of freedom:

$$\begin{cases} \chi^2(V_x^2/\sigma_{V_x}^2; 1) = \frac{1}{\sqrt{2\pi V_x^2/\sigma_{V_x}^2}} \cdot \exp(-V_x^2/2\sigma_{V_x}^2), \\ \chi^2(V_y^2/\sigma_{V_y}^2; 1) = \frac{1}{\sqrt{2\pi V_y^2/\sigma_{V_y}^2}} \cdot \exp(-V_y^2/2\sigma_{V_y}^2), \end{cases} \quad (4.54)$$

and,

$$\begin{cases} \left\langle \frac{V_x^2}{\sigma_{V_x}^2} \right\rangle = \left\langle \frac{V_y^2}{\sigma_{V_y}^2} \right\rangle = 1, \\ Var \left[ \frac{V_x^2}{\sigma_{V_x}^2} \right] = Var \left[ \frac{V_y^2}{\sigma_{V_y}^2} \right] = 2. \end{cases} \quad (4.55)$$

Thus,

$$\begin{cases} \langle V_x^2 \rangle = \langle V_y^2 \rangle = \sigma_V^2, \\ Var [V_x^2] = Var [V_y^2] = 2\sigma_V^4. \end{cases} \quad (4.56)$$

The denominators of three Stokes parameters have the identical form “ $2+V_x^2+V_y^2$ ”. Since  $V_x$  and  $V_y$  are both following  $N(0, \sigma_V^2)$ , the sum of squares “ $V_x^2/\sigma_V^2 + V_y^2/\sigma_V^2$ ” is following Chi-squared distribution with 2 degree of freedom:

$$\chi^2(V^2/\sigma_V^2; 2) = \frac{1}{2} \exp\left(-\frac{V^2}{2\sigma_V^2}\right), \quad (4.57)$$

and,

$$\begin{cases} \left\langle \frac{V_x^2}{\sigma_{V_x}^2} + \frac{V_y^2}{\sigma_{V_y}^2} \right\rangle = 2, \\ Var \left[ \frac{V_x^2}{\sigma_{V_x}^2} + \frac{V_y^2}{\sigma_{V_y}^2} \right] = 4. \end{cases} \quad (4.58)$$

Thus

$$\begin{cases} \langle 2 + V_x^2 + V_y^2 \rangle = 2 + 2\sigma_V^2, \\ Var [2 + V_x^2 + V_y^2] = 4\sigma_V^4. \end{cases} \quad (4.59)$$

Since  $\phi \sim N(0, \sigma_\phi^2)$ , we can calculate the mean value of  $e^{j\phi} = \cos(\phi) + j \sin(\phi)$  as:

$$\begin{aligned} \langle e^{j\phi} \rangle &= \int_{-\infty}^{+\infty} e^{j\phi} \cdot \frac{1}{\sigma_\phi \sqrt{2\pi}} \exp\left(-\frac{\phi^2}{2\sigma_\phi^2}\right) d\phi \\ &= e^{(j\sigma_\phi)^2/2} \cdot \int_{-\infty}^{+\infty} \frac{1}{\sigma_\phi \sqrt{2\pi}} \exp\left[-\frac{(\phi - j\sigma_\phi^2)^2}{2\sigma_\phi^2}\right] d\phi \\ &= e^{-\sigma_\phi^2/2}. \end{aligned} \quad (4.60)$$

Thus, the imaginary part  $\langle \sin(\phi) \rangle = 0$  and the real part  $\langle \cos(\phi) \rangle = e^{-\sigma_\phi^2/2}$ . The variance of  $\sin(\phi)$  and  $\cos(\phi)$  can be calculated as:

$$\begin{aligned} Var[\sin(\phi)] &= \langle \sin^2(\phi) \rangle - \langle \sin(\phi) \rangle^2 \\ &= \left\langle \frac{1}{2} [1 - \cos(2\phi)] \right\rangle - 0 \\ &= \frac{1}{2} (1 - e^{-2\sigma_\phi^2}), \end{aligned} \quad (4.61)$$

$$\begin{aligned} Var[\cos(\phi)] &= \langle \cos^2(\phi) \rangle - \langle \cos(\phi) \rangle^2 \\ &= \left\langle \frac{1}{2} [1 + \cos(2\phi)] \right\rangle - e^{-\sigma_\phi^2} \\ &= \frac{1}{2} (1 - e^{-\sigma_\phi^2})^2. \end{aligned} \quad (4.62)$$

Considering the physical interpretation of  $S_1$ ,  $S_2$  and  $S_3$ , we can conclude that when the right or left circularly polarized light propagates through the free space, its Stokes parameters  $S_1$  and  $S_2$  are following the identical distribution. Hence, we can obtain the following relations:

$$\langle S_1 \rangle = \langle S_2 \rangle, \quad (4.63)$$

$$Var[S_1] = Var[S_2], \quad (4.64)$$

which means

$$\langle V_x^2 - V_y^2 \rangle = \langle -2 \sin(\phi) \rangle, \quad (4.65)$$

$$Var[V_x^2 - V_y^2] = Var[-2 \sin(\phi)]. \quad (4.66)$$

Since  $V_x$  and  $V_y$  are interchangeable and  $\langle \sin(\phi) \rangle = 0$ , Equation(4.65) can be written as:

$$\langle V_x^2 - V_y^2 \rangle = \langle -2 \sin(\phi) \rangle = 0. \quad (4.67)$$

Based on Equation(4.59), variance of  $V_x^2 - V_y^2$  can be calculated as:

$$\begin{aligned} Var[V_x^2 - V_y^2] &= \langle (V_x^2 - V_y^2)^2 \rangle \\ &= \langle V_x^4 - 2V_x^2V_y^2 + V_y^4 \rangle \\ &= \langle V_x^4 \rangle + \langle V_y^4 \rangle - 2\langle V_x^2V_y^2 \rangle \\ &= Var[V_x^2] + \langle V_x^2 \rangle^2 + Var[V_y^2] + \langle V_y^2 \rangle^2 - 2\langle V_x^2V_y^2 \rangle \\ &= 4\sigma_V^4. \end{aligned} \quad (4.68)$$

The variance of  $[-2 \sin(\phi)]$  is:

$$\text{Var}[-2 \sin(\phi)] = 4\text{Var}[\sin(\phi)] = 2 \left(1 - e^{-2\sigma_\phi^2}\right) \quad (4.69)$$

Substituting the Equation(4.68), (4.69) into Equation(4.66) yields:

$$\sigma_\phi^2 = -\frac{1}{2} \ln(1 - 2\sigma_V^4). \quad (4.70)$$

Since  $\sigma_V^4$  is high-order minim, Equation(4.70) can be approximated to:

$$\sigma_\phi^2 = \sigma_V^4. \quad (4.71)$$

The distribution of the phase difference can be expressed as:

$$N_\phi(\phi) = \frac{1}{\sqrt{2\pi\sigma_\phi^2}} \exp\left(-\frac{\phi^2}{2\sigma_\phi^2}\right). \quad (4.72)$$

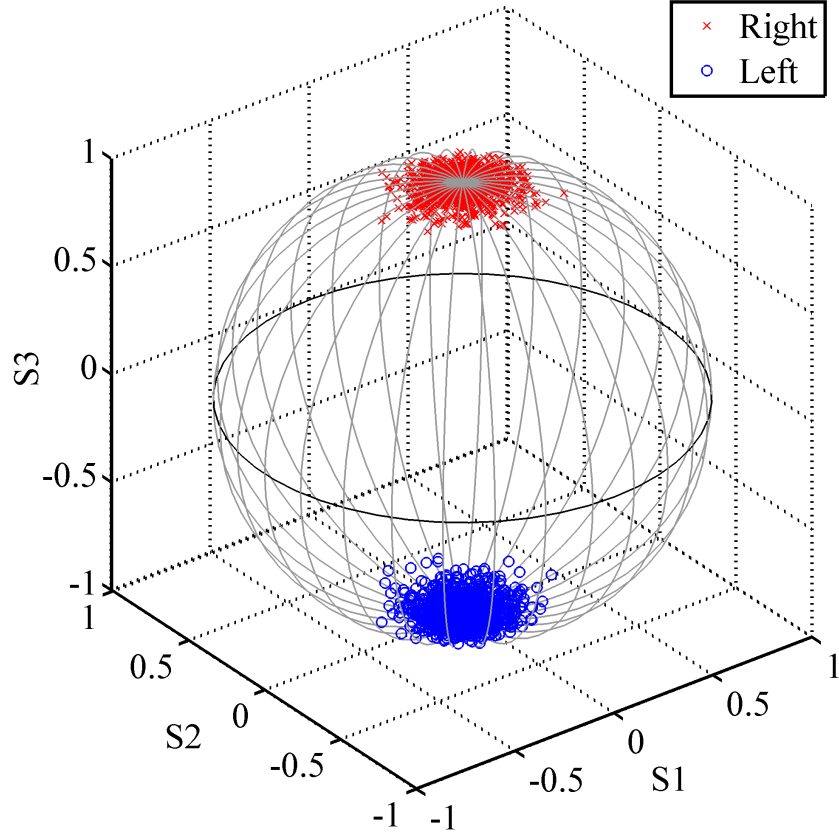


Figure 4.18 Polarization Characters of the CPolSK-Based FSO System Working in Space-to-Ground Links. [7]

By running a simulation to the Stocks parameters, we can have a vivid impression on the polarization fluctuation. Figure 4.18 shows the distortion of the Stocks parameters when the circular polarized light propagating through the space-to-ground channel. We can find that the distortion range of the parameter  $S_3$  is less than 1%.

#### 4.4.2 CPolSK-Based FSO System Structure

We will introduce the principle of the transceiver structures of the CPolSK-based FSO system at this segment. In order to visually view the optical processing, we will discuss the situation of transmitting the signal '1' and analyze the optical states in different parts of the system with considering the turbulence effects. Technical details about optical devices in this section are specified in [103–106].

##### 4.4.2.1 Transmitter

The transmitter structure of the CPolSK-based FSO system is illustrated in Figure 4.19. A polarizer is used to get the  $45^\circ$  polarized light. Then a polarization beam

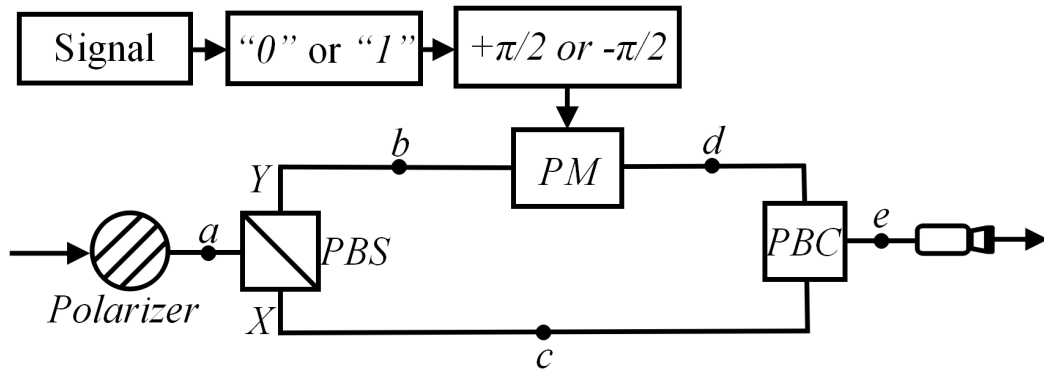


Figure 4.19 Diagram of the CPolSK-Based FSO System Transmitter. [7]

splitter ( $PBS$ ) splits the light into two orthogonal polarization directions components  $X$  and  $Y$ . Then the  $Y$  component will be modulated by a phase modulator ( $PM$ ). The  $PM$  can make a  $+\pi/2$  phase difference to the  $Y$  component light when the transmitted signal is '0' and make a  $-\pi/2$  phase difference when the signal is '1'. Finally, the  $X$  component light and  $Y$  component light are combined by a polarization beam combiner ( $PBC$ ) and transmitted through the space-to-ground channel.

When the signal is '1', the polarization states corresponding to the points  $a$ ,  $b$ ,  $c$ ,  $d$  and  $e$  in Figure 4.19 are given in Figure 4.20. Since the  $Y$  component light is

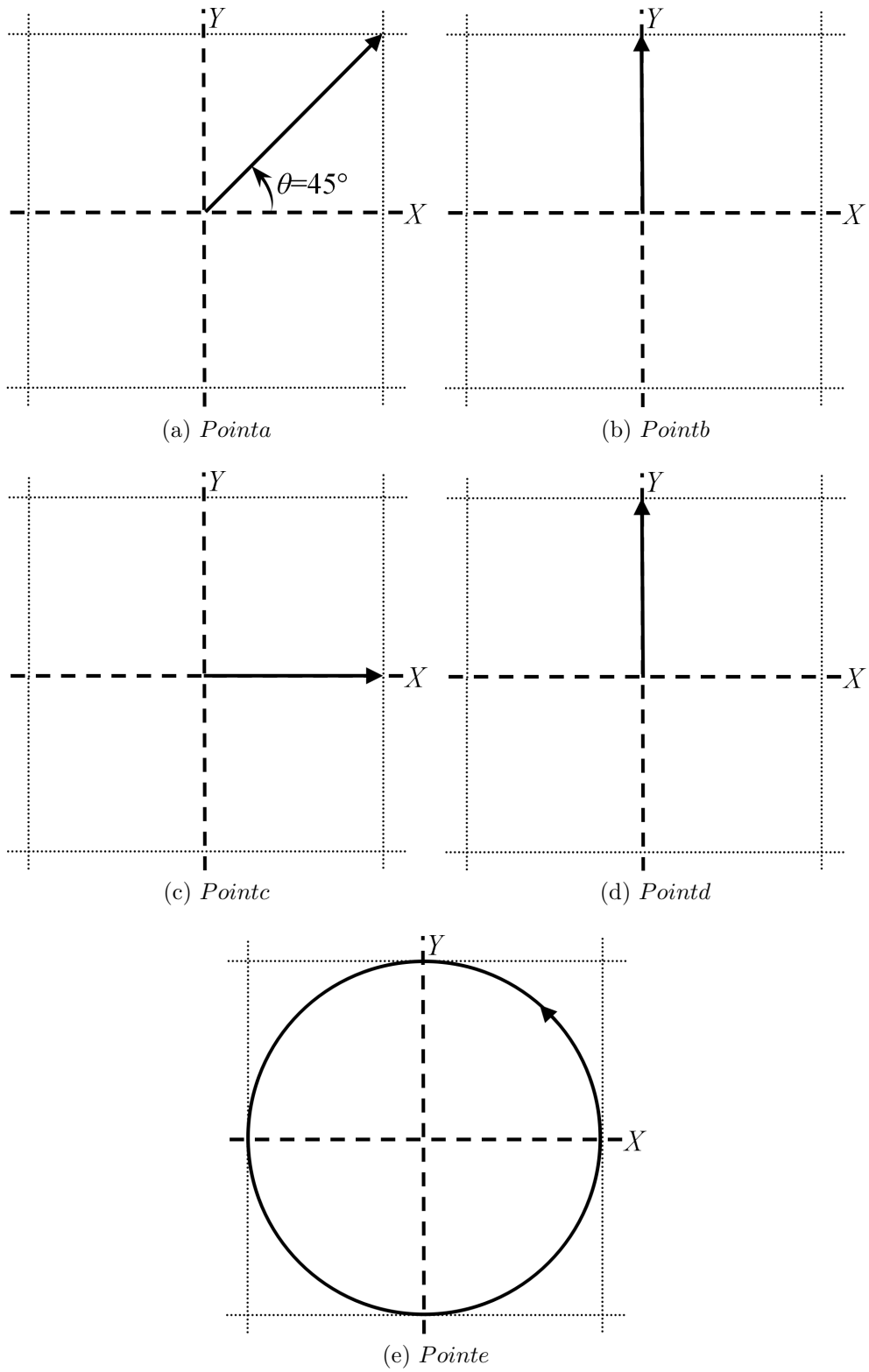


Figure 4.20 Polarization States in The Transmitter. [7]

having a  $-\pi/2$  phase changing, the combined light is left circle polarized as showed in Figure 4.20.(e).

#### 4.4.2.2 Receiver

The receiver structure of the CPolSK-based FSO system is illustrated in Figure 4.21.

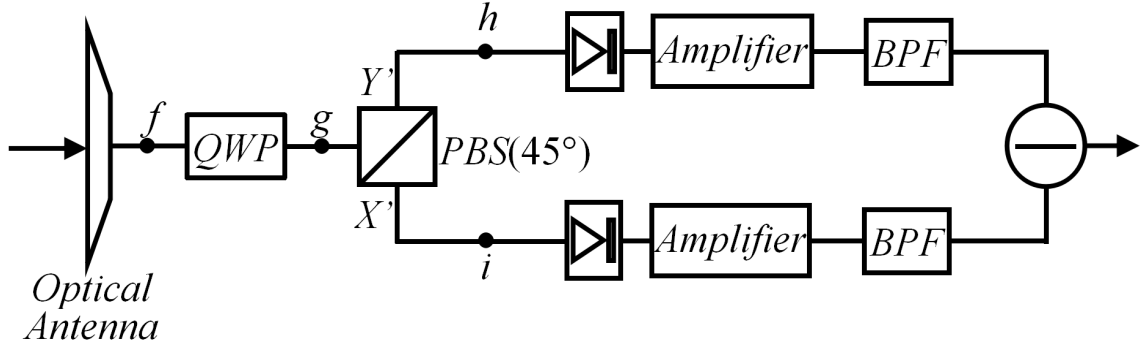


Figure 4.21 Diagram of the CPolSK-Based FSO System Receiver. [7]

After propagating through the space-to-ground atmospheric channel, the received optical intensity can be expressed as:

$$P_R = [\langle E_x^* E_x \rangle + \langle E_y^* E_y \rangle] \cdot C. \quad (4.73)$$

The optical signal is detected by an optical antenna and coupled into the optical fiber. The quarter wave plate (*QWP*) will give the *Y* component light a  $+\pi/2$  phase changing, thus the optical wave electric vector is converted to:

$$E = (E_x + jE_y) \cdot C^{\frac{1}{2}}. \quad (4.74)$$

We should notice that this *Y* direction has no need to be identical with the *Y* direction in the transmitter, since the received light is either left or right handed polarized. Then the light is split into two polarization components *X'* and *Y'* which have a  $45^\circ$  rotation from the *X* and *Y* directions corresponding to the *QWP*. The vectors  $E_{x'}$  and  $E_{y'}$  are given as:

$$\begin{cases} E_{x'} = \left[ \frac{\sqrt{2}}{2} E_x + j \frac{\sqrt{2}}{2} E_y \right] \cdot C^{\frac{1}{2}}, \\ E_{y'} = \left[ \frac{\sqrt{2}}{2} E_x - j \frac{\sqrt{2}}{2} E_y \right] \cdot C^{\frac{1}{2}}. \end{cases} \quad (4.75)$$

The optical intensity of the  $X'$  and  $Y'$  component light is converted into electric current  $I_{x'}$  and  $I_{y'}$  by two photo-detectors ( $PD$ ), respectively:

$$\begin{cases} I_{x'} = \rho \langle E_{x'}^* E_{x'} \rangle + n_{x'}, \\ I_{y'} = \rho \langle E_{y'}^* E_{y'} \rangle + n_{y'}, \end{cases} \quad (4.76)$$

where  $\rho$  is the responsivity of the  $PD$ s,  $n_{x'}$  and  $n_{y'}$  are related current noise. After passing through the amplifier and the band-pass filter ( $BPF$ ),  $I_{x'}$  and  $I_{y'}$  are doing  $I_{x'} - I_{y'}$  calculation in a subtracter:

$$I = I_{x'} - I_{y'} = GC\rho j [\langle E_x^* E_y \rangle - \langle E_y^* E_x \rangle] + n = -GS_3\rho P_R + n, \quad (4.77)$$

where  $n$  is current noise,  $G$  denotes gain of the amplifiers.

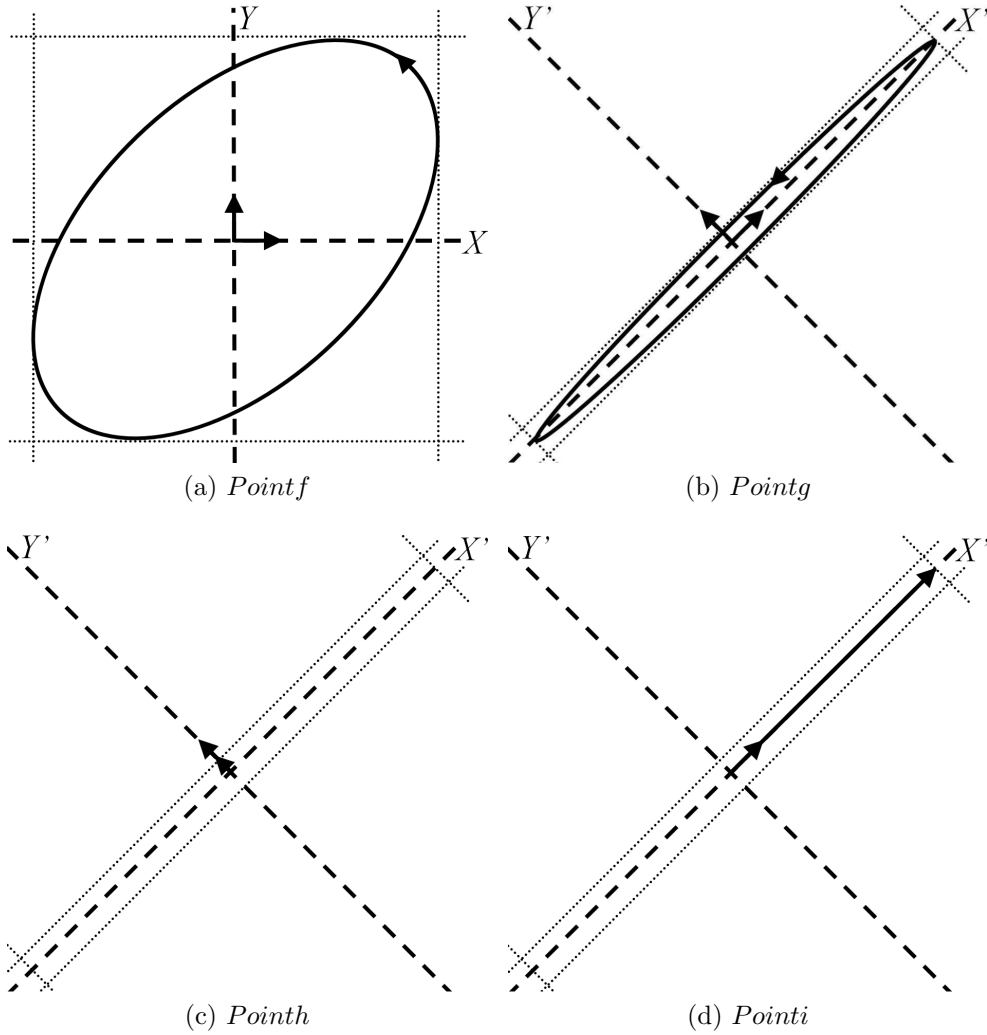


Figure 4.22 Polarization States in The Receiver. [7]

We can find that the desired signal is relative to one Stocks parameter ' $S_3$ '. If the result is positive, the received light manifesting a left handed polarization, thus the signal is '1'; if the result is negative, the received light manifesting a right handed polarization, thus the signal is '0'.

Figure 4.22 shows the polarization states corresponding to the points  $f$ ,  $g$ ,  $h$  and  $i$  in Figure 4.21, when the signal transmitted in Figure 4.20 is detected by the system receiver. The received optical wave as showed in Figure 4.22.(f) has suffered the scintillation, the depolarization and phase distortion while propagating through the space-to-ground atmospheric channel. Two vectors at the origin denote the depolarized light. The polarization state become elliptical from circular since the phase noise caused by the turbulence. When the  $Y$  component light has a  $+\pi/2$  phase changing, the polarization state is showed in Figure 4.22.(g) and is elliptical since the phase noise. The polarized and depolarized light are both split into  $X'$  and  $Y'$  directions as showed in Figure 4.22.(h) and Figure 4.22.(i). Since the intensity of the  $X'$  component light in Figure 4.22.(i) is stronger than the intensity of the  $Y'$  component light in Figure 4.22.(h), the subtraction result must be positive, which means the received signal is '1'.

### 4.4.3 System Performance

In this section, we propose the equations representing the proposed system performance, in terms of signal-noise-ratio (SNR), bit-error-ratio (BER) and the outage probability  $P_{out}$ . We run the simulation under different atmosphere conditions and give a comparison with the OOK-based FSO system.

#### 4.4.3.1 Theoretical Analysis

Based on Equation (4.77), power of the desired signal can be expressed as:

$$S_D = [-GS_3\rho P_R]^2 = [GS_3\rho\langle P_R\rangle C]^2. \quad (4.78)$$

The system noise is consider as Additive White Gaussian noise (AWGN) which is consist of the thermal noise, the shot noise and the relative intensity noise (RIN) [2]. The noise power is given as:

$$N_{AWGN} = N_{th} + N_{shot} + N_{RIN}, \quad (4.79)$$

where

$$\begin{cases} N_{th} = \frac{4K_B T_{abs} F}{T_s R_L}, \\ N_{shot} = \frac{2q |G S_3 \rho C \langle P_R \rangle|}{T_s}, \\ N_{RIN} = \frac{RIN \cdot [G S_3 \rho C \langle P_R \rangle]^2}{T_s}, \end{cases} \quad (4.80)$$

where  $K_B$  represents the Boltzmann's constant,  $T_{abs}$  denotes the absolute temperature,  $F$  is the noise figure of the receiver electronics,  $R_L$  denotes the  $PD$  load resistor, and  $q$  is the electron charge.  $T_s$  represents the signal duration.  $RIN$  denotes relative intensity noise.

The instantaneous SNR of the proposed system is given as:

$$SNR(I, C, S_3) = \frac{S_D}{N_{AWGN}}. \quad (4.81)$$

Signal processing of the CPolSK-based FSO system is equivalent to a binary bipolar baseband system. The instantaneous BER can be expressed as:

$$BER(I, C, S_3) = \frac{1}{2} \operatorname{erfc} \left( \sqrt{\frac{SNR}{2}} \right). \quad (4.82)$$

Based on the results of section 4.4.1, Stocks parameter  $S_3$  is varying within the range of 1% . Therefore, the approximate expressions of the average SNR and the average BER are given as:

$$\langle SNR(I) \rangle \approx \int_0^{+\infty} SNR(I, C, \langle S_3 \rangle) f_C(C) dC, \quad (4.83)$$

$$\langle BER(I) \rangle \approx \int_0^{+\infty} BER(I, C, \langle S_3 \rangle) f_C(C) dC. \quad (4.84)$$

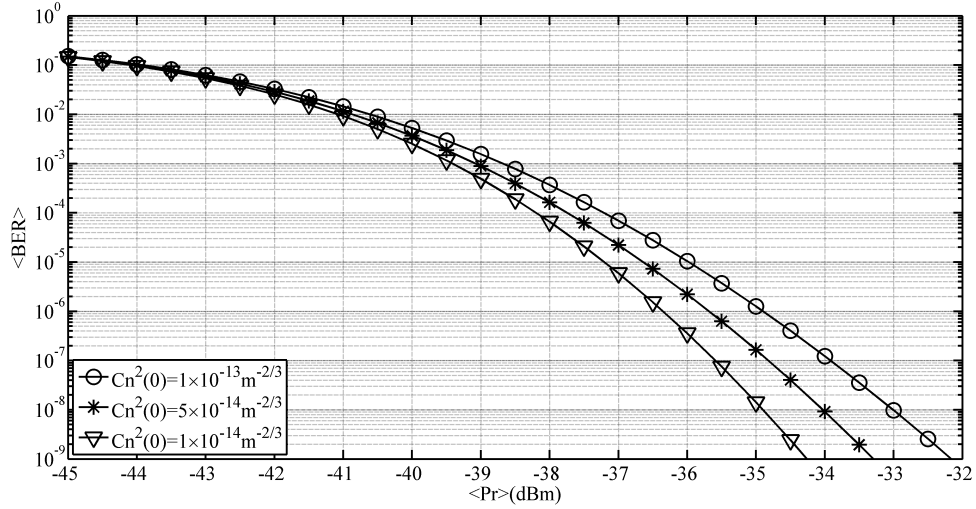
Another major parameter to evaluate the communication system performance is the outage probability  $P_{out}$  which is defined as the probability of the instantaneous SNR lower than the system threshold  $SNR_{th}$ . Therefore, the  $P_{out}$  should be expressed as:

$$P_{out} = P [SNR(I, C, S_3) < SNR_{th}]. \quad (4.85)$$

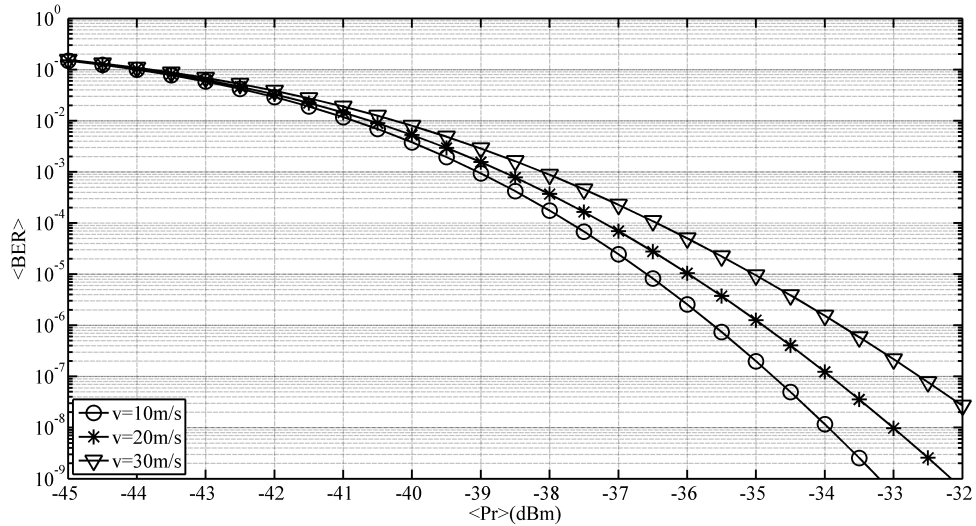
In this case, the communication can be seen as failed.

#### 4.4.3.2 Numerical Results Analysis

In this section, simulation results about the CPolSK-based FSO system performance working in space-to-ground channel are demonstrated. We compare the performance of the proposed system with the OOK-based FSO system under different atmospheric conditions. The simulation parameters can be found in Table 4.4.



(a)  $v = 20\text{m/s}$

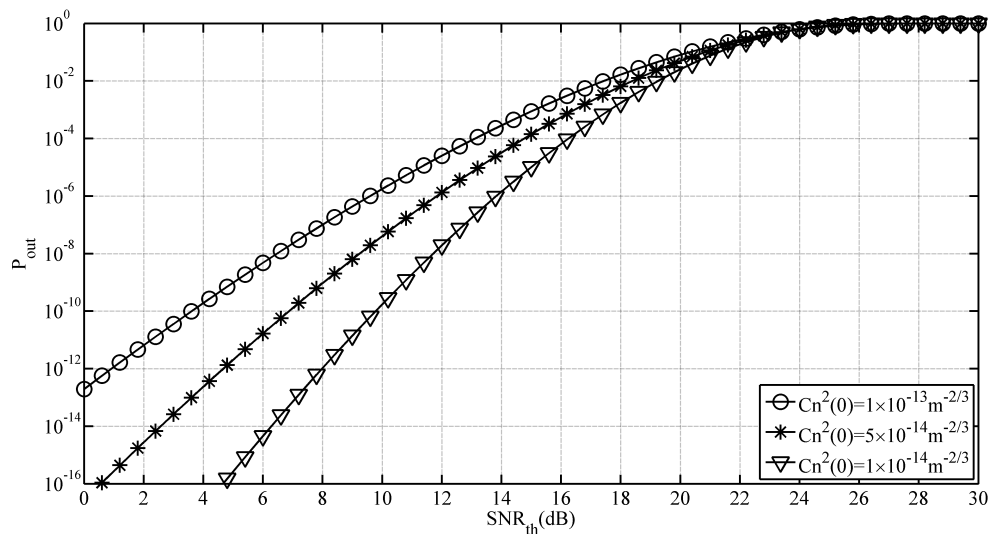


(b)  $C_n^2(0) = 1 \times 10^{-13}m^{-2/3}$

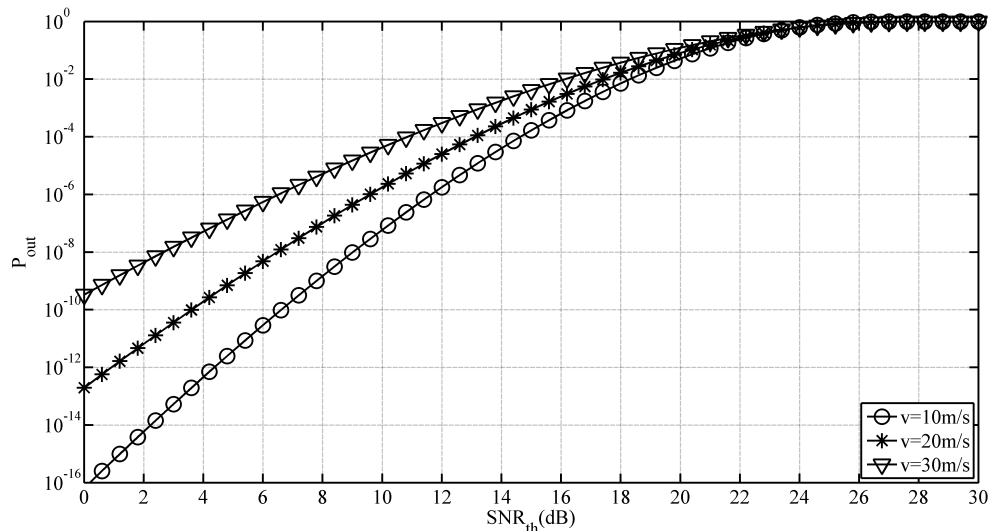
Figure 4.23 Effects of  $C_n^2(0)$  and  $v$  to The  $\langle BER \rangle$  Performance of CPolSK-Based FSO System Working in Space-to-Ground Channel. [7]

Figure 4.23 presents the effects of the  $C_n^2(0)$  and the pseudo-wind to the  $\langle BER \rangle$  performance of the proposed system working in the space-to-ground channel under

the varying average received optical power  $\langle P_r \rangle$ . We can find that an increasing of the received power can decrease the  $\langle BER \rangle$  of the system. The system performance is affected by the atmospheric conditions. In Figure 4.23.(a), when the pseudo-wind  $v$  is fixed on 20m/s, the  $\langle BER \rangle$  is rising with the  $C_n^2(0)$ . On the other hand, when the pseudo-wind is getting stronger, the  $\langle BER \rangle$  performance is deteriorating as showed in Figure 4.23.(b).



(a)  $v = 20m/s$

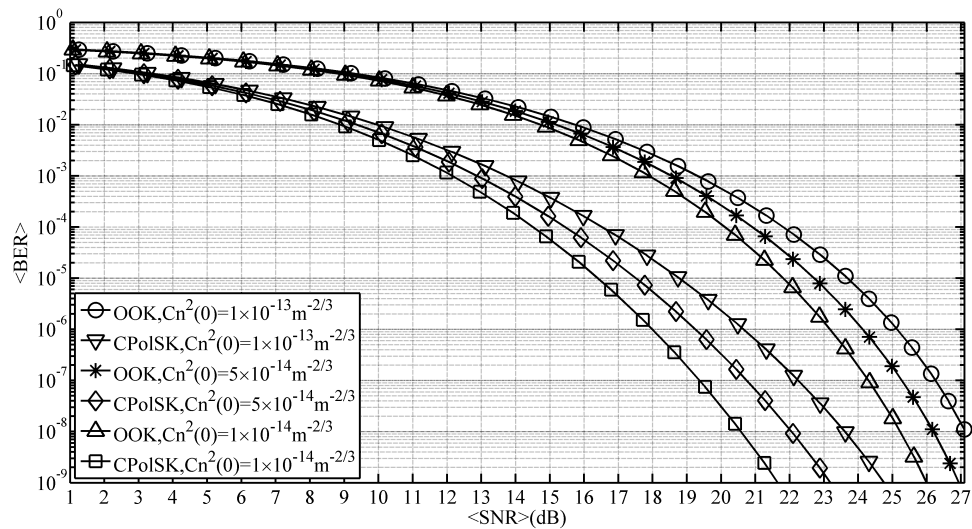


(b)  $C_n^2(0) = 1 \times 10^{-13}m^{-2/3}$

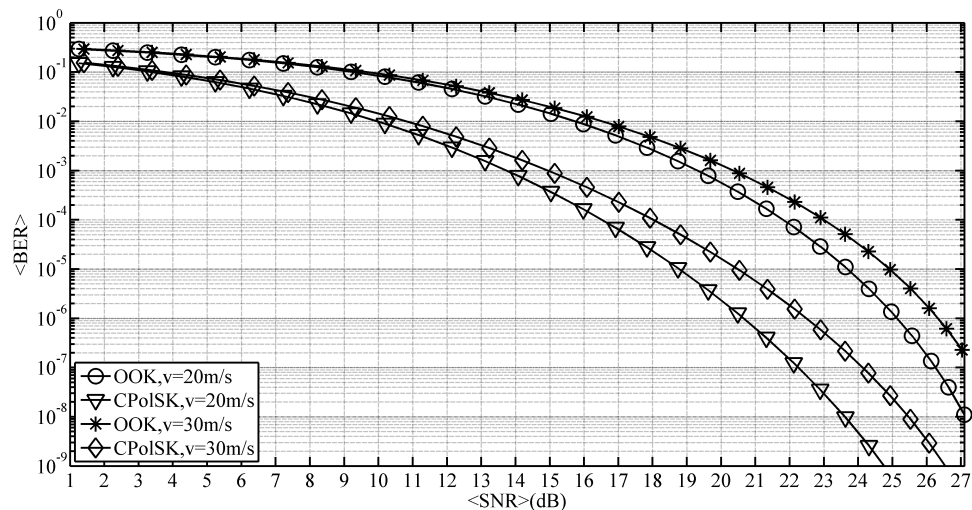
Figure 4.24 Effects of  $C_n^2(0)$  and  $v$  to The  $P_{out}$  Performance of CPolSK-Based FSO System Working in Space-to-Ground Channel. [7]

Figure 4.24 shows the effects of the  $C_n^2(0)$  and the pseudo-wind to the outage

probability  $P_{out}$  of the proposed system working in the space-to-ground channel under the varying threshold  $\langle SNR_{th} \rangle$ . In Figure 4.24.(a), when the  $C_n^2(0)$  becoming more intense, the system outage probability is rising. And in Figure 4.24.(b), it is clear that a stronger pseudo-wind will cause a higher  $P_{out}$ .



(a)  $v = 20m/s$



(b)  $C_n^2(0) = 1 \times 10^{-13}m^{-2/3}$

Figure 4.25 Comparison of  $\langle BER \rangle$  Versus  $\langle SNR \rangle$  in the CPolSK- and OOK-Based FSO System Working in Space-to-Ground Channel. [7]

Figure 4.25 presents a comparison of  $\langle BER \rangle$  versus  $\langle SNR \rangle$  between the CPolSK- and OOK-based FSO system working in the space-to-ground channel. The performance of both systems are sensitive to the turbulence effects. We can find that in the

same atmospheric condition, the OOK-based FSO system needs to provide a higher  $\langle SNR \rangle$  than the CPolSK-based FSO system in order to arrive at the same level of  $\langle BER \rangle$ .

Table 4.4 Simulation Parameters

Parameter	Value
Transmission Distance ( $L$ )	959.8km
Optical Wavelength ( $\lambda$ )	847nm
Symbol Duration ( $T_s$ )	0.1ns
Gain of the Amplifiers ( $G$ )	20dB
Absolute Temperature ( $T_{abs}$ )	300K
PD Load Resistor ( $R_L$ )	50 $\Omega$
Detector Responsivity ( $\rho$ )	0.8A/W
Relative Intensity Noise ( $RIN$ )	-130dB/Hz
Noise Figure of The Receiver Electronics ( $F$ )	2dB
Boltzmanns Constant ( $K_B$ )	1.38e <sup>-23</sup> J/K
Electron Charge ( $q$ )	1.602e <sup>-19</sup> C

In this section, we analyzed the performance of the CPolSK-based FSO link and establish the equations to describe the system performance working in the space-to-ground channel. We set reliable simulation parameters of the proposed system and give a comparison with the OOK-based FSO system. It is turned out that the CPolSK-based FSO system has a significant improvement in reducing the channel fading caused by the atmospheric turbulence.

# Chapter 5

## Conclusion

### 5.1 Summary and discussion

FSO communications have been achieving a growing attention in the past decades, since researches about the wireless RF communications have met with the bottleneck. The optical frequency is so much higher than the radio frequency, which means FSO links can provide a wider communication bandwidth and a higher transmission speed than the traditional RF links. The inherent narrow laser beam can provide the superior directivity for the FSO links, that FSO systems can support ultra-long distance communications (satellite communications, deep space communications, etc.). The optical telescopes for the FSO communications are more mass saving, more portable and more energy efficient than the antennas for the RF communications. The FSO scheme can also be an ideal alternative option to the optical fiber networks in special situations (natural disaster areas, mountainous areas, etc.), in which the optical fiber structures are too expensive or impossible to be established. As many as 75% customers are distributed within one mile distance around the backbone optical fiber, this so called last mile problem is growing more and more serious and the FSO communication is considered as a desired solution.

In Chapter 1, we have given a brief introduction to the concept of the FSO communications. The current development situation of the FSO has been presented. The advantages of the FSO systems stimulate our research motivation. Under the consideration of the mainly constraints of the FSO systems, the atmosphere influence, we can affirm our research orientation on reducing the channel fading in FSO links.

In Chapter 2, the analysis about the influence of the atmospheric channel to the laser beam transmission has been demonstrated. The atmospheric turbulence generates both the intensity fluctuations and the polarization distortions of the optical wave. These detrimental effects have far-reaching consequences in the performance

of the FSO links. We have described the physical form of the atmospheric turbulence and explained the widely-used turbulence spectrum models. By associating with the turbulence parameters dynamic changing laws, we established the statistic model describing the intensity fluctuations and the polarization distortions of the optical wave propagating through the atmosphere channel. We ran the simulation based on the mathematic model. According to the estimation, we can find that the optical polarization is far more stable than the optical intensity suffered from the turbulence disturbing.

In Chapter 3, based on the channel analysis in chapter 2, we proposed four methods to be applied in FSO system designment:

1. The OFDM technology has the advantages in against channel dispersion and time varying environment.
2. The method aperture average mitigates the channel fading by increasing the size of the receiving lens. The aperture average promoting the performance of FSO systems with the plane/spherical/Gaussian wave are simulated. We can find that the optical fluctuation is reduced with the aperture size increasing.
3. The multiple reception reduces the weight and cost of the FSO system by replacing one huge lens to several smaller lenses. We establish the mathematical model of the correlation coefficient between different lenses corresponding to their central distance and the turbulence conditions. The intensity relationship between two individual lenses are presented.
4. The PM modulates signals into optical polarization states to promote the system performance, since the optical polarization is the most stable property when laser beam propagating through the atmosphere channel. The principle of three types of PM methods, the PolSK, the CPolM and the CPolSK, are expressed by polarization states figures.

In Chapter 4, we analyze the performance of the FSO systems applying the technologies discussed in Chapter 3. It includes:

1. The performance of the OFDM FSO system with aperture average is simulated. The numerical result can present that the optimum OFDM modulation index is between 0.01% to 0.1%. By increasing the diameter of lens, the performance of the proposed system is promoted, efficiently. The proposal can reduce the system average BER under the varying atmospheric turbulence strength.

2. The multiple reception scheme is replacing one huge lens to several smaller lenses. Under the condition of the identical receiving area, we run the simulations about the multiple reception OFDM FSO systems. We compared the average BER performance of the single reception, the dual reception and the ternary reception schemes. The numerical results show that the increasing number of lens can improve the average BER performance, efficiently. When the lens quantity is fixed, the superior performance comes from a lower correlation coefficient.
3. According to the estimation in Chapter 2, the optical polarization is the most stable property of the laser beam when propagating through the atmospheric channel. In order to take full advantages of the polarization stability, we modulate the OFDM signal into a consecutive linear polarization state and name this method as CPolM (consecutive polarization modulation). Based on the comparison between the CPolM-based OFDM FSO system with the IM-based OFDM FSO system, we can achieve the conclusion that the proposal emerges the superiority in mitigating channel effects.
4. The linear polarization state is not suitable in a mobile environment, since a random rotation will lead to a misalignment of the polarized direction. Hence, we apply the circular polarization states to represent signals and simulate the system working in the space-to-ground channel. The simulation results can present that even after 959.8km data transmission the right\left handed circularly polarized states are remaining stable. Comparing the numerical results of the CPolSK-based FSO system with the IM-based FSO system, we can find the proposed system needs about 3dB less SNR than the conventional system to achieve the same level of BER.

## 5.2 Future work

In this thesis, we proposed four methods applying in the FSO system designment. Although the results show that our proposals are efficiently promoting the FSO system performance, the scope of this field can not be completely covered. Some of the potential research in future can be list as follows:

1. The underwater FSO systems:  
FSO systems utilizing the blue-green laser diodes can support the underwater links over the kilometer level distances. Compared to the acoustic sonar systems, FSO systems can provide wider bandwidths, higher transmission speed,

and lower multi-path fading. However the undersea environment is much more complicated than the atmospheric channel, the requirement to the solution for mitigating the underwater channel fading is highly urgent.

2. The quantum communication systems:

Since the laser beam is natural narrow, the FSO information is hard to be captured. In order to further enhance the security of FSO system, we can transmit the signal on the single photon. The transmitter can immediately realize that the information has been hacked owing to the entangled quantum effect.

3. The pointing, acquisition and tracing (PAT) systems:

The laser's narrow beam can provide to the FSO system the advantage of well directivity and power concentration, as well as, the disadvantage of the difficulty of building a communication link. Thus, a well-performed PAT system is urgently needed.

# References

- [1] L. C. Andrews and R. L. Phillips, *Laser Beam Propagation through Random Media*, 2nd ed. Washington, USA: SPIE, 2005.
- [2] Y. Su and T. Sato, “A key technology for standardizing outdoor optical wireless communications,” *ICT Express*, vol. 3, no. 2, pp. 62–66, 2017.
- [3] W. Shieh and I. Djordjevic, *OFDM for Optical Communications*. Academic Press, ELSEVIER, 2010.
- [4] J. Armstrong, “Ofdm for optical communications,” *Journal of Lightwave Technology*, vol. 27, no. 3, pp. 189–204, 2009.
- [5] Y. Su, F. Bai, and M. Matsumoto, “Transmission analysis of a ternary diversity reception based on ofdm fso system over correlated log-normal fading channel.” Guangzhou China: PIERS Proceedings, August 2014, pp. 1721–1725.
- [6] Y. Su, F. Bai, and T. Sato, “Transmission analysis of cpolm-based ofdm fso system in atmospheric turbulence,” *Optics Communications*, vol. 369, pp. 111–119, 2016.
- [7] Y. Su and T. Sato, “Analysis of cpolsk-based fso system working in space-to-ground channel,” *Optics Communications*, vol. 410, pp. 660–667, 2018.
- [8] A. Siamarou, “Broadband wireless local-area networks at millimeter waves around 60 ghz,” *Antennas and Propagation Magazine, IEEE*, vol. 45, no. 1, pp. 177–181, Feb 2003.
- [9] R. Honer and A. Mahdy, “Emerging urban applications of broadband optical wireless networking,” in *Emerging Network Intelligence, 2009 First International Conference on*, Oct 2009, pp. 39–42.

- [10] G. Peng, Y. Luo, J. Zhang, J.H.and Wen, Y. B.B., and J. Canning, “Recent development of new active optical fibres for broadband photonic applications,” pp. 5–9, Oct 2013.
- [11] E. Leitgeb and T. Plank, “Combination of free space optics (fso) and rf for different wireless application scenarios,” pp. 1–4, April 2015.
- [12] J. S. S. Bloom, E. Korevaar and H. Willebrand., “Understanding the performance of free-space optics,” pp. 178–200, April 2003.
- [13] S. Hranilovic., “Wireless optical communication system,” 2004.
- [14] M. Toyoshima, T. Sasaki, H. Takenaka, Y. Shoji, Y. Takayama, Y. Koyama, H. Kunimori, M. Akioka, M. Fujiwara, and M. Sasaki, “Research and development of free-space laser communications and quantum key distribution technologies at nict,” in *Space Optical Systems and Applications (ICSOS), 2011 International Conference on*, May 2011, pp. 1–7.
- [15] J. Lesh, “Free space laser communications,” in *Summaries of Papers Presented at the Conference on Lasers and Electro-Optics, Baltimore, MD, USA, c1999: 1-5.*, May 1999.
- [16] A. Boucouvalas, “Reliability of indoor and short range fso - paper not available at publishing time,” in *Transparent Optical Networks, 2005, Proceedings of 2005 7th International Conference*, vol. 1, July 2005, pp. 402–402.
- [17] H. Hemmati, “Laser communications: From terrestrial broadband to deep-space,” in *Transparent Optical Networks (ICTON), 2014 16th International Conference on*, July 2014, pp. 1–3.
- [18] R. Sharma, H. Kaushal, and P. Sharma, “Analysis of indoor fso link under diffused channel topology,” in *2015 International Conference on Computing, Communication Automation (ICCCA)*, May 2015, pp. 1268–1272.
- [19] J. Vitasek, P. Siska, J. Latal, S. Hejduk, A. Liner, and V. Vasinek, “The transmitter for indoor free space optic networks,” in *2013 36th International Conference on Telecommunications and Signal Processing (TSP)*, July 2013, pp. 290–293.

- [20] N. Nor, E. Fabiyi, M. Abadi, X. Tang, Z. Ghassemlooy, and A. Burton, "A laboratory demonstration investigation of moderate-to-strong turbulence effects on free space optics," in *2015 13th International Conference on Telecommunications (ConTEL)*, July 2015, pp. 1–5.
- [21] D. Kedar and S. Arnon, "Urban optical wireless communication networks: the main challenges and possible solutions," *Communications Magazine, IEEE*, vol. 42, no. 5, pp. S2–S7, May 2004.
- [22] S. Arnon, "Optimization of urban optical wireless communication systems," *IEEE Transactions on Wireless Communications*, vol. 2, no. 4, pp. 626–629, July 2003.
- [23] S. Muhammad, P. Kohldorfer, and E. Leitgeb, "Channel modeling for terrestrial free space optical links," in *Proceedings of 2005 7th International Conference on Transparent Optical Networks*, vol. 1, July 2005, pp. 407–410 Vol. 1.
- [24] M. Cordeiro, C. Colvero, and J. von der Weid, "Experimental comparison of scintillation effects in far and near infrared wavelengths in fso systems," in *2005 SBMO/IEEE MTT-S International Conference on Microwave and Optoelectronics*, July 2005, pp. 393–395.
- [25] H. E. Nistazakis, E. Karagianni, A. Tsigopoulos, M. Fafalios, and G. Tombras, "Average capacity of optical wireless communication systems over atmospheric turbulence channels," *Journal of Lightwave Technology*, vol. 27, no. 8, pp. 974–979, April 2009.
- [26] T. Singh, "Calculations of the impact on atmospheric turbulence conditions on free space optical communication links using gamma-gamma model," in *2013 Fourth International Conference on Computing, Communications and Networking Technologies (ICCCNT)*, July 2013, pp. 1–5.
- [27] T. Joseph, H. Kaushal, V. Jain, and S. Kar, "Performance analysis of oofdm modulation scheme with spatial diversity in atmospheric turbulence," in *2014 23rd Wireless and Optical Communication Conference (WOCC)*, May 2014, pp. 1–3.
- [28] A. Johnsi and V. Saminadan, "Performance of diversity combining techniques for fso-mimo system," in *2013 International Conference on Communications and Signal Processing (ICCSP)*, April 2013, pp. 479–483.

- [29] A. Viswanath, V. Jain, and S. Kar, “Experimental evaluation of the effect of aperture averaging technique on the performance of free space optical communication link for different intensity modulation schemes,” in *2015 7th International Conference on Communication Systems and Networks (COMSNETS)*, Jan 2015, pp. 1–5.
- [30] M. Toyoshima, S. Yamakawa, T. Yamawaki, K. Arai, K. Yabe, and K. Shiratama, “Reconfirmation of the optical performances of the laser communications terminal onboard the oicets satellite,” *Acta Astronautica*, vol. 55, no. 3-9, pp. 261–269, 2004.
- [31] S. Navidpour, M. Uysal, and M. Kavehrad, “Ber performance of free-space optical transmission with spatial diversity,” *IEEE Transactions on Wireless Communications*, vol. 6, no. 8, pp. 2813–2819, August 2007.
- [32] F. Bai, Y. Su, and T. Sato, “Performance evaluation of a dual diversity reception base on ofdm rofso systems over correlated log-normal fading channel,” in *ITU Kaleidoscope Academic Conference: Living in a converged world - Impossible without standards?, Proceedings of the 2014*, June 2014, pp. 263–268.
- [33] C. Chen, Y. H.M., J. Fan, X. Feng, C. Han, and Y. Ding, “Model for outage probability of free-space optical links with spatial diversity through atmospheric turbulence,” in *ICIC '09 Second International Conference on Information and Computing Science*, vol. 4, May 2009, pp. 209–211.
- [34] M. Toyoshima, T. Takahashi, K. Suzuki, S. Kimura, K. Takizawa, T. Kuri, W. Klaus, M. Toyoda, H. Kunimori, T. Jono, Y. Takayama, and K. Arai, “Ground-to-satellite laser communication experiments,” *IEEE Aerospace and Electronic Systems Magazine*, vol. 23, pp. 10–18, 2008.
- [35] W. Gappmair, S. Hranilovic, and E. Leitgeb, “Ook performance for terrestrial fso links in turbulent atmosphere with pointing errors modeled by hoyt distributions,” *IEEE Communications Letters*, vol. 15, no. 8, pp. 875–877, August 2011.
- [36] M. Toyoshima, H. Takenaka, Y. Shoji, Y. Takayama, Y. Koyama, and H. Kunimori, “Polarization measurements through space-to-ground atmospheric propagation paths by using a highly polarized laser source in space,” *Optics Express*, vol. 17, no. 25, pp. 22 333–22 340, 2009.

- [37] X. Tang, Z. Ghassemlooy, S. Rajbhandari, W. Popoola, C. Lee, E. Leitgeb, and V. Ahmadi, "Free-space optical communication employing polarization shift keying coherent modulation in atmospheric turbulence channel," *2010 7th International Symposium on Communication Systems Networks and Digital Signal Processing (CSNDSP)*, pp. 615–620, July 2010.
- [38] J. Strohbehn and S. Clifford, "Polarization and angle-of-arrival fluctuations for a plane wave propagated through a turbulent medium," *IEEE Transactions on Antennas and Propagation*, vol. 15, no. 3, pp. 416–421, May 1967.
- [39] S. Florez, "Circular polarization and availability in free space optics (fso) communication systems," in *2010 IEEE Latin-American Conference on Communications*, Sept 2010, pp. 1–6.
- [40] Y. Zhao, X.H. and Yao, Y. Sun, and C. Liu, "Circle polarization shift keying with direct detection for free-space optical communication," *J. Opt. Commun. Netw.*, vol. 1, no. 4, pp. 307–312, Sep 2009.
- [41] K. Sasaki, N. Minato, T. Ushikubo, and Y. Arimoto, "First ocdma experimental demonstration over free space and optical fiber link," *Conference on Optical Fiber communication/National Fiber Optic Engineers Conference*, pp. 1–3, Feb 2008.
- [42] N. C. Ben, A. Bekkali, K. Wakamori, and M. Matsumoto, "Performance analysis of cdma-based wireless services transmission over a turbulent rf-on-fso channel," May 2011, pp. 475–486.
- [43] P. Kumar, "Comparative analysis of ber performance for direct detection and coherent detection fso communication systems," pp. 369–374, April 2015.
- [44] D. Ly-Gagnon, S. Tsukamoto, K. Katoh, and K. Kikuchi, "Coherent detection of optical quadrature phase-shift keying signals with carrier phase estimation," *Journal of Lightwave Technology*, vol. 24, no. 1, pp. 12–21, Jan 2006.
- [45] H. T. T. Pham, N. T. Dang, L. T. Vu, and H. T. Bui, "A survey of performance improvement methods for free-space optical communication systems," in *International Conference on Advanced Technologies for Communications*, Hanoi, 2014, pp. 770–775.

- [46] Z. Wang and C. Zhong, W.D.and Yu, “Dynamic decision threshold and adaptive coherent detection in fso communication system,” in *2011 8th International Conference on Information, Communications and Signal Processing (ICICS)*, Dec 2011, pp. 1–5.
- [47] F. Bai, Y. Su, and T. Sato, “Performance analysis of polarization modulated directdetection optical cdma systems over turbulent fso links modeled by the gamma-gamma distribution,” *Photonics*, vol. 2, no. 1, p. 139, 2015.
- [48] —, “Performance analysis of rofso links with diversity reception for transmission of ofdm signals under correlated log-normal fading channels,” *Journal of ICT standardization*, vol. 2, pp. 129–150, 2014.
- [49] K. Peppas and P. Mathiopoulos, “Free-space optical communication with spatial modulation and coherent detection over h-k atmospheric turbulence channels,” *Journal of Lightwave Technology*, vol. 33, no. 20, pp. 4221–4232, Oct 2015.
- [50] F. Bai, Y. Su, and T. Sato, “Performance analysis of heterodyne-detected ocdma systems using polsk modulation over a free-space optical turbulence channel,” *Electronics*, vol. 4, pp. 785–798, 2015.
- [51] <https://en.wikipedia.org/wiki/Photophone>.
- [52] C. Fan, “Engineering innovation: Prof. charles k. kao’s nobel prize,” in *2010 19th Annual Wireless and Optical Communications Conference (WOCC)*, May 2010, pp. 1–4.
- [53] <http://opticalcomm.jpl.nasa.gov/PAGES/flight.html>.
- [54] <http://global.jaxa.jp/>.
- [55] L. Hutcheson, “Fttx: Current status and the future,” *IEEE Communications Magazine*, vol. 46, no. 7, pp. 90–95, July 2008.
- [56] A. Ghosh, D. Wolter, J. Andrews, and R. Chen, “Broadband wireless access with wimax/802.16: current performance benchmarks and future potential,” *IEEE Communications Magazine*, vol. 43, no. 2, pp. 129–136, Feb 2005.
- [57] E. Leitgeb, T. Plank, M. Loschnigg, and P. Mandl, “Free space optics in different (civil and military) application scenarios in combination with other wireless technologies,” in *2014 16th International Telecommunications Network Strategy and Planning Symposium (Networks)*, Sept 2014, pp. 1–7.

- [58] R. Paudel, Z. Ghassemlooy, L. Hoa, S. Rajbhandari, and B. Livingstone, “Investigation of fso ground-to-train communications in a laboratory environment,” in *2011 Second Asian Himalayas International Conference on Internet (AH-ICI)*, Nov 2011.
- [59] E. Zedini and M. Alouini, “Multihop relaying over im/dd fso systems with pointing errors,” *Journal of Lightwave Technology*, vol. PP, no. 99, pp. 1–1, 2015.
- [60] K. Prabu, S. Bose, and D. Kumar, “Analysis of optical modulators for radio over free space optical communication systems and radio over fiber systems,” in *2012 Annual IEEE India Conference (INDICON)*, Dec 2012, pp. 1176–1179.
- [61] C. Mary, “Signaling safety [electrical safety],” *Industry Applications Magazine, IEEE*, vol. 17, no. 1, pp. 6–6, Jan 2011.
- [62] <http://esc.gsfc.nasa.gov/267/271/335.html>.
- [63] N. Agrawal, C. Davis, and S. Milner, “Free space optical sensor networking for underwater sensing applications,” in *2009 5th International Conference on Intelligent Sensors, Sensor Networks and Information Processing (ISSNIP)*, Dec 2009, pp. 475–480.
- [64] Z. Ghassemlooy, S. Arnon, M. Uysal, and J. Xu, Z.Y.and Chen, “Emerging optical wireless communications-advances and challenges,” *IEEE Journal on Selected Areas in Communications*, vol. 33, no. 9, pp. 1738–1749, Sept 2015.
- [65] V. Silva, A. Barbero, and R. Ribeiro, “A new triangulation-like technique for the evaluation of the refractive index structure constant ( $c_n^2$ ) in free-space optical links,” *Journal of Lightwave Technology*, vol. 29, no. 24, pp. 3603–3610, Dec 2011.
- [66] M. Abaza, R. Mesleh, A. Mansour, and E. Aggoune, “Spatial diversity for fso communication systems over atmospheric turbulence channels,” in *2014 IEEE Wireless Communications and Networking Conference (WCNC)*, April 2014, pp. 382–387.
- [67] A. Malpani and A. Malpani, “Performance analysis of fso communication with aperture averaging under varying atmospheric turbulence regimes,” in *2012 Ninth International Conference on Wireless and Optical Communications Networks (WOCN)*, Sept 2012, pp. 1–6.

- [68] T. Tsiftsis, H. Sandalidis, G. Karagiannidis, and M. Uysal, "Fso links with spatial diversity over strong atmospheric turbulence channels," in *IEEE International Conference on Communications*, May 2008, pp. 5379–5384.
- [69] X. Zhu and J. Kahn, "Performance bounds for coded free-space optical communications through atmospheric turbulence channels," vol. 51, no. 8, Aug 2003, pp. 1233–1239.
- [70] H. Samimi and P. Azmi, "Performance analysis of adaptive subcarrier intensity-modulated free-space optical systems - retracted," *Optoelectronics, IET*, vol. 5, no. 4, pp. 168–174, August 2011.
- [71] X. Tang, S. Rajbhandari, W. Popoola, Z. Ghassemlooy, E. Leitgeb, S. Muhammad, and G. Kandung, "Performance of bpsk subcarrier intensity modulation free-space optical communications using a log-normal atmospheric turbulence model," in *2010 Symposium on Photonics and Optoelectronic (SOPO)*, June 2010, pp. 1–4.
- [72] W. Popoola and Z. Ghassemlooy, "Bpsk subcarrier intensity modulated free-space optical communications in atmospheric turbulence," *Journal of Lightwave Technology*, vol. 27, no. 8, pp. 967–973, April 2009.
- [73] A. Bekkali, C. Ben Naila, K. Kazaura, K. Wakamori, and M. Matsumoto, "Transmission analysis of ofdm-based wireless services over turbulent radio-on-fso links modeled by gamma-gamma distribution," vol. 2, no. 3, June 2010, pp. 510–520.
- [74] X. Zhao, Y. Yao, Y. Sun, J. Xu, X. C. Tian, and C. Liu, "Condition of keeping polarization property unchanged in the circle polarization shift keying system," *Journal of Optical Communications and Networking, IEEE/OSA*, vol. 2, no. 8, pp. 570–575, August 2010.
- [75] Z. Ghassemlooy, X. Tang, and S. Rajbhandari, "Experimental investigation of polarisation modulated free space optical communication with direct detection in a turbulence channel," *Communications, IET*, vol. 6, no. 11, pp. 1489–1494, July 2012.
- [76] M. A. Khalighi and M. Uysal, "Survey on free space optical communication: A communication theory perspective," *IEEE Communications Surveys & Tutorials*, vol. 16, no. 4, pp. 2231–2258, 2014.

- [77] H. Al-Raweshidy and S. Komaki, *Radio Over Fiber Technologies for Mobile Communications Networks*. Artech, 2002.
- [78] <https://www.itu.int/rec/T-REC-G.640-200603-I/en>.
- [79] D. Skraparlis, M. Sandell, V. Sakarellos, A. Panagopoulos, and J. Kanellopoulos, “On the effect of correlation on the performance of dual diversity receivers in lognormal fading,” *Communications Letters, IEEE*, vol. 14, no. 11, pp. 1038–1040, November 2010.
- [80] Z. Chen, S. Yu, T. Wang, G. Wu, and W. Wang, S.L. and Gu, “Channel correlation in aperture receiver diversity systems for free-space optical communication,” *Journal of Optics*, 2012.
- [81] M. Khalighi, N. Schwartz, N. Aitamer, and S. Bourennane, “Fading reduction by aperture averaging and spatial diversity in optical wireless systems,” *IEEE/OSA Journal of Optical Communications and Networking*, vol. 1, no. 6, pp. 580–593, November 2009.
- [82] G. Hooshang and M. M. Karbassian, in *Optical CDMA Networks: Principles, Analysis and Applications*. Wiley-IEEE Press, 2012.
- [83] X. Tang, Z. Ghassemlooy, S. Rajbhandari, W. Popoola, and C. Lee, “Differential circular polarization shift keying with heterodyne detection for free space optical links with turbulence channel,” in *2011 16th European Conference on Networks and Optical Communications (NOC)*, July 2011.
- [84] K. Wakafuji and T. Ohtsuki, “Performance analysis of atmospheric optical subcarrier multiplexing systems and atmospheric optical code division multiplexing systems,” in *2004 IEEE International Conference on Communications*, vol. 6, June 2004, pp. 3336–3340.
- [85] P. Liu, P. Dat, K. Wakamori, and M. Matsumoto, “A new scheme on time-diversity atmospheric ocdma system over atmospheric turbulence channels,” in *2010 IEEE GLOBECOM Workshops (GC Wkshps)*, Dec 2010, pp. 1020–1025.
- [86] K. Iversen, J. Muechenhein, and D. Junghanns., “Performance evaluation of optical cdma using polsk-dd to improve bipolar capacity,” 1995, pp. 319–329.
- [87] G. Yang and W. Kwong, *Prime Codes with Applications to CDMA Optical and Wireless Networks*. Artech House, 2002.

- [88] M. Karbassian and H. Ghafouri-Shiraz, "Transceiver architecture for incoherent optical cdma networks based on polarization modulation," *Journal of Lightwave Technology*, vol. 26, no. 24, pp. 3820–3828, Dec 2008.
- [89] K. Iversen, J. Muechenhein, and D. Junghanns., "On the combination of optical cdma and polsk," *J. Opt. Commun.*, pp. 126–130, 1994.
- [90] T. OFarrell and S. Lochmann, "Performance analysis of an optical correlator receiver for sik ds-cdma communication systems," *Electronics Letters*, vol. 30, no. 1, pp. 63–65, Jan 1994.
- [91] O. Adamchik, V.S.; Marichev, "The algorithm for calculating integrals of hypergeometric type functions and its realization in reduce system," *In Proceedings of the International Conference Symbolic Algebraic.*, pp. 212–224, August 1990.
- [92] M. Jazayerifar and J. Salehi, "Atmospheric optical cdma communication systems via optical orthogonal codes," *IEEE Transactions on Communications*, vol. 54, no. 9, pp. 1614–1623, Sept 2006.
- [93] X. Tang, Z. Ghassemlooy, S. Rajbhandari, W. Popoola, and C. Lee, "Coherent heterodyne multilevel polarization shift keying with spatial diversity in a free-space optical turbulence channel," *Journal of Lightwave Technology*, vol. 30, no. 16, pp. 2689–2695, Aug 2012.
- [94] L. J. LopeZ and C. Rodriguez Hidalgo, "Interconnecting university networks using a full-duplex fso system using coherent detection and polarization-division multiplexing: Design and simulation," in *2015 IEEE Optical Interconnects Conference (OI)*, April 2015, pp. 106–107.
- [95] I. Kim and E. K. B. McArthur, "Comparison of laser beam propagation at 785 nm and 1550 nm in fog and haze for optical wireless communications," *Proceeding of SPIE*, vol. 4214, pp. 26–37, February 2001.
- [96] N. Wang and J. Cheng, "Moment-based estimation for the shape parameters of the gamma-gamma atmospheric turbulence model," *Opt. Express*, vol. 18, no. 12, pp. 12 824–12 831, Jun 2010.
- [97] I. Kay, M. Jens, and J. Dirk, "Performance evaluation of optical code division multiple access (cdma) using polarization shift keying direct detection (polsk-dd) to improve bipolar capacity," pp. 319–329, 1995.

- [98] K. Takahashi, “A study on signal-mode-fiber direct coupling type optical wireless communication systems,” PH.D. Thesis, The University of Electro-Communications, Tokyo, Japan, 2011.
- [99] A. Mansour, R. Mesleh, and M. Abaza, “New challenges in wireless and free space optical communications available,” *Optics and Lasers in Engineering*, vol. 89, pp. 95–108, 2017.
- [100] H. Hemmati, *Deep Space Optical Communications*. John Wiley & Sons, Inc., 2006.
- [101] H. Henniger and O. Wilfert, “An introduction to free-space optical communications,” *Radio Engineering*, vol. 19, no. 2, pp. 203–212, 2010.
- [102] K. Takahashi, “A study on signal-mode-fiber direct coupling type optical wireless communication systems,” Ph.D. dissertation, The University of Electro-Communications, Tokyo, Japan, 2011.
- [103] S. L. Chuang, *Physics of Photonic Devices*. John Wiley & Sons, Inc., 2008.
- [104] K. Chang, *Fiber and Electro-Optical Components*. John Wiley & Sons, Inc., 1991.
- [105] H. Nishihara, M. Haruna, and T. Suhara, *Optical Integrated Circuits*. McGraw-Hill, 1989.
- [106] T. Tamir, G. Griffel, and H. L. Bertoni, *Guided-Wave Optoelectronics: Device Characterization, Analysis, and Design*. Springer, 1995.

## 早稲田大学 博士（工学） 学位申請 研究業績書

(List of research achievements for application of doctorate (Dr. of Engineering), Waseda University)

氏名 蘇昱瑋 (SU Yuwei) 印

(As of October, 2017)

種 類 別 (By Type)	題名、 発表・発行掲載誌名、 発表・発行年月、 連名者(申請者含む)(theme, journal name, date & year of publication, name of authors inc. yourself)
Articles in Refereed Journals	<p>○[1] <b>Yuwei Su</b> and Fan Bai and Takuro Sato, “Transmission Analysis of CPolM-based OFDM FSO System in Atmospheric Turbulence”, Optics Communications, Volume 369, pp. 111-119, 2016, ISSN 0030-4018.</p> <p>○[2] <b>Yuwei Su</b> and Takuro Sato, “A Key Technology for Standardizing Outdoor Optical Wireless Communications”, ICT Express, Volume 3, Issue 2, 2017, Pages 62-66, ISSN 2405-9595.</p> <p>○[3] <b>Yuwei Su</b> and Takuro Sato, “Analysis of CPolSK-based FSO System Working in Space-to-Ground Channel” , Optics Communications, Volume 410, Pages 660-667, 2018, ISSN 0030-4018,.</p> <p>[4] Fan Bai, <b>Yuwei Su</b> and Takuro Sato, “Performance Analysis of Heterodyne-Detected OCDMA Systems Using PolSK Modulation over a Free-Space Optical Turbulence Channel”, MDPI, Electronics, 4(4), pp .785-798, 16 October, 2015, ISSN 2079-9292.</p> <p>[5] Fan Bai, <b>Yuwei Su</b> and Takuro Sato, “Performance Analysis of Polarization Modulated Direct Detection Optical CDMA Systems over Turbulent FSO Links Modeled by the Gamma-Gamma Distribution”, MDPI, Photonics, 2(1), pp.139-155, 29 January, 2015, ISSN 2304-6732.</p> <p>[6]Fan Bai, <b>Yuwei Su</b> and Takuro Sato, “Performance Analysis of RoFSO Links with Diversity Reception for Transmission of OFDM Signals under Correlated Log-normal Fading Channels”, Journal of ICT standardization, 2(2), pp .129-150, 10 November, 2014, ISSN 2245-800X.</p>
International Conferences	<p>○[1] <b>Yuwei Su</b>, Fan Bai and Mitsuji Matsumoto, “Transmission Analysis of a Ternary Diversity Reception Based on OFDM FSO System over Correlated Log-normal Fading Channel”, Progress in Electromagnetics Research Symposium (PIERS), Guangzhou, China, August, 2014.</p> <p>[2] Fan Bai, <b>Yuwei Su</b> and Takuro Sato, “Performance Evaluation of a Dual Diversity Reception Base on OFDM RoFSO Systems over Correlated Log-normal Fading Channel”, ITU Kaleidoscope Academic Conference: Living in a converged world - Impossible without standards, 263-268, Russia, June, 2014.</p>